# Geophysical Surveys Near Tucson Electric Power Sundt Generating Station

**Geophysics Field Camp 2014**
**LASI-14-1**

**May 10, 2014**

Lujain Ali Alghannam
Wadyan Osama Ayyad
Carla Gabriela Do Lago Montenegro
Wanjie Feng
Christopher A. Jones
Mikhail D. Samoylov
Ben K. Sternberg
Chak Hau Tso
Sean T. Wright

## Abstract

Tucson Electric Power (TEP) is carrying out subsurface investigations in order to locate more groundwater for cooling at the Sundt power-generating plant. To assist with this investigation, the University of Arizona GEN/GEOS 416/516 Field Studies in Geophysics class conducted geophysics surveys in an area just south of Davis-Monthan Air Force Base and between UTM coordinates 508,555 to 511,753 East and 3,553,705 to 3,556,895 North. Four geophysics methods (Gravity, Magnetics, Transient Electromagnetics (TEM), and Passive Seismic) were employed to locate a postulated fault, which may be correlated with ground water flow. A broad regional magnetic anomaly was mapped, as the magnetic field decreases steadily from NE to SW. There are no significant magnetic field anomalies that could be related to a potential fault. The Gravity results show a regional gravitational gradient, steadily decreasing from NE to SW, with a large isolated anomaly apparent around 1500m from the base station at the NE corner of the survey area. But, this large anomaly is a localized, and does not appear on the adjacent parallel survey lines, therefore it is not related to a potential fault contact. The Passive Seismic survey detected a deep boundary at 100m to 160m in elevation, but the depths interpreted from the 11 stations are scattered and do not show a clear trend. The Transient Electromagnetic (TEM) data show a consistent difference in depth to a low-resistivity layer along the profile line. The four TEM stations north of Interstate 10 (I10) have an average elevation for the 10 Ohm-m contour line of 720 meters. The four TEM stations south of I10 have an average elevation for the 10 Ohm-m contour line of 670 meters. This offset may be related to the postulated fault.

# Acknowledgements

The University of Arizona Geophysics Field Camp class, GEN/GEOS 416/516, would like to thank Tucson Electric Power for providing the funding for this project. In particular, we would like to thank Byron Brandon of TEP for his coordination of the project. Without this funding and support, we would not have been able to offer the class this year.

We would also like to thank the U.S. Geological Survey for their support of the class, including identifying this project, and making the cooperation with Tucson Electric Power possible. In particular, we would like to thank Don Pool for his coordination of the project. The USGS also provided the passive seismic equipment.

Buck Schmidt, Principal Hydrologist of Basin Wells Associates, PLLC, presented the geological background and objective of this project in an early class. His presentation and assistance in this class were of great help to us in understanding the requirements of this project.

Jamie P. Macy, USGS Hydrologist, Arizona Water Science Center, Flagstaff Programs, provided the TEM equipment and assisted us in the TEM field surveys. He taught us the procedures for data acquisition and data processing. His willingness in sharing his expertise with this class was invaluable for us.

We really appreciated the help from Don Pool. He arranged for our use of the Passive Seismic equipment. He also taught us how to obtain the data and trained us on using the processing software, Geopsy. He also double checked our processing results. His help let us be confident in our processing results.

Zonge International provided data processing software to the class. Zonge International has played a vital role in our Geophysics Field Camp for the past 27 years. We sincerely appreciate that they have continued to provide our students with the opportunity to use state-of-the-art electrical geophysics methods.

# Table of Contents

# 1. Introduction

## 1.1 Tucson Basin Geology

Based on a deep exploration well commissioned by Exxon, Houser et al. (2004) describe in detail the geologic settings of the Tucson Basin. This is among one of the best descriptions of the Tucson Basin available, and is summarized in the following paragraphs. The Tucson Basin was formed around the late Cenozoic, however Proterozoic and Paleozoic geologic events shaped the area of the present Tucson Basin. The basin is located in the upper plate of the Catalina detachment fault. Based on the deep exploration well logs, it was found that granitoid rocks were penetrated beneath 3,658m of Mesozoic and Cenozoic sedimentary and volcanic rocks. Uplift of the adjacent Catalina Mountains has altered the subsurface geometry of the Basin. A stratigraphic section from Pleistocene to middle Miocene covers the top 1,880m of the area. The Tucson Basin is a large structural basin, sediment filled and separated by mountain ranges. It is 15 to 40km wide; 80km long, and the elevation is about 727m above sea level.

The top 1,880m of basin-fill sedimentary rocks can be divided about equally into the lower basin-fill and upper basin-fill deposits. They consist of alluvial-fan, alluvial-plain, and playa facies. The first 341m thick unit is an alluvial fan deposit that is a major aquifer in the Tucson Basin. At about 908m there is a boundary that separates an unconsolidated and undeformed upper-basin fill from a denser and more faulted lower-basin fill, indicating two stages of basin filling. The Pontano Formation follows the sedimentary layers and it extends deeper than the focus of this study.

## 1.2 Project Background and Outline

Tucson Electric Power (TEP) Sundt Power Plant has plans for expanding and improving its well field to supply sufficient groundwater resources for power generation and cooling. An aging well field along with declining groundwater levels has resulted in operational water supply challenges with respect to groundwater yield and quality, and sand production. The improved well field has to be able to provide at least 5500 gallons per minute (gpm) and the water must have low temperature and total dissolved solids (TDS), since the water is used for cooling purposes in the power plant. The TEP Sundt Groundwater Resource Investigation/Groundwater

Action Plan (GAP) is a project commissioned in order to find additional water resources in an area close to TEP. The study area of the GAP is shown in Figure 1.1 (Bostic and Schmidt, 2013). A regional aquifer in a stratigraphic unit called the Upper Tinaja Beds (TSU) is the optimal aquifer for meeting the requirements. This is because the yield potential of a shallower, perched aquifer is too low and the existing deeper regional aquifer is expected to have unacceptably high temperatures. Figure 1.2 shows the water depth of the regional aquifer in the study area. Figure 1.3 shows a table with these stratigraphic units.

In order to assist with these goals, the GEN/GEOS 416-516 Field Studies in Geophysics class performed four different geophysics surveys (Gravity, Magnetics, Transient Electromagnetics (TEM), and Passive Seismic) in the area (Figures 1.1 and 1.2) where a postulated fault crosses the regional and deep regional aquifers. The exact location of the fault is unknown, as well as the exact depths of the aquifers. The proposed depth and location of the fault is shown in Figures 1.4 and 1.5. The purpose of the geophysical studies and this report is to provide additional information regarding the fault and the depths of the aquifers and aquitards, and provide information for the proposed well locations. The following sections discuss each of the geophysical surveys performed and the results obtained.

## 1.3 References

Bostic, Michael W., R.G Werner 'Buck' Schmidt, 2013, Tucson Electric Power - Sundt Generating Station, Preliminary Groundwater Resource Investigation, Tucson, Arizona, Prepared For Tucson Electric Power, September 4, 2013, Basinwells Associates Pllc Project No. 13-003

Houser, B., Peters, L., Esser, R., & Gettings, M. (2004, January 1). Stratigraphy and Tectonic History of the Tucson Basin, Pima County, Arizona, Based on the Exxon State (32)-1 Well. *Stratigraphy and Tectonic History of the Tucson Basin, Pima County, Arizona, Based on the Exxon State (32)-1 Well*. Retrieved April 20, 2014, from http://pubs.usgs.gov/sir/2004/5076/

Schmidt, Buck (February 3, 2014), *TEP Sundt Groundwater Reource Investigation/Groundwater Action Plan (GAP)*, PowerPoint presentation, Power point presentation, BasinWells Associates, PLLC, Tucson AZ

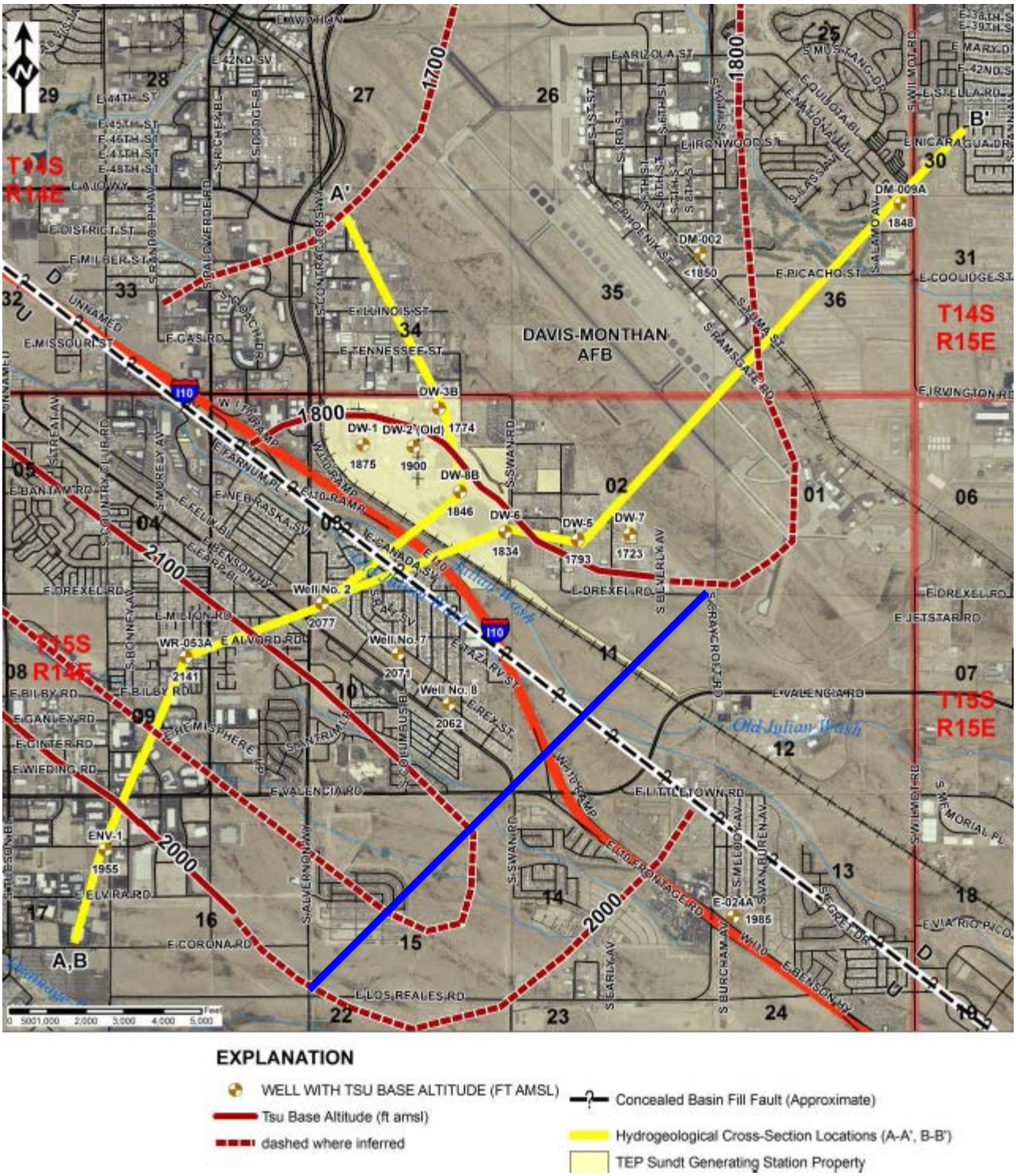


**Figure 1.1** GAP study area. The blue line represents the profile line of our survey area. The yellow lines correspond with the cross sections shown in Figures 1.3 (A-A`) and 1.4 (B-B`), courtesy of BasinWells Associates PLLC.

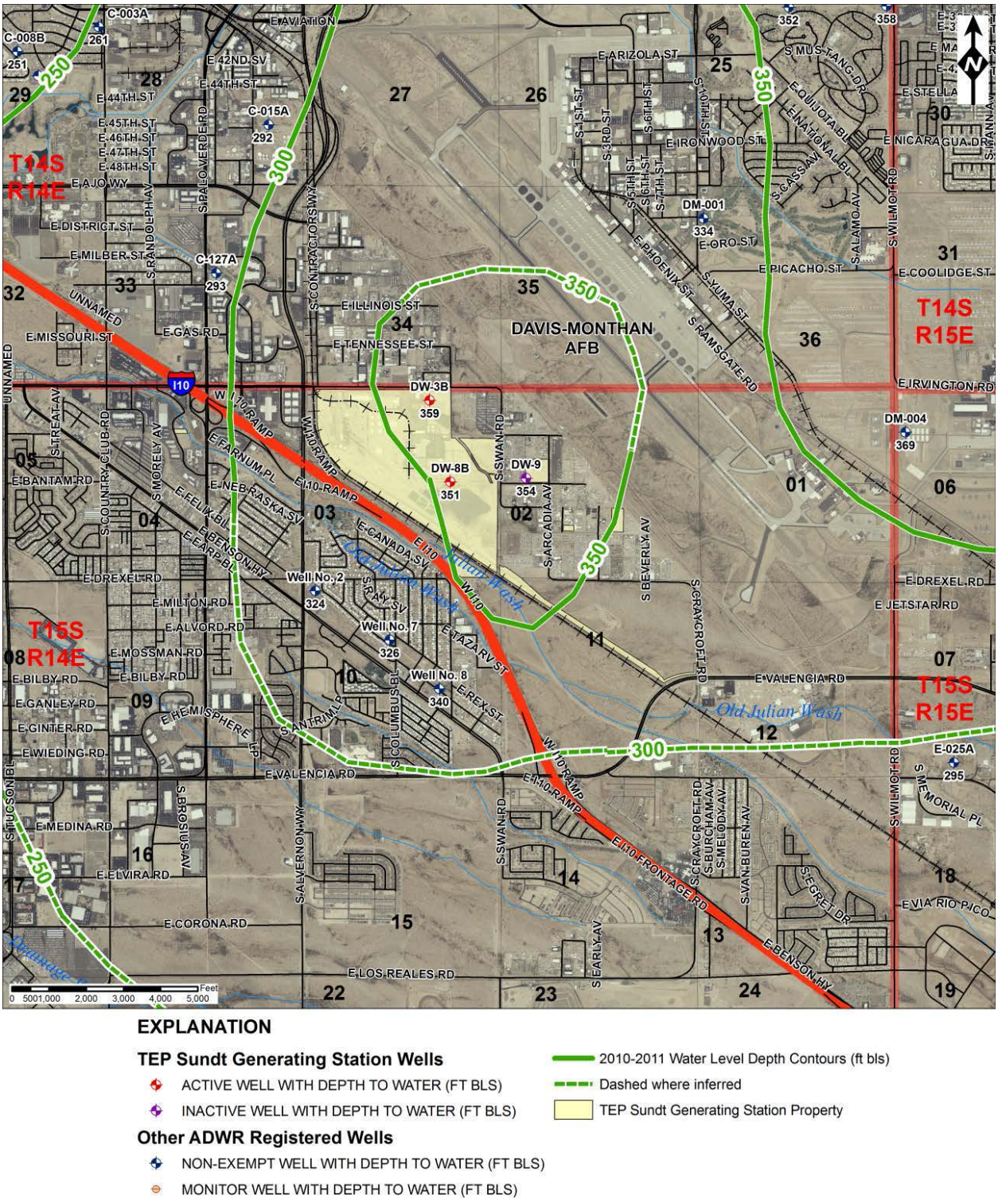


**Figure 1.2** Depth to water of regional aquifer in the survey area.

| SUMMARY OF AQUIFER SYSTEM AND STRATIGRAPHIC UNITS | | | | |
|---|---|---|---|---|
| **AQUIFER** | **STRATIGRAPHIC UNIT** | **YIELD POTENTIAL** | **GENERAL GROUNDWATER QUALITY** | **GENERAL TEMP. OF GROUNDWATER** |
| **PERCHED** | FORT LOWELL FORMATION (QF) | POOR | FAIR | MODERATE |
| **AQUITARD** | CLAY ZONE IN FORT LOWELL FORMATION (QF) | | | |
| **REGIONAL** | UPPER TINAJA BEDS (TSU) | FAIR TO GOOD | GOOD | MODERATE |
| **AQUITARD** | MIDDLE TINAJA BEDS (TSM) | POOR | POOR | MODERATE |
| **DEEP REGIONAL** | LOWER TINAJA BEDS (TSL) | GOOD | UNKNOWN | WARM TO HOT |

**Figure 1.3** Stratification, courtesy of BasinWells Associates PLLC.

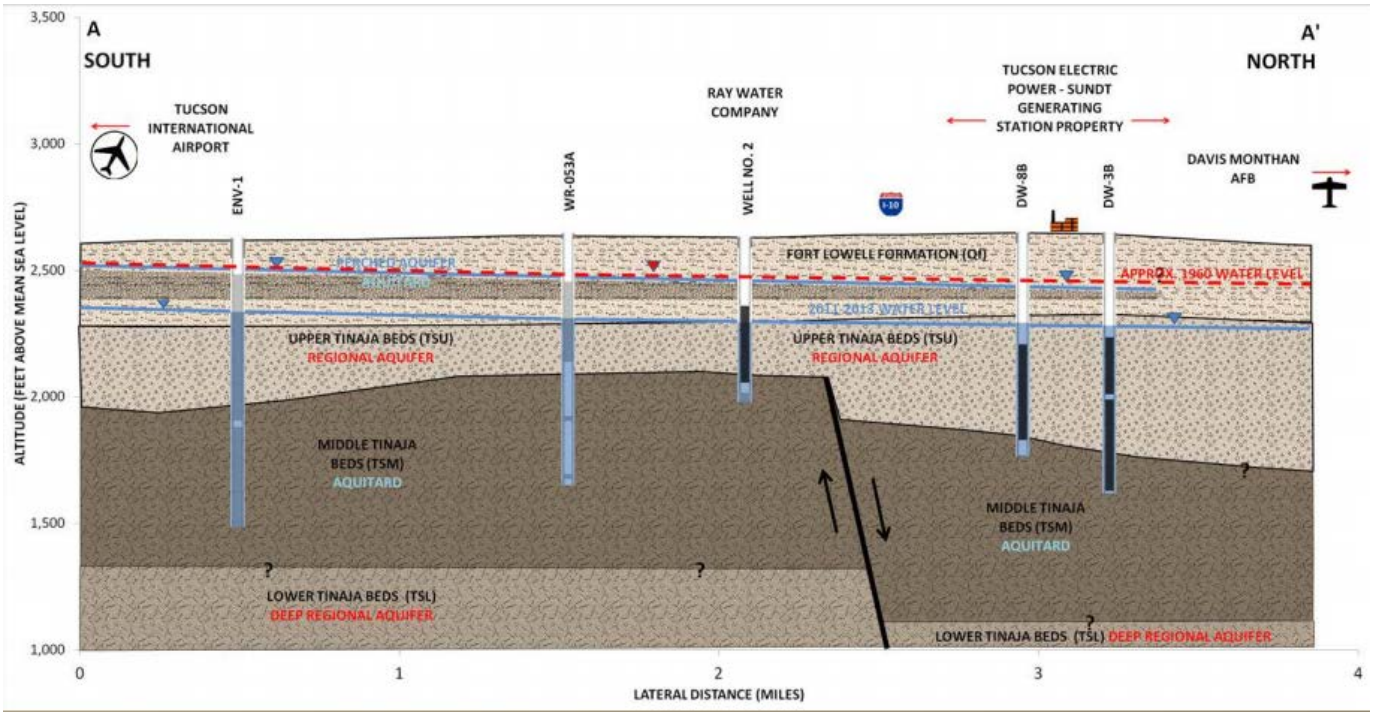


**Figure 1.4** Hydrogeologic cross section A-A`, courtesy of BasinWells Associates PLLC.

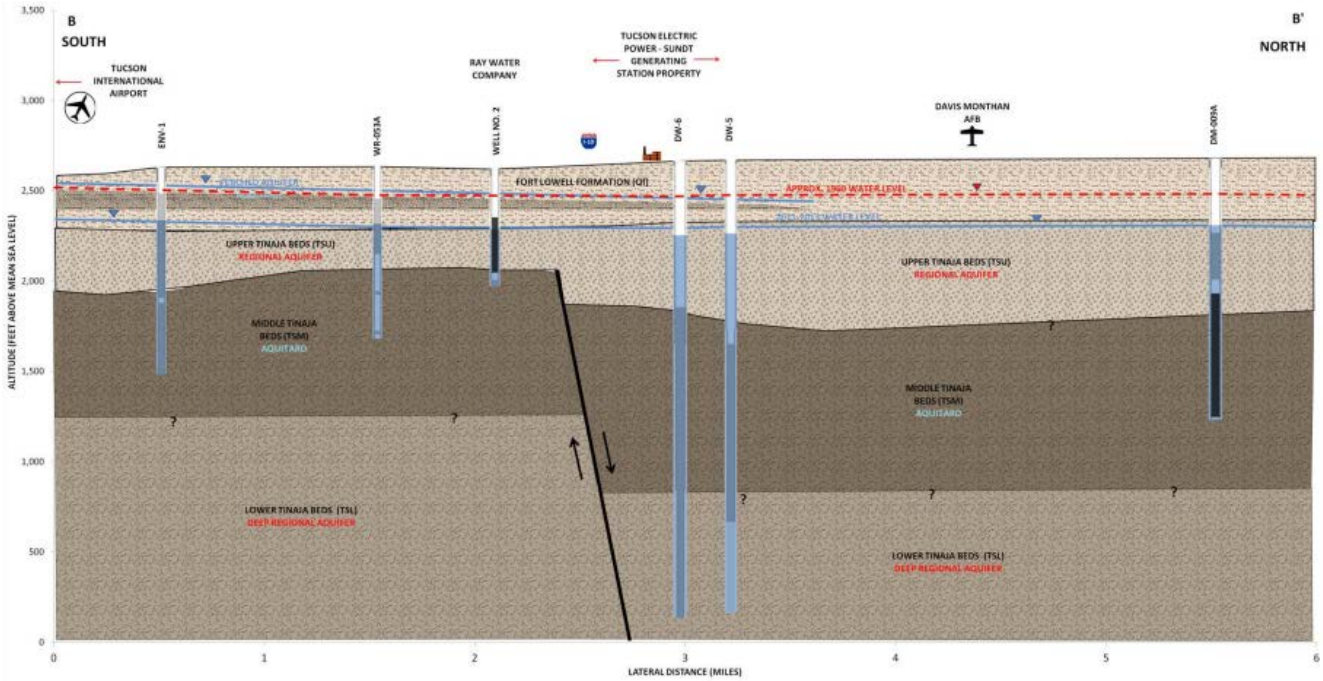


**Figure 1.5** Hydrogeologic cross section B-B`, courtesy of BasinWells Associates PLLC.

# 2. Location maps

## 2.1 Geographic location

The survey area is located near the southern boundary of Tucson, just south of Davis-Monthan Air Force Base, and with UTM coordinates 508,555 to 511,753 East and 3,553,705 to 3,556,895 North. The main profile is from the north-east corner of Section 11 to the south-west corner of Section 15. Near the north-east corner of Section 11, a large solar array obstructs the main profile line. Directly south of the solar array, two rail tracks cross the main profile. Further southwest, Interstate 10 (I-10) bisects the main profile. A housing subdivision is located at the south-west corner of the survey area. Four different geophysics methods (Gravity, Magnetics, Passive Seismic and Transient Electromagnetics) were used in these surveys. The survey locations for the four methods are shown in Figure 2.1.

## 2.2 Gravity Survey Location

A relative gravity meter was employed for the gravity survey. There are 38 Gravity stations in total and 4 profiles. The direction of each profile is approximately NE-SW, 45 degree NE. From a base station in the north-east corner to the last station in the south-west corner, the overall length of the main profile line is 4335 m, with 11 stations. The gravity profile north-west of the main transect is 700 m in length, with 8 stations. The central profile line straddles the main profile and is 920 m long, with 8 stations. South-east of the main profile, another profile was surveyed; it is 1000 m, comprised of 11 stations. The locations of these gravity stations and profiles are shown in Figure 2.2.

## 2.3 Magnetic Survey Location

The magnetic survey was carried out along the main diagonal line of the survey area. A total of 89 stations were measured. When encountering the solar array and subdivision, the magnetic measurements were taken at least 20m away from the solar array fence and 50m away from the subdivision to avoid interference from structures. The whole profile length is 4336m. Figure 2.3 shows the locations of the 89 magnetic stations.

## 2.4 TEM Survey Location

It is necessary to use a large transmitting loop for a TEM survey. The size of each loop used for this study was 200m X 200m. A total of eight loops were recorded, four on the north-east side of I-10, and four on the south-west side of I-10. Due to the location of the solar array, I-10, cacti, and the subdivision, the quantity and locations of these TEM loops were limited (Figure 2.4).

## 2.5 Passive Seismic Survey Location

The passive seismic survey consists of eleven locations throughout the study area (Figure 2.5). These measurements were located primarily along the diagonal line of the survey area in the northeast portion of the study area. Seismic measurements are more dispersed in the southwest portion.

## 2.6 Culture interference

A number of structures limited our ability to follow a line orthogonal to the postulated regional fault. Around the north east corner, there is a solar array. At the south-west side of the solar array, a rail-track cuts through the main profile. High-voltage power lines and the I-10 bisect the main profile line. A subdivision is at the south-west corner of the survey area. The main profile also encountered cacti and bushes.

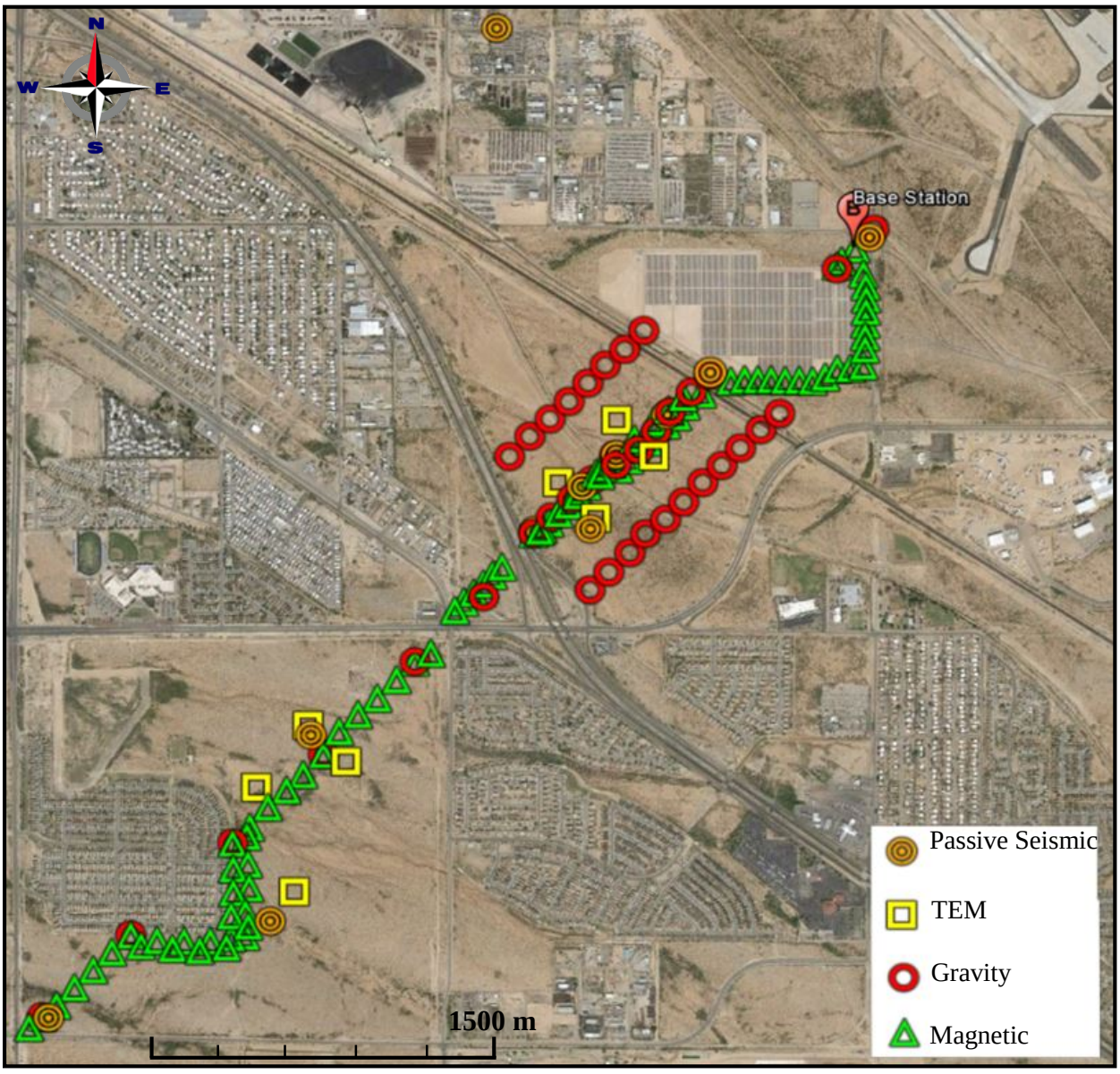


**Fig 2.1.** Google Earth image of the survey area. Four geophysical methods applied along a Northeast-Southwest profile.

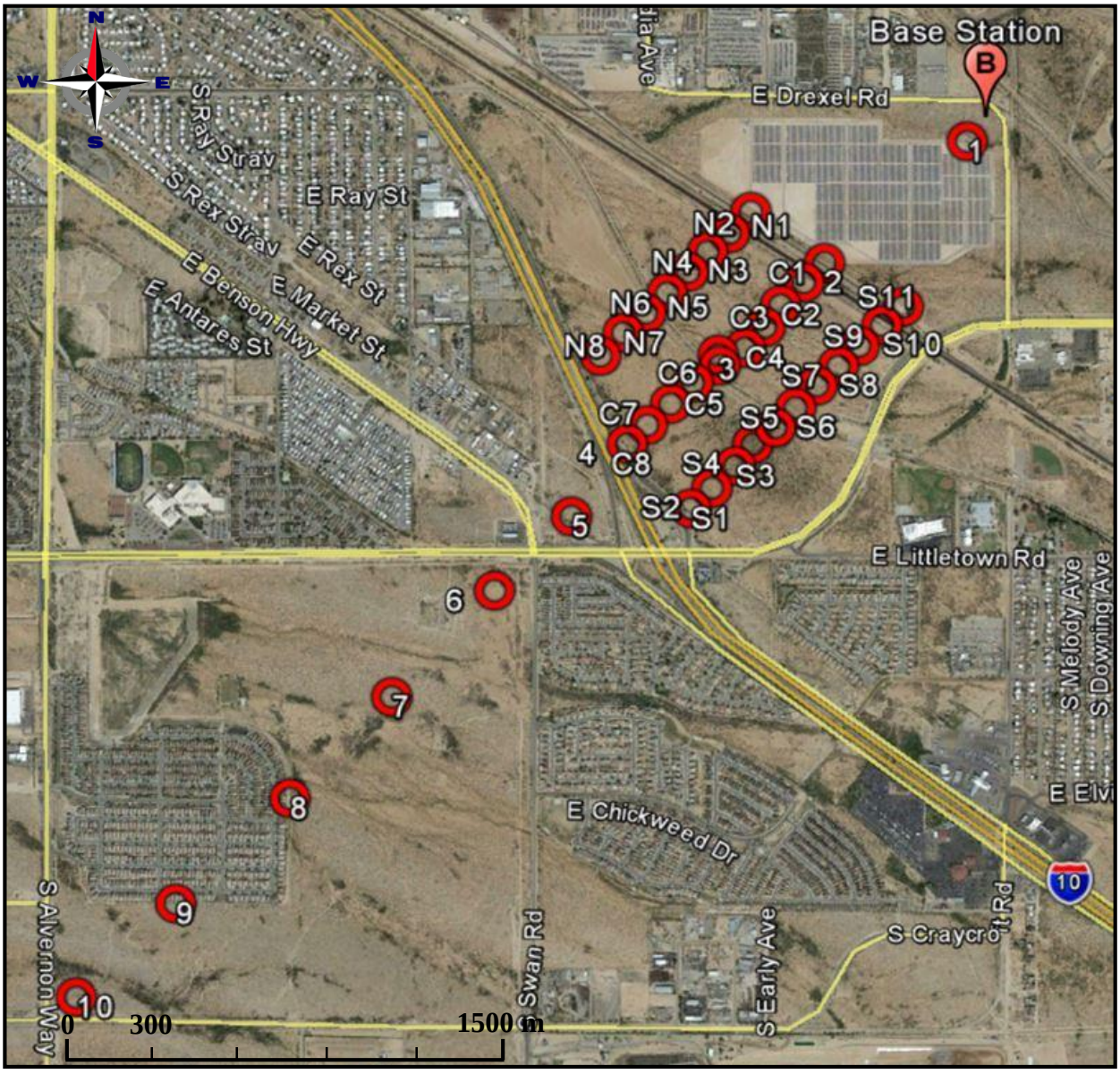


**Figure 2.2** Gravity stations in the survey area; a total of 38. Two additional profiles, lateral from the primary Southwest-Northeast profile, were taken between I-10 and Rail track in order to locate the position of fault.

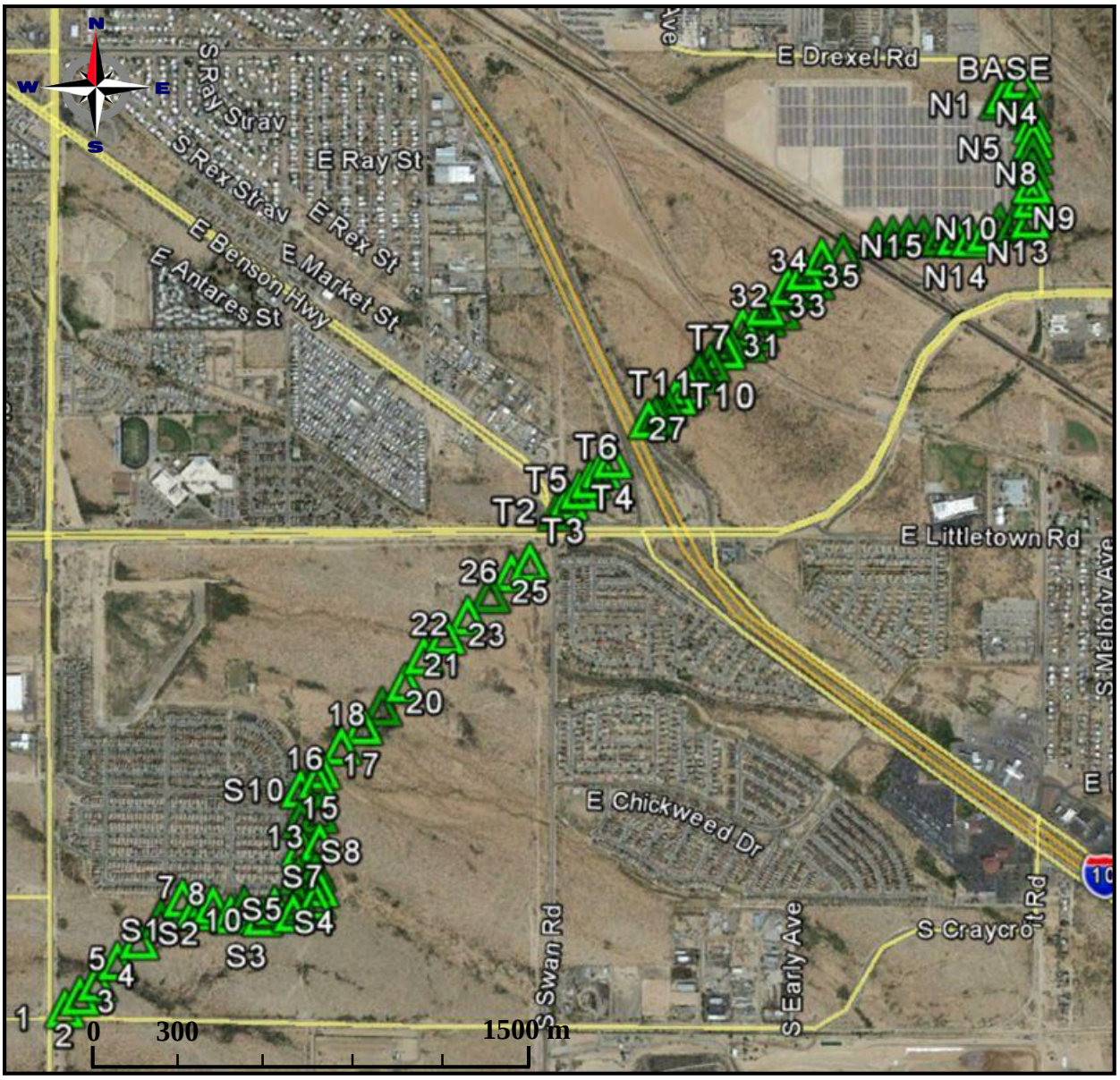


**Figure 2.3.** Magnetic survey stations. The magnetic survey are mainly from the north-east corner to the south-west corner. There are 89 stations in total.

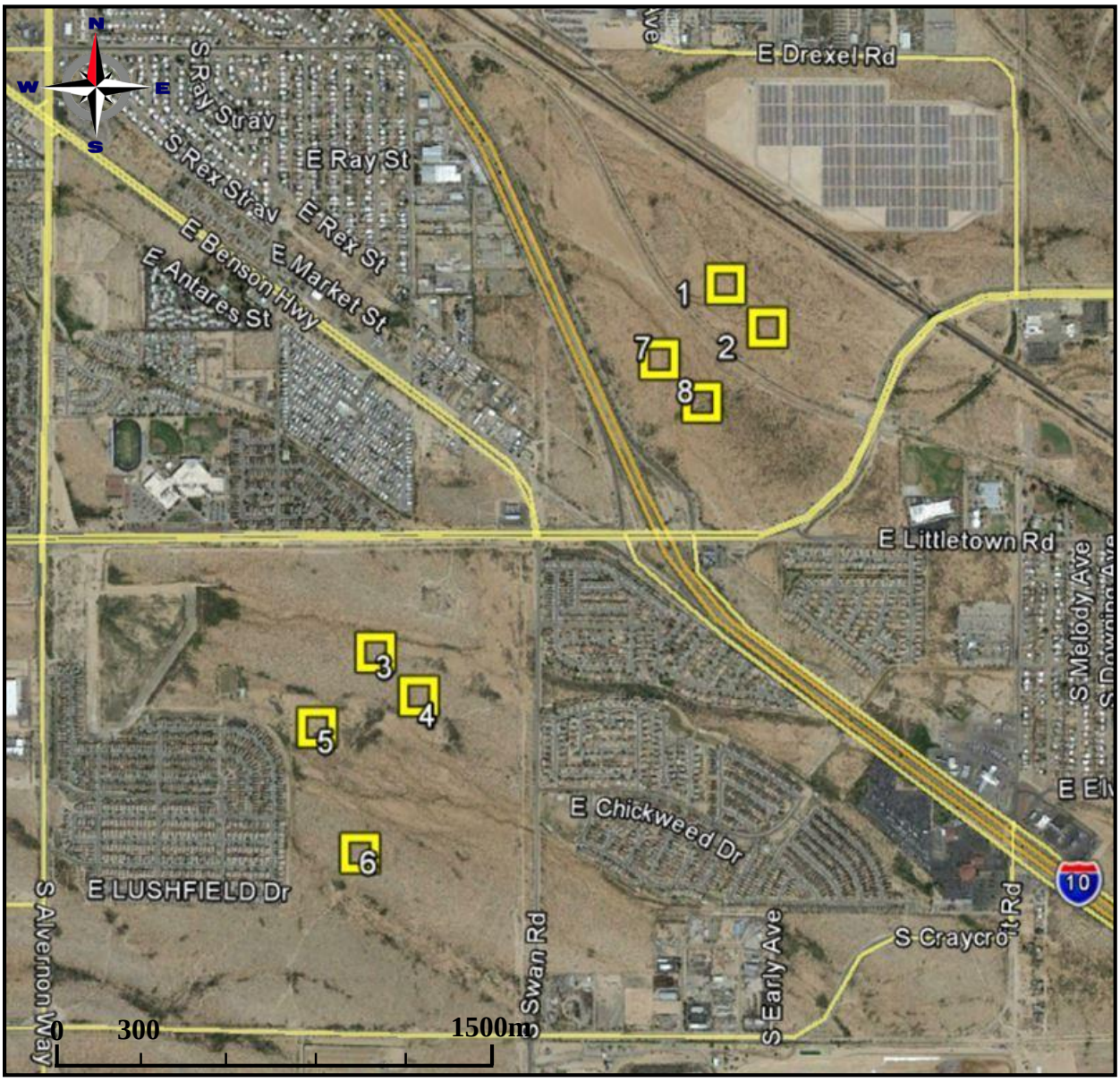


**Figure 2.4.** TEM survey stations. The loop size for TEM survey is 200m × 200m. There are 8 loops in the survey area.

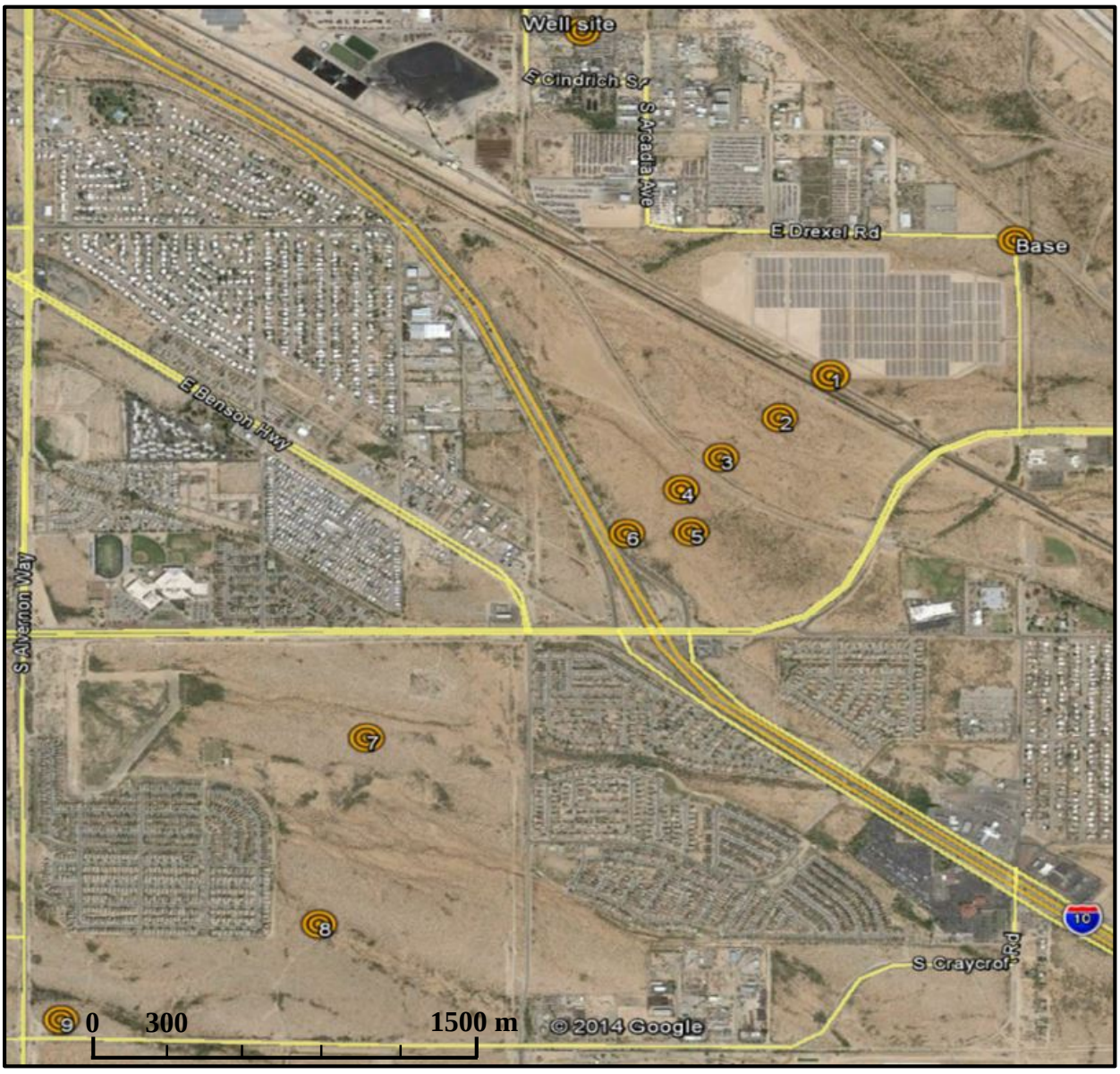


**Figure 2.5.** Passive Seismic survey stations. There are 11 stations in total.

# 3. Magnetic Survey

## 3.1 Introduction

Magnetic surveys are one of the tools that exploration geophysicists use in order to map oil, water, minerals, or other buried structures by measuring the Earth's magnetic-field intensity. The magnetic-field measurements respond to variations in the magnetic susceptibility of the Earth materials. A large number of stations are needed to measure the magnetic field using approximately constant distances between stations over the desired region and must be away from metallic materials and roadways. In addition, a base station was set up to measure the magnetic field simultaneously with the moving station. The base station is used to remove temporal variations in the Earth's magnetic field. A profile of the magnetic field can be generated, which can illustrate the location of the anomalous body (U.S. Army Corps of Engineers, 1995, 6-1).

## 3.2 Dates and Location

The magnetic field survey took place on February 8, 9, and 22, and April 6 of 2014. The magnetic field data were collected in the south part of Tucson, along a diagonal line that crosses Interstate 10 from northeast to southwest. A total of 89 stations were recorded along the profile line, which encountered a solar array (northeast of I-10), and a subdivision (southwest of I-10) that required shifts in the line. Measurements were not possible near the railroad and Interstate 10. Figure 3.1 shows the locations at which magnetic field measurements were taken.

## 3.3 Instrument and Field procedures.

The magnetometers used for this survey were the GEM Systems GSM-19 Overhauser Magnetometer, the EDA OMNI IV Magnetometer, and the EDA OMNI Plus Magnetometer. We used Garmin 530HX GPS receivers (Garmin International Inc. 2007) to determine the locations of the stations. On the first weekend, a base station was set up at the beginning of the line at the southwest corner between Craycroft road and Drexel road. We started to take measurements every 50m along the main profile. During that first weekend (Feb 7th-8th) measurements around the solar array were skipped because the solar array cuts through the main profile line. The data

collected along the main profile were linked to the base station every time they were taken. Both of the measurements, base station and measurements along the main profile, were taken within a difference of a few seconds using two different sets of magnetometers. During the second weekend (Feb, 22nd), the area around the solar array was revisited and data offset from the fence of the solar array were collected. Also, a big portion of the profile was revisited as well because the data along the line could not be referenced to the base station. On the third weekend (April 6th), surveys were needed between I-10 and Valencia road due to a gap in data in that area. That area is essential because it is very close to the hypothesized fault location. To mitigate the effect of metallic objects creating false anomalies, we have experimentally determined the change in magnetic field as a function of distance away front the solar array fence on February 23, 2014 (Figure 3.2). Results indicate that the fence had no effect on the magnetic field at a point that is 20m away from it. Therefore, all of the measurements along the profile line reported are at least 20 m away from metal objects like fences and railroads.

### 3.4 Data Processing

The magnetic field data and GPS coordinates are recorded and imported to Microsoft Excel for further processing.

The effect of ambient magnetic drift is corrected by subtraction of a correction factor which is calculated by subtracting the base station reading when a profile reading is collected to that measured at a reference time. Therefore, the corrected magnetic field is given by:

$$y_{corrected}(x) = y_{measured}(x,t) - (y_{base,t}(t) - y_{base,ref})$$

The measurements were also projected to a profile line where the end points are the base station and the northeast corner of the intersection of S. Alvernon Way and Los Reales Road. The coordinates of the measurement locations are recorded using the UTM system. The projection is done by the following transformation equation:

$$x_m = \frac{b(bx_p - ay_p) - ac}{a^2 + b^2} \qquad y_m = \frac{b(-bx_p - ay_p) - bc}{a^2 + b^2}$$

where ax+by+c = 0 is the equation representing a straight line which goes through (x1,y1) and (x2,y2); (xp,yp) is the point where a measurement is taken; and (xm,ym) is the projected point on the profile line.

Figure 3.3 shows the corrected and projected magnetic field profile. Each line represents data collected on a particular day. A table is also included in Appendix A, which lists the raw and corrected data.

### 3.5 Interpretation

From the results in Figure 3.4, we do not observe any significant anomalies that can potentially be attributed to a fault. However, a regional anomaly was identified as the magnetic field is found to decrease from NE to SW. There are also several short wavelength, small amplitude fluctuations. Those are probably not attributed to faults. They are more likely to be associated with anthropogenic features such as metal trash. The sampling spacing is between 50-100m so that the spatial resolution is high enough to detect any anomalies of interest. Also, the measured data used simultaneous measurements at the base station, which were used to correct for any shift in the ambient magnetic field. In summary, the magnetic field data do not show evidence of any fault in the study area.

## 3.6 Reference

Garmin International Inc. 2007. Owner's Manual for Rino® 520-530HCx 2-way radio and GPS.

U.S. Army Corps of Engineers. 1995. Geophysical Exploration for Engineering and Environmental Investigations. USACE EM 1110-1-1802

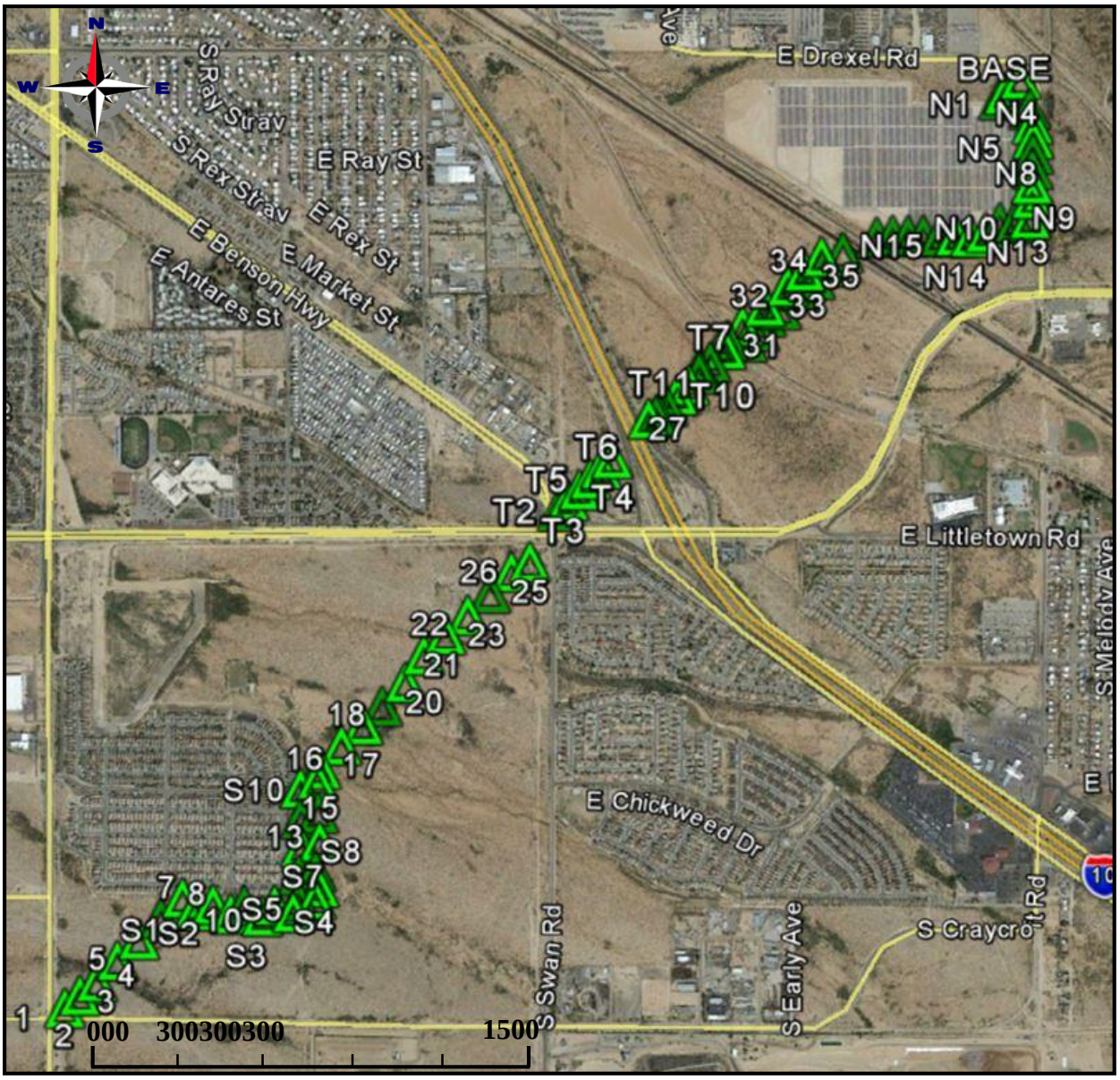


**Figure 3.1** Location map for magnetic field measurements.

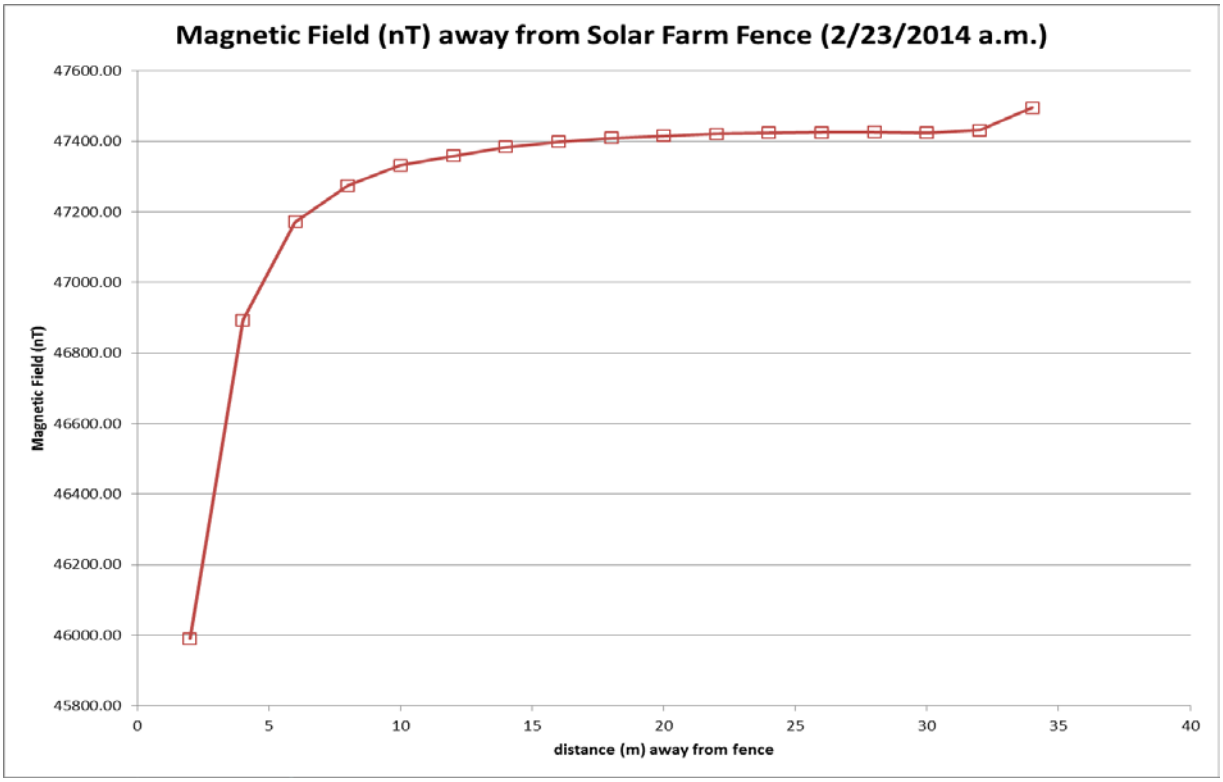


**Figure 3.2** Magnetic field as a function of distance away from the fence of the solar array.

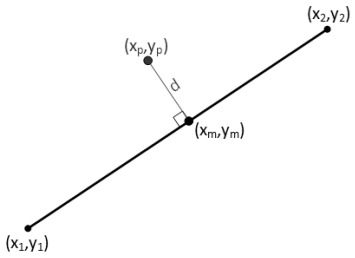


**Figure 3.3** Magnetic profile line along transect.

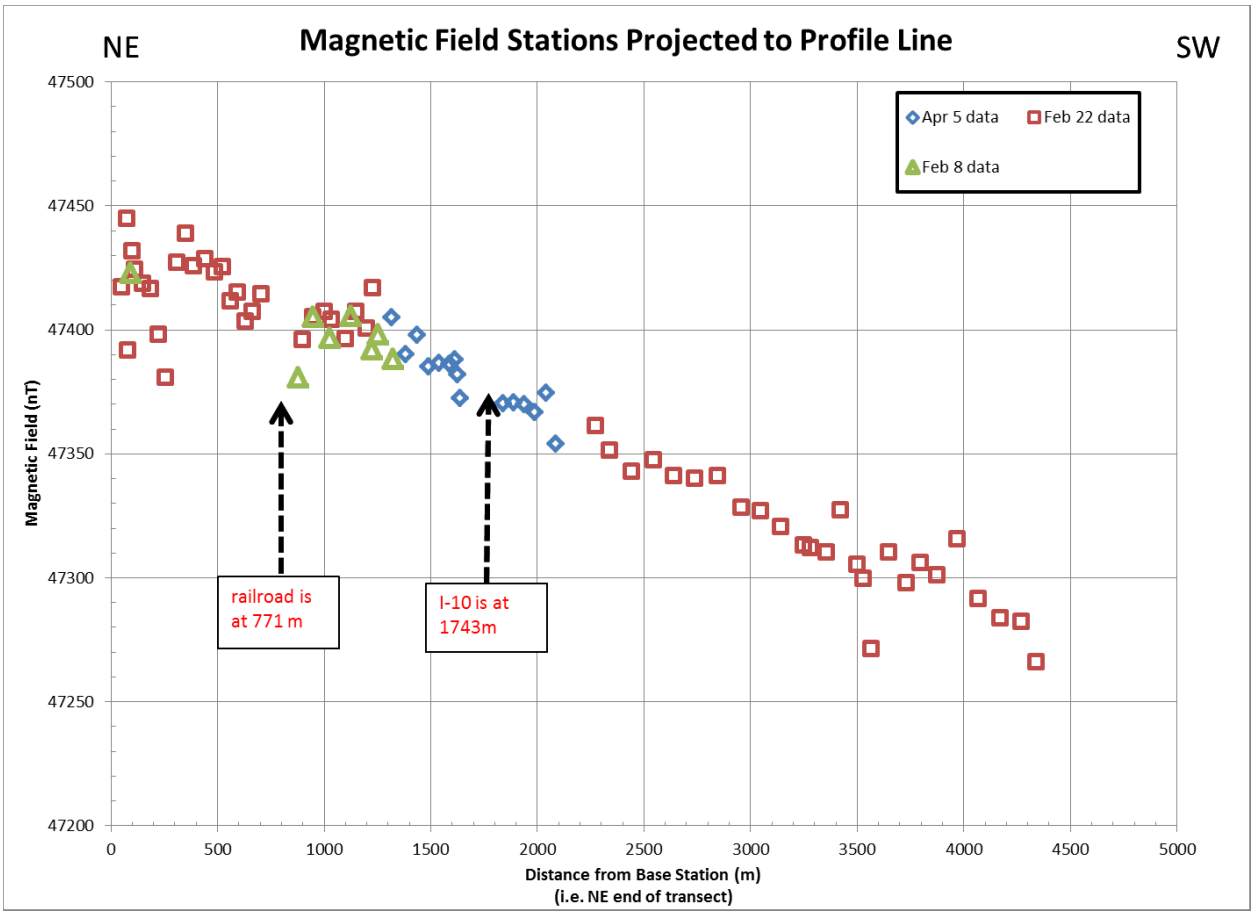


**Figure 3.4** Magnetic profile line along transect.

# 4. Gravity Survey

## 4.1 Introduction, Instrumentation and Data Collection

A gravity survey was conducted to investigate the possibility of gravity anomalies in the study area that may be indicative of subsurface geological features. The gravity meter used in this survey was a LaCoste Romberg model G-575. A designated pair of operators worked in tandem for the duration of the survey. After a station was chosen and the meter was leveled, operator A took and recorded a measurement, immediately followed by operator B, always in the same order. The time was recorded along with GPS coordinates for each station. The first recording station was designated the base station; repeat measurements were taken at the base station every two hours to account for instrument drift.

## 4.2 Locations

An initial survey was made along the main NE-SW transect line of the study area. The stations were located approximately 400m-600m apart depending on local obstacles, and spanned the entire length of the study area diagonal. After analysis of this initial coarse survey, a focus area was chosen between the solar array and the Interstate-10 (I-10). A second survey was conducted there, consisting of three parallel survey lines: one along the main diagonal, and one each 300m NW and SE of the central line (Figure 4.1). Stations were selected 100m apart down all three lines. Station locations along the offset lines were projected orthogonally onto the main transect for data analysis.

## 4.3 Data Processing

The gravity values recorded by each operator were averaged to produce a single measurement value at each station. See Figure 4.2 for a complete table of raw measurements. This combined value was then corrected for instrument drift, latitude, free-air and Bouguer anomalies (Figure 4.3). Correction calculations were performed as per “An Introduction to Geophysical Exploration”, Keary, Brooks, and Hill, 3$^{rd}$ ed, 6.8.3 (drift corr.) and 6.8.6 (free air/Bouguer). These relative gravity anomaly data were then converted to absolute gravity using a tie-in point in the Harshbarger/Mines building on the University of Arizona campus (1133 E North Campus Dr, Tucson AZ 85721) where absolute gravity is known.

## 4.4 Results

The full length, coarse transect shows a regional gravitational gradient, steadily decreasing from NE to SW, with a large anomaly apparent around 1500m from the base station, between the railroad tracks and the I-10 (Figure 4.4). The central high-resolution line along the main transect appears to repeat this anomaly; however, the offset lines show no repetition of such an anomaly (Figure 4.5). Rather, they show very little change in value, indicating the anomaly along the main transect is a local one, and not consistent with a NW-SE trending fault contact.

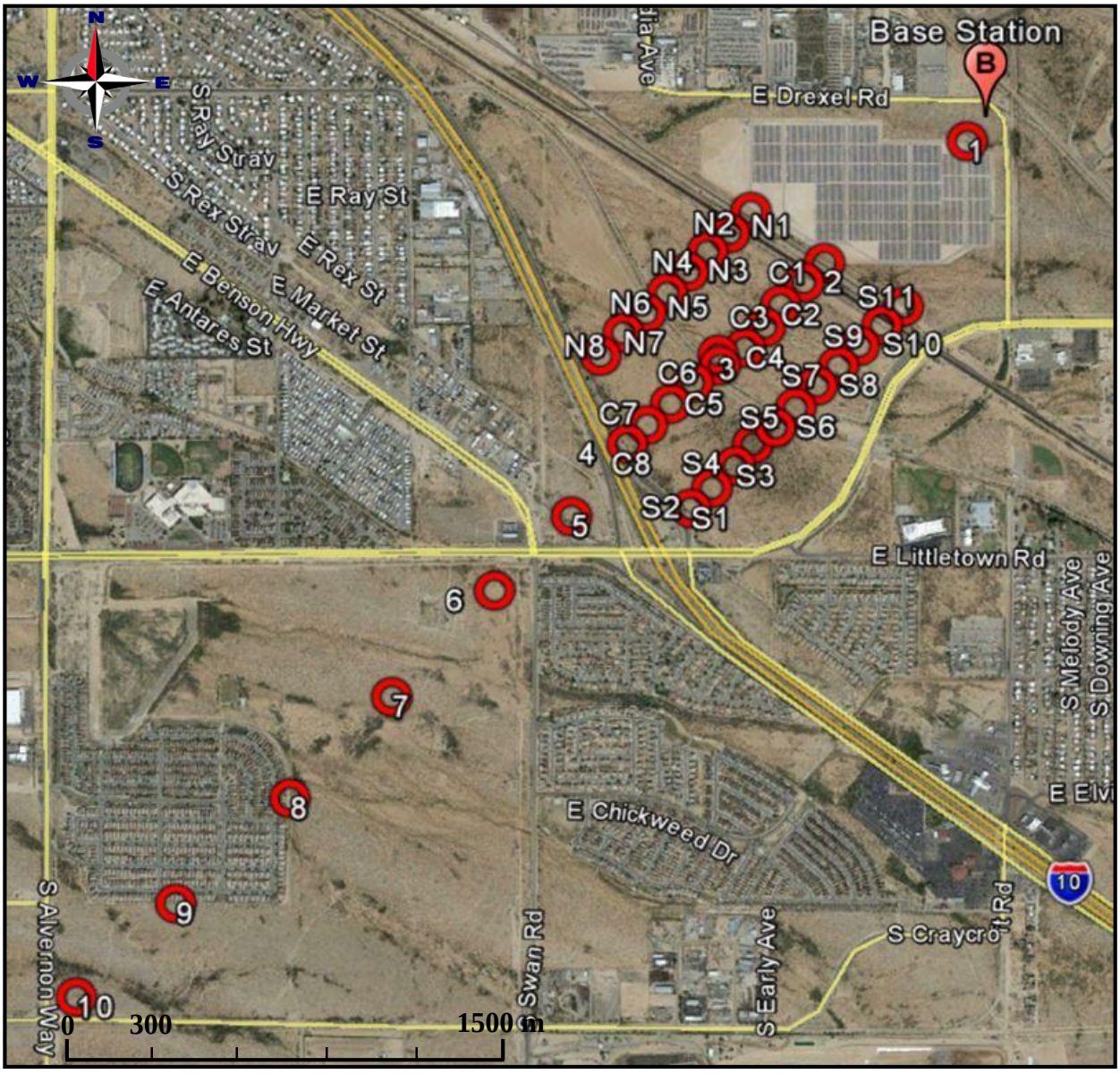


**Figure 4.1** Gravity stations in the survey area; a total of 38. Two additional profiles, lateral from the primary Southwest-Northeast profile, were taken between I-10 and Rail track in order to locate the position of fault.

## Field Measurements

| Station | Gravity Meter Reading | Gravity value (mGal) | GPS | | Elevation (ft) | Projected Distance | Time |
|---|---|---|---|---|---|---|---|
| Base | 2793.94 | 2864.882562 | 511709 | 3556853 | 2700.6 | | 10:05 AM |
| Base | 2793.65 | 2864.584836 | | | | | 10:08 AM |
| CL-01 | 2794.44 | 2865.395882 | 511100 | 3556273 | 2680.36 | 840.7118185 | 10:21 AM |
| CL-01 | 2794.25 | 2865.20082 | | | | | 10:23 AM |
| CL-02 | 2794.28 | 2865.231619 | 511021 | 3556194 | 2678.8 | 952.4345101 | 10:29 AM |
| CL-02 | 2794.06 | 2865.005758 | | | | | 10:30 AM |
| CL-03 | 2794.01 | 2864.954426 | 510969 | 3556117 | 2677.22 | 1043.682855 | 10:35 AM |
| CL-03 | 2793.94 | 2864.882562 | | | | | 10:37 AM |
| CL-04 | 2794.05 | 2864.995492 | 510902 | 3556044 | 2675.12 | 1142.685257 | 10:41 AM |
| CL-04 | 2793.65 | 2864.584836 | | | | | 10:42 AM |
| CL-05 | 2794.32 | 2865.272685 | 510817 | 3555983 | 2672.96 | 1245.892233 | 10:47 AM |
| CL-05 | 2794.07 | 2865.016025 | | | | | 10:48 AM |
| CL-06 | 2794.32 | 2865.272685 | 510726 | 3555923 | 2674.12 | 1352.625856 | 10:54 AM |
| CL-06 | 2793.99 | 2864.933894 | | | | | 10:56 AM |
| CL-07 | 2794.22 | 2865.170021 | 510651 | 3555849 | 2675.85 | 1457.983328 | 11:02 AM |
| CL-07 | 2793.96 | 2864.903094 | | | | | 11:04 AM |
| CL-08 | 2794.21 | 2865.159754 | 510572 | 3555775 | 2678.51 | 1566.164148 | 11:08 AM |
| CL-08 | 2793.94 | 2864.882562 | | | | | 11:09 AM |
| SL-01 | 2793 | 2863.91752 | 510719 | 3555485 | 2682.12 | 1667.83466 | 11:17 AM |
| SL-01 | 2792.73 | 2863.640327 | | | | | 11:18 AM |
| SL-02 | 2793 | 2863.91752 | 510790 | 3555556 | 2681.34 | 1567.425659 | 11:23 AM |
| SL-02 | 2792.89 | 2863.80459 | | | | | 11:25 AM |
| SL-03 | 2793.11 | 2864.03045 | 510869 | 3555633 | 2681.25 | 1457.119716 | 11:30 AM |
| SL-03 | 2792.86 | 2863.77379 | | | | | 11:32 AM |
| SL-04 | 2793.2 | 2864.122848 | 510928 | 3555709 | 2681.31 | 1361.638887 | 11:37 AM |
| SL-04 | 2793.04 | 2863.958586 | | | | | 11:39 AM |
| SL-05 | 2793.08 | 2863.999651 | 511004 | 3555767 | 2682.79 | 1266.909567 | 11:44 AM |
| SL-05 | 2792.9 | 2863.814856 | | | | | 11:46 AM |
| SL-06 | 2793.15 | 2864.071516 | 511072 | 3555836 | 2682.26 | 1170.034825 | 11:50 AM |
| SL-06 | 2792.89 | 2863.80459 | | | | | 11:52 AM |
| SL-07 | 2793.14 | 2864.06125 | 511144 | 3555913 | 2682.64 | 1064.669741 | 11:57 AM |
| SL-07 | 2792.93 | 2863.845655 | | | | | 11:58 AM |
| SL-08 | 2793.25 | 2864.17418 | 511216 | 3555981 | 2683.14 | 965.6800254 | 12:02 PM |
| SL-08 | 2793.02 | 2863.938053 | | | | | 12:04 PM |
| SL-09 | 2793.19 | 2864.112582 | 511286 | 3556051 | 2684.54 | 866.6852354 | 12:07 PM |
| SL-09 | 2792.85 | 2863.763524 | | | | | 12:09 PM |
| SL-10 | 2793.24 | 2864.163914 | 511363 | 3556124 | 2685.93 | 760.6244636 | 12:13 PM |
| SL-10 | 2792.98 | 2863.896987 | | | | | 12:14 PM |
| SL-11 | 2793.29 | 2864.215246 | 511434 | 3556188 | 2689.08 | 665.1740824 | 12:18 PM |
| SL-11 | 2793.13 | 2864.050983 | | | | | 12:20 PM |
| Base | 2793.94 | 2864.882562 | | | | | 12:29 PM |
| Base | 2793.68 | 2864.615635 | | | | | 12:31 PM |
| NL-01 | 2795.49 | 2866.473854 | 510921 | 3556519 | 2672.19 | 792.7965594 | 12:59 PM |
| NL-01 | 2795.11 | 2866.08373 | | | | | 1:00 PM |
| NL-02 | 2795.47 | 2866.453321 | 510849 | 3556444 | 2671.4 | 896.7448949 | 1:05 PM |
| NL-02 | 2795.32 | 2866.299325 | | | | | 1:07 PM |
| NL-03 | 2795.41 | 2866.391722 | 510775 | 3556381 | 2670.84 | 993.6044127 | 1:12 PM |
| NL-03 | 2795.17 | 2866.145329 | | | | | 1:13 PM |
| NL-04 | 2795.34 | 2866.319858 | 510710 | 3556309 | 2671.88 | 1090.486766 | 1:17 PM |
| NL-04 | 2795.11 | 2866.08373 | | | | | 1:19 PM |
| NL-05 | 2795.28 | 2866.258259 | 510639 | 3556236 | 2672.14 | 1192.312516 | 1:23 PM |
| NL-05 | 2795.14 | 2866.11453 | | | | | 1:25 PM |
| NL-06 | 2795.34 | 2866.319858 | 510567 | 3556166 | 2669.19 | 1292.71898 | 1:30 PM |
| NL-06 | 2795.14 | 2866.11453 | | | | | 1:32 PM |
| NL-07 | 2795.33 | 2866.309591 | 510491 | 3556097 | 2668.79 | 1395.240418 | 1:36 PM |
| NL-07 | 2795.05 | 2866.022132 | | | | | 1:37 PM |
| NL-08 | 2795.15 | 2866.124796 | 510414 | 3556016 | 2669.6 | 1506.968184 | 1:42 PM |
| NL-08 | 2795.01 | 2865.981066 | | | | | 1:43 PM |
| Base | 2793.87 | 2864.810697 | | | | | 2:14 PM |
| Base | 2793.61 | 2864.54377 | | | | | 2:16 PM |

**Figure 4.2** Raw field data with GPS and time information.

## Data Processing

| Gravity correction | | | | Shift Correction | | | | | | Simple Bouguer Gravity Anomaly | | |
|---|---|---|---|---|---|---|---|---|---|---|---|---|
| Relative elevation | Free Air Correction | Bouguer Correction | Gravity Meter shift | Time pass | Shift correction | Base | Station (m) | G Value | Latitude | Theoretical Gravity (mGal) | Relative ThG | Simple Bouguer Anomaly (mGal) |
| 0 | 0 | 0 | 0 | 0:00:00 | 0 | CL-01 | 841 | 2864.083602 | 32.14283 | 979495.9517 | 0 | 2864.508975 |
| | | | | 0:00:00 | | CL-02 | 952.69355 | 2863.809684 | 32.14211 | 979495.8931 | -0.483973802 | 2864.293658 |
| -20.24 | -1.9037744 | -0.690641424 | | 0:16:00 | 0.001615 | CL-03 | 1043.69344 | 2863.514035 | 32.14142 | 979495.8369 | -0.540133093 | 2864.054168 |
| | | | | 0:15:00 | | CL-04 | 1142.68543 | 2863.259298 | 32.14076 | 979495.7832 | -0.593850061 | 2863.853148 |
| -21.8 | -2.050508 | -0.74387268 | | 0:24:00 | 0.002369 | CL-05 | 1246.01926 | 2863.483377 | 32.14021 | 979495.7385 | -0.638613742 | 2864.121991 |
| | | | | 0:22:00 | | CL-06 | 1353.21432 | 2863.510978 | 32.13968 | 979495.6953 | -0.681749258 | 2864.192727 |
| -23.38 | -2.1991228 | -0.797786388 | | 0:30:00 | 0.003123 | CL-07 | 1458.55408 | 2863.547076 | 32.13901 | 979495.6408 | -0.736278506 | 2864.283355 |
| | | | | 0:29:00 | | CL-08 | 1566.79705 | 2863.690572 | 32.13833 | 979495.5855 | -0.791620991 | 2864.482193 |
| -25.48 | -2.3966488 | -0.869443848 | | 0:36:00 | 0.003661 | SL-01 | 1002.71332 | 2862.663742 | 32.13572 | 979495.3731 | -1.004032543 | 2863.667775 |
| | | | | 0:34:00 | | SL-02 | 902.308151 | 2862.698368 | 32.13636 | 979495.4251 | -0.951947822 | 2863.650316 |
| -27.64 | -2.5998184 | -0.943148664 | | 0:42:00 | 0.004308 | SL-03 | 791.991162 | 2862.733286 | 32.13705 | 979495.4813 | -0.895793348 | 2863.629079 |
| | | | | 0:40:00 | | SL-04 | 696.761796 | 2862.874725 | 32.13774 | 979495.5374 | -0.839638218 | 2863.714363 |
| -26.48 | -2.4907088 | -0.903566448 | | 0:49:00 | 0.005169 | SL-05 | 601.781522 | 2862.829215 | 32.13826 | 979495.5798 | -0.797317975 | 2863.626533 |
| | | | | 0:48:00 | | SL-06 | 504.923757 | 2862.827601 | 32.13889 | 979495.631 | -0.746044874 | 2863.573646 |
| -24.75 | -2.327985 | -0.84455435 | | 0:57:00 | 0.006031 | SL-07 | 399.656102 | 2862.865131 | 32.13958 | 979495.6872 | -0.689887991 | 2863.555019 |
| | | | | 0:56:00 | | SL-08 | 300.621024 | 2862.997117 | 32.14019 | 979495.7368 | -0.640241504 | 2863.637359 |
| -22.09 | -2.0777854 | -0.753768234 | | 1:03:00 | 0.006569 | SL-09 | 201.675482 | 2862.962428 | 32.14082 | 979495.7881 | -0.588966725 | 2863.551394 |
| | | | | 1:01:00 | | SL-10 | 95.58765561 | 2863.1376 | 32.14148 | 979495.8418 | -0.535249702 | 2863.67285 |
| -18.48 | -1.7382288 | -0.630585648 | | 1:12:00 | 0.007538 | SL-11 | 0 | 2863.428421 | 32.14206 | 979495.889 | -0.488043337 | 2863.916464 |
| | | | | 1:10:00 | | NL-01 | 0 | 2864.600414 | 32.14505 | 979496.1324 | -0.244679026 | 2864.845093 |
| -19.26 | -1.8115956 | -0.657201276 | | 1:18:00 | 0.008292 | NL-02 | 103.966341 | 2864.65607 | 32.14437 | 979496.0825 | -0.294573784 | 2864.950644 |
| | | | | 1:17:00 | | NL-03 | 200.897984 | 2864.520037 | 32.1438 | 979496.0307 | -0.346421459 | 2864.866458 |
| -19.35 | -1.820061 | -0.66027231 | | 1:25:00 | 0.009046 | NL-04 | 297.692795 | 2864.520284 | 32.14315 | 979495.9778 | -0.399326672 | 2864.919611 |
| | | | | 1:24:00 | | NL-05 | 399.515957 | 2864.525455 | 32.1425 | 979495.9249 | -0.452231303 | 2864.977686 |
| -19.29 | -1.8144174 | -0.658224954 | | 1:32:00 | 0.0098 | NL-06 | 499.924994 | 2864.385256 | 32.14186 | 979495.8728 | -0.504321447 | 2864.889578 |
| | | | | 1:31:00 | | NL-07 | 602.481535 | 2864.314447 | 32.14125 | 979495.8231 | -0.553969339 | 2864.868416 |
| -17.81 | -1.6752086 | -0.607723506 | | 1:39:00 | 0.010554 | NL-08 | 714.18345 | 2864.255052 | 32.14051 | 979495.7629 | -0.61419724 | 2864.86925 |
| | | | | 1:38:00 | | | | | | | | |
| -18.34 | -1.7250604 | -0.625808484 | | 1:45:00 | 0.0112 | | | | | | | |
| | | | | 1:44:00 | | | | | | | | |
| -17.96 | -1.6893176 | -0.612841896 | | 1:52:00 | 0.011846 | | | | | | | |
| | | | | 1:50:00 | | | | | | | | |
| -17.46 | -1.6422876 | -0.5957805 96 | | 1:57:00 | 0.012492 | | | | | | | |
| | | | | 1:56:00 | | | | | | | | |
| -16.06 | -1.5106036 | -0.548008956 | | 2:02:00 | 0.01303 | | | | | | | |
| | | | | 2:01:00 | | | | | | | | |
| -14.67 | -1.3798602 | -0.500578542 | | 2:08:00 | 0.013569 | | | | | | | |
| | | | | 2:06:00 | | | | | | | | |
| -11.52 | -1.0835712 | -0.393092352 | | 2:13:00 | 0.014215 | | | | | | | |
| | | | | 2:12:00 | | | | | | | | |
| | | | 0 | 2:24:00 | 0 | | | | | | | |
| | | | 0.0307992 | 2:23:00 | | | | | | | | |
| -28.41 | -2.6722446 | -0.969423066 | | 2:54:00 | -0.024444 | | | | | | | |
| | | | | 2:52:00 | | | | | | | | |
| -29.2 | -2.746552 | -0.99637992 | | 3:00:00 | -0.029919 | | | | | | | |
| | | | | 2:59:00 | | | | | | | | |
| -29.76 | -2.7992256 | -1.015488576 | | 3:07:00 | -0.035248 | | | | | | | |
| | | | | 3:05:00 | | | | | | | | |
| -28.72 | -2.7014032 | -0.980001072 | | 3:12:00 | -0.039892 | | | | | | | |
| | | | | 3:11:00 | | | | | | | | |
| -28.46 | -2.6769476 | -0.971129196 | | 3:18:00 | -0.044879 | | | | | | | |
| | | | | 3:17:00 | | | | | | | | |
| -31.41 | -2.9544246 | -1.071790866 | | 3:25:00 | -0.050696 | | | | | | | |
| | | | | 3:24:00 | | | | | | | | |
| -31.81 | -2.9920486 | -1.085439906 | | 3:31:00 | -0.055194 | | | | | | | |
| | | | | 3:29:00 | | | | | | | | |
| -31 | -2.91586 | -1.0578006 | | 3:37:00 | -0.060181 | | | | | | | |
| | | | -0.0718648 | 3:35:00 | | | | | | | | |
| | | | -0.0718648 | 4:09:00 | -0.087264 | | | | | | | |
| | | | | 4:08:00 | | | | | | | | |

**Figure 4.3** Data processing spreadsheat.

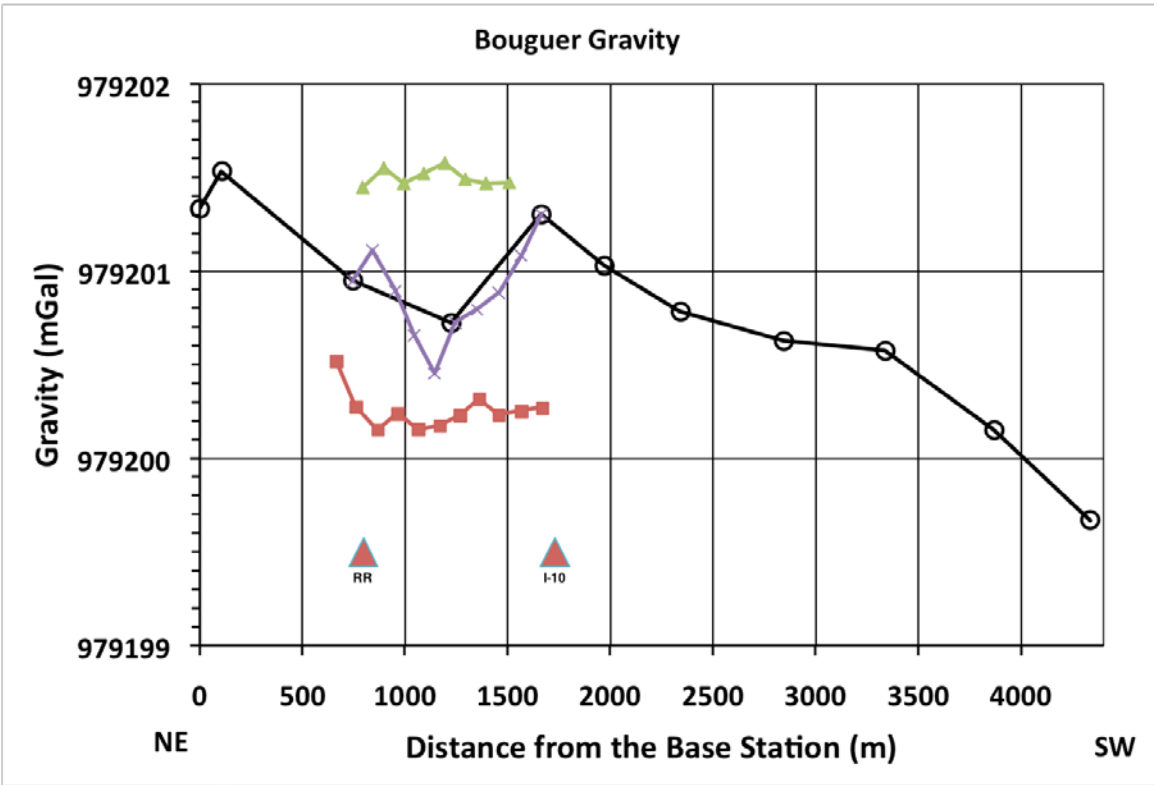


**Figure 4.4** All data plotted as absolute gravity values. Railroad and I-10 marked.

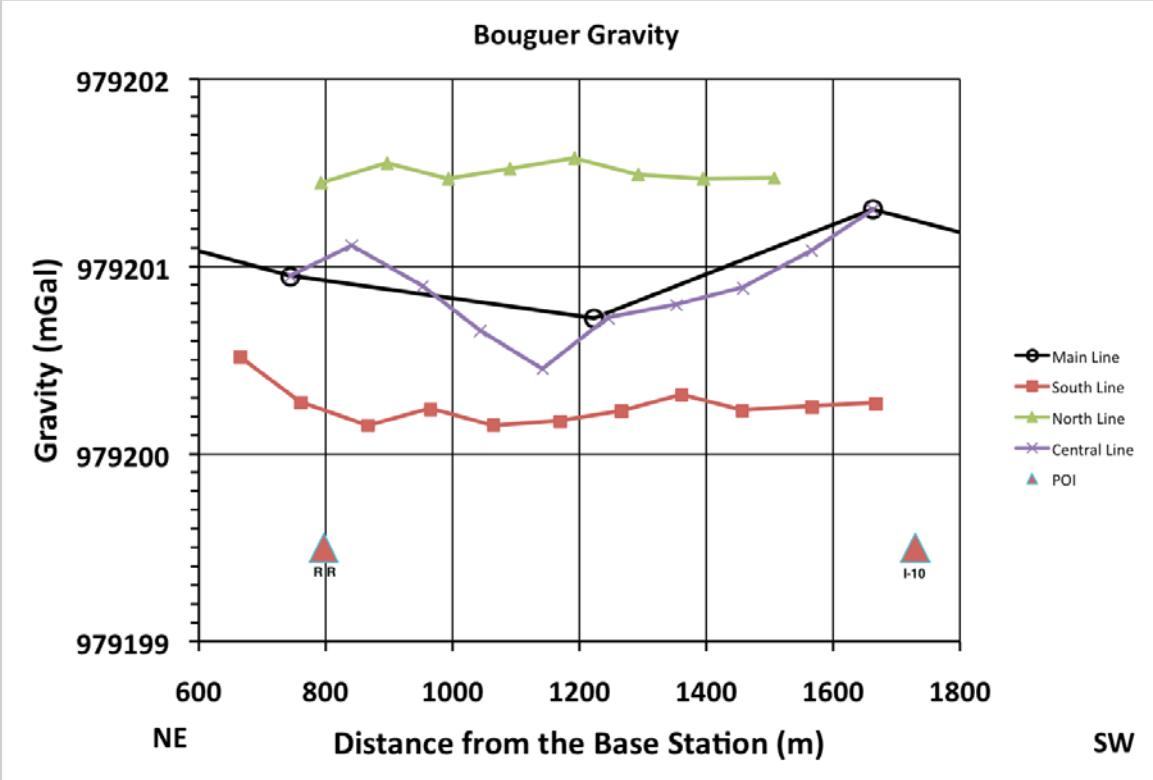


**Figure 4.5** Zoom plot of the offset lines.

# 5. Passive-Seismic Survey

## 5.1 Introduction

Passive-seismic analysis is one of the methods used to analyze the subsurface structure of the study area. The horizontal-to-vertical spectral ratio method (H/V) was used to interpret the data. The H/V method relies on ambient seismic noise and can be used for estimating the thickness of unconsolidated deposits. A change in the seismic properties of the subsurface is shown as a peak in the H/V spectral ratio. This is the primary resonant frequency (shear wave) of the overburden and an empirical relationship is used to determine the thickness from the frequency.

Passive seismic analysis is an inexpensive and relatively fast method for obtaining seismic data. It is limited by interference from human activity and works better in low-population areas. Passive seismic analysis is intended to be a supplement to other geophysical methods as was the case in this study.

## 5.2 Instrumentation and Field Procedures

The measurements were performed perpendicular to the postulated fault location. These measurements started at the base station located near E. Drexel Rd and S. Craycroft Rd and were collected along a line running southwest toward E. Los Reales Rd and S. Alvernon Way. Data were also collected near an existing test well site. Figure 5.1 shows the locations where passive seismic instruments were set up for data collection.

Three Guralp CMG-6TD seismometers were used in the study, the sensor IDs were A834, B74 and B76. Table 5.1 shows the coordinates of each station corresponding to locations in Figure 5.1. A gravity meter plate was used as a leveling plate everywhere except for the base station (Figure 5.2). A tilted table was used in some cases in order to block some of the wind. At the base station a shallow hole was dug for the seismometer and the seismometer was leveled on the ground at the bottom of the hole. This method kept the equipment safer and reduced interference caused by wind.

| Site ID | Sensor ID | Easting | Northing | Proj. Dist. From Base (m) | Elevation AMSL(m) | file(s) |
|---|---|---|---|---|---|---|
| Base Station | A834 | 511709.3 | 3556853 | 0 | 822.23 | 2014_1856-0000 |
| Well DW-9 | B74 | 510420 | 3557722 | 295 | 808.63 | 20140222_1928-2000 |
| 1 | B76 | 511172 | 3556351 | 735 | 816.92 | 20140222_2331_0000 |
| 2 | B76 | 511008 | 3556183 | 970 | 816.42 | 20140222_2252-2300 |
| 3 | B76 | 510817 | 3556024 | 1217 | 814.8 | 20140222_2007 |
| 4 | B76 | 510688 | 3555896 | 1399 | 815.31 | 20140222_2152-2200 |
| 5 | B74 | 510720 | 3555728 | 1496 | 816.42 | 20140316_2319<br>20140317_0000 |
| 6 | B76 | 510511 | 3555721 | 1648 | 817.23 | 20140222_2100_57 |
| 7 | B74 | 509665 | 3554905 | 2823 | 811.67 | 20140316_2128_2200 |
| 8 | B74 | 509512 | 3554162 | 3260 | 816.48 | 20140222_2239 |
| 9 | B74 | 508671 | 3553778 | 4024 | 811.39 | 20140222_2127 |

**Table 5.1** Passive-seismic locations, seismometer Id#, projected distances from base station and the corresponding files created during data collection on 2/22/14 and 3/10/14.

## 5.3 Data and Results

The intended scheme for data collection was to retain proximity to the main profile line, which runs northeast to southwest, more or less orthogonal to the postulated fault in the area. This was adhered to in the northeastern region of the study area despite many structural obstacles. In the southwest area of study it was somewhat more difficult, and therefore, measurements are more disperse.

Once these data were collected and downloaded, a data-processing program called Geopsy, (Wathelet et al., 2008) was used to identify the maximum sediment depth. Due to the fact that often several files were created by the seismometer during data collection at a given site, files were merged using Geopsy prior to data processing. Before the H/V spectral ratio can be

generated, it is necessary to consider the length of the time window. Based on the duration of each site survey and the recommendations outlined by SESAME (2004), we selected a 50 second window for the majority of the processing.

A major consideration when processing seismic data is the significant influence nearby industrial noise can have on the interpretation of data. This is of particular importance because much of the study area lies within a kilometer of a busy interstate and a railroad. The damping tool in Geopsy can detect the frequency of local industrial noises (Fig. 5.3). For this reason, the data were subsequently processed with two filters. A high-pass filter set to 0.9 Hz and a band-reject filter set for a range of 0.9 – 1.1 Hz.

The frequency at the peak of the spectral ratio ($f_{H/V}$) is of primary interest to determine the sediment thickness, depth to bedrock, ($h_{min}$) using Equation 5.1. Shear wave velocity ($v_s$) can range from 300-12,000 ft/sec. Previous work in the Tucson Basin by Loy (1990) determined the alluvium in this area to be 5500 feet/sec.

$$h_{min} = \frac{v_s}{4 f_{H/V}} \qquad \textbf{5.1}$$

| Site ID | Sensor | Proj. Dist. From Base Station (m) | f H/V (Hz) | Amp. Of fH/V | Predicted elevation AMSL (m) | Predicted Depth (m) |
|---|---|---|---|---|---|---|
| Base Station | A834 | 0 | 0.594 | 2.89 | 117 | 706 |
| Well DW-9 | B74 | 295 | 0.597 | 10.03 | 106 | 702 |
| 1 | B76 | 735 | 0.589 | 1.98 | 105 | 712 |
| 2 | B76 | 970 | 0.609 | 5.48 | 128 | 689 |
| 3 | B76 | 1217 | 0.606 | 2.30 | 123 | 692 |
| 4 | B76 | 1399 | 0.613 | 8.66 | 132 | 684 |
| 5 | B74 | 1496 | 0.591 | 2.13 | 107 | 709 |
| 6 | B76 | 1648 | 0.612 | 2.78 | 132 | 685 |
| 7 | B74 | 2823 | 0.622 | 1.76 | 137 | 674 |
| 8 | B74 | 3411 | 0.640 | 3.55 | 160 | 655 |
| 9 | B74 | 4321 | 0.590 | 4.10 | 100 | 711 |

**Table 5.2** Passive-seismic locations and predicted depth to the deep boundary of the subsurface layer.

The peak frequency can be identified during the processing of the data once the spectra are generated in Geopsy (Figs. 5.4-5.14). Results of these data are seen in Table 5.2 and Figures 5.15-17.

## 5.4 Data Interpretation

The H/V processing results of the passive seismic surveys have the primary peak $f_{H/V}$ at a range from 0.5 to 0.7Hz (Table 5.2). For most cases, we can clearly see this peak and get the $f_{H/V}$. The amplitudes of these peaks range from 1.7 to 10.0 (Table 5.2). However, there aren't obvious secondary peaks. This makes it difficult to predict boundary depths for other layers. Thus, from our processing results, we can only detect a deep layer boundary. This boundary is much deeper than the results from the TEM method. The final processing results of the H/V are shown in Figures 5.15-5.17.

In Figure 5.17 we see that the calculated elevations (AMSL) of the ten stations are highly variable. On the north-east side of I-10, elevations are from 105m to 132m, typically close to 130m. Elevations predicted on the south-west side of I-10, range from 100m to 162m. It is possible that the variations in the elevation of this boundary represent a facies change rather than an offset due to a fault. The drop in predicted elevation at the location 1495m from the base station (Station 5) is significant relative to the nearby stations, which may be caused by nearby noise. This can be seen from a smaller $f_{H/V}$ produced by the high-pass filter than the band-reject filter (Figure 5.15). Though the noise effect is also seen in the last station, the drop at this station may indicate a fault offset in this area. Unfortunately, we have only one station at this area and it is not possible to predict detailed variations around this station. In general, the underground layer detected by the passive-seismic survey has identified a boundary increasing from north-east to south-west. A possible reason for this is that a facies change defines the depth of this deep layer.

## 5.5 Discussion and Conclusion

One of the possible reasons why only one boundary is found is because the H/V technique is effective when there is a large acoustic impedance contrast. If the underground layers are very similar in acoustic impedance, it is difficult to find a peak in the H/V plot. Thus, we can only see the deep boundary using the passive-seismic method, since the shallow layers

have close acoustic impedances. Due to the limited time and number of seismometers in our array, the seismic data do not have the highest precision. Despite these limitations, a boundary ranging from 100m to 162m in elevation was detected using this technique. Coupled with the geological information, this technique may indicate that there is a possible facies change in the layer detected by passive seismic. On the south-west side of I-10, the deep boundary of this layer is around 150m in elevation, and on the north-east side of I-10 the deep boundary is around 130m in elevation.

## 5.6 References

Loy, K. (1990) Subsurface structure of the Southern and Central Tucson Basin, Pima County, Arizona, M.Sc., p81.

SESAME European research project, 2004, Guidelines for the implementation of the H/V spectral ratio technique on ambient vibrations measurements, processing and interpretation.

Wathelet, M., D. Jongmans, M. Ohrnberger, and S. Bonnefoy-Claudet, 2008, Array performances for ambient vibrations on a shallow structure and consequences over Vs inversion. Journal of Seismology, 12, 1-19.

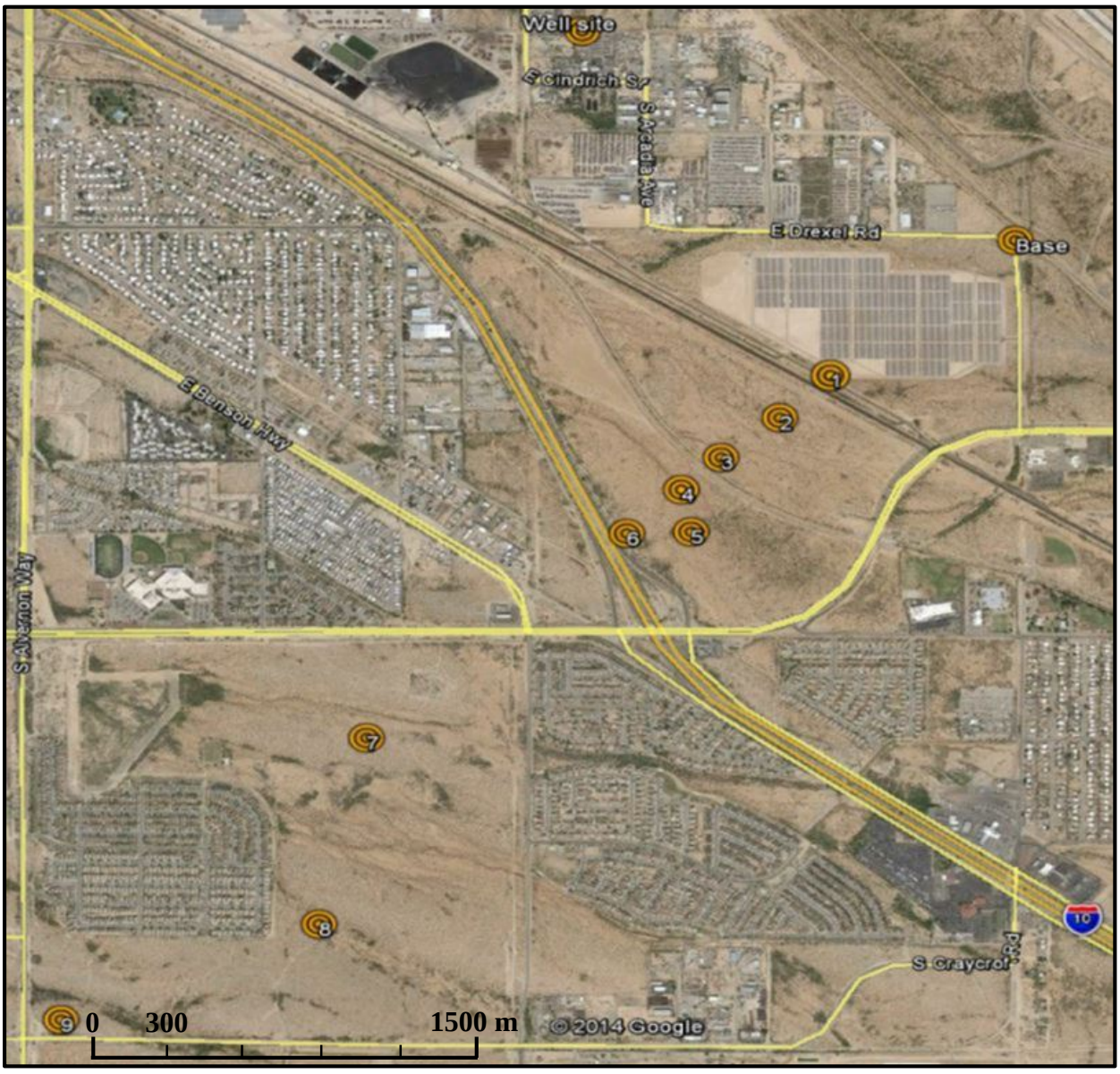


**Figure 5.1** Displays the locations of the passive seismic data collection stations

**Figure 5.2** Seismometer in the field taking measurements. The battery is housed in the cooler.

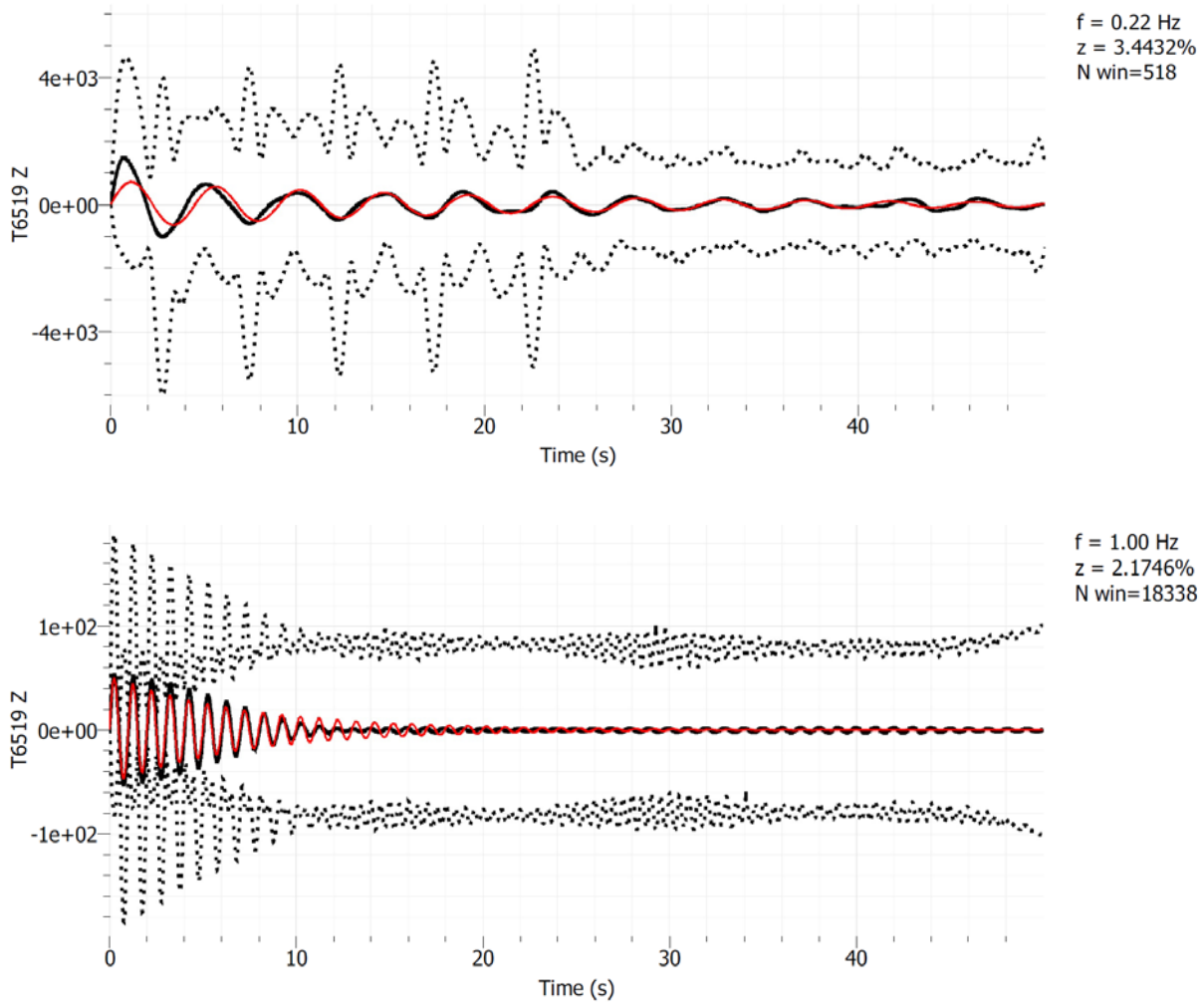


**Figure 5.3** The damping tool identifies the frequency at which industrial noise is detected. These results are from Site 1, which lies between the solar array and railroad tracks, show an industrial source at 0.22 Hz decaying at a rate of 3.44% per sec and at 1Hz decaying at a rate of 2.17% per sec. The damping tool was applied to all passive-seismic survey sites.

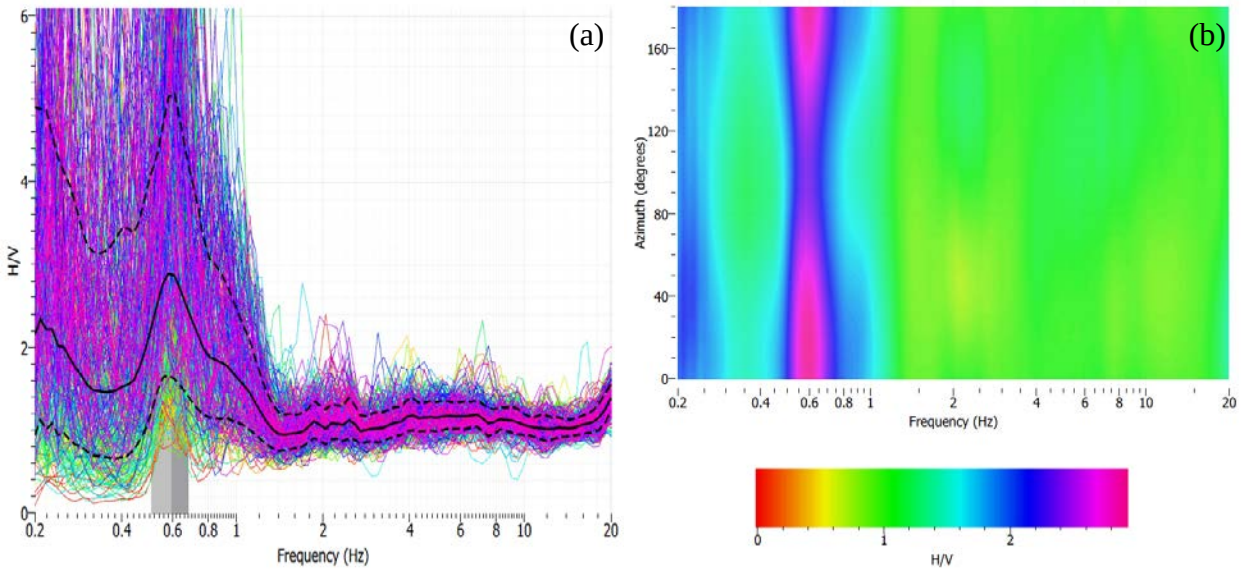


**Figure 5.4** Processing results of Base Station. (a) H/V processing results, and (b) H/V rotate analysis, indicating an around 0.6Hz seismic source which seems to come in all directions and concentrates from 0 degree to 70 degree and from 140 degree to 180 degree.

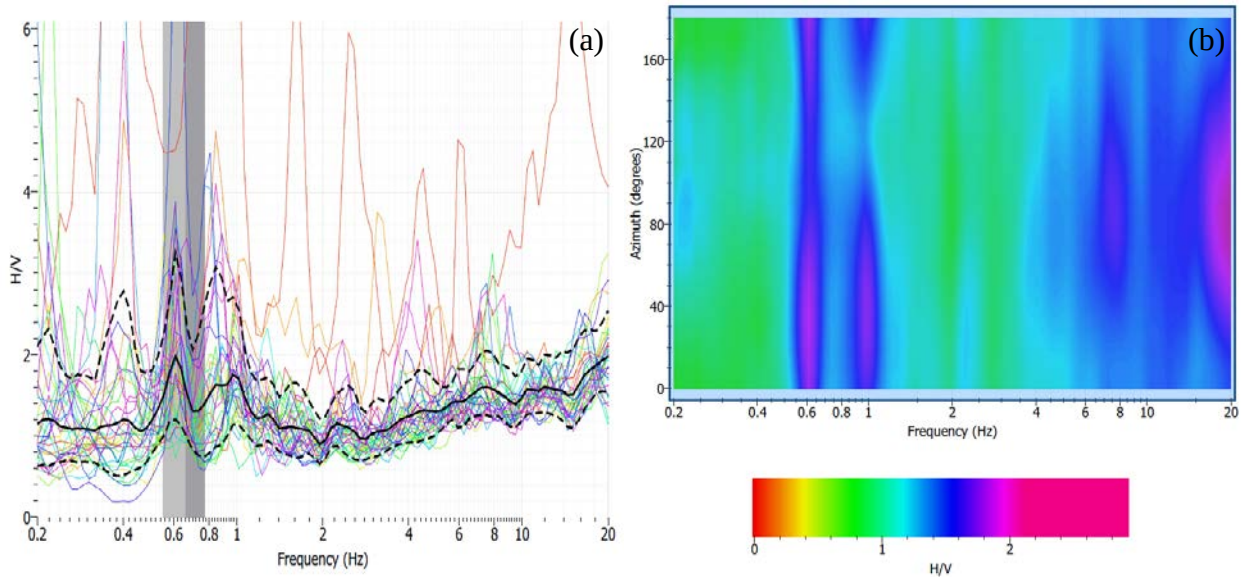


**Figure 5.5** Processing results of Station 1. (a) H/V processing results, and (b) H/V rotate analysis, indicating an around 0.6Hz seismic source which seems to come in all directions and concentrates from 0 degree to 80 degree and from 140 degree to 180 degree. The source around 1Hz and 20Hz are noise, we don't use them.

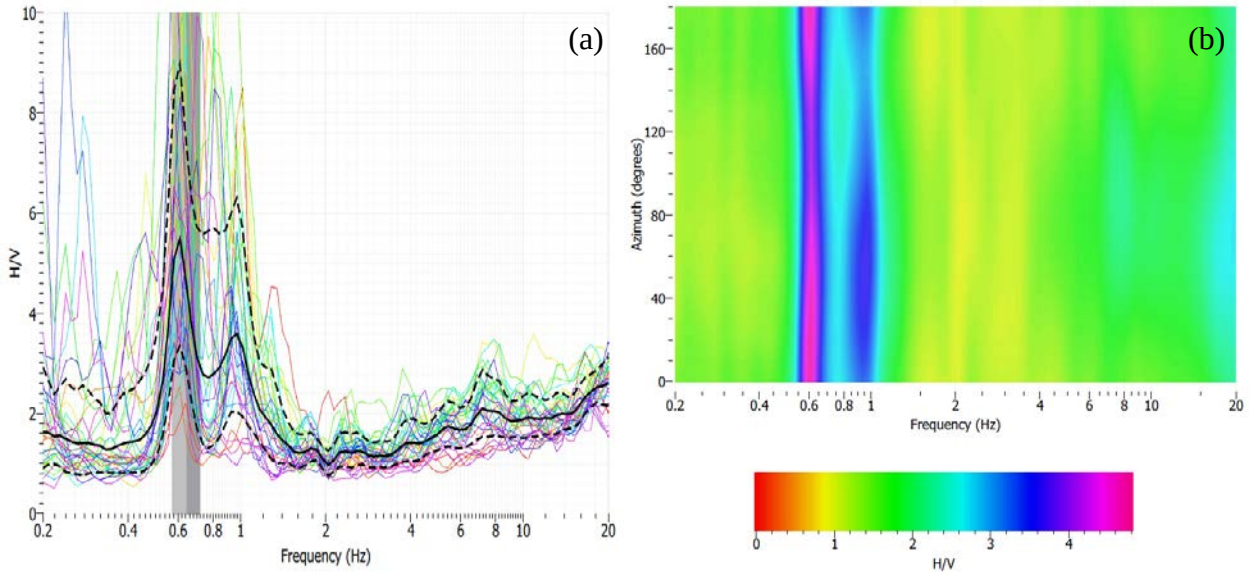


**Figure 5.6** Processing results of Station 2. (a) H/V processing results, and (b) H/V rotate analysis, indicating an around 0.6Hz seismic source which seems to come in all directions. The source around 1Hz is noise, we don't use it.

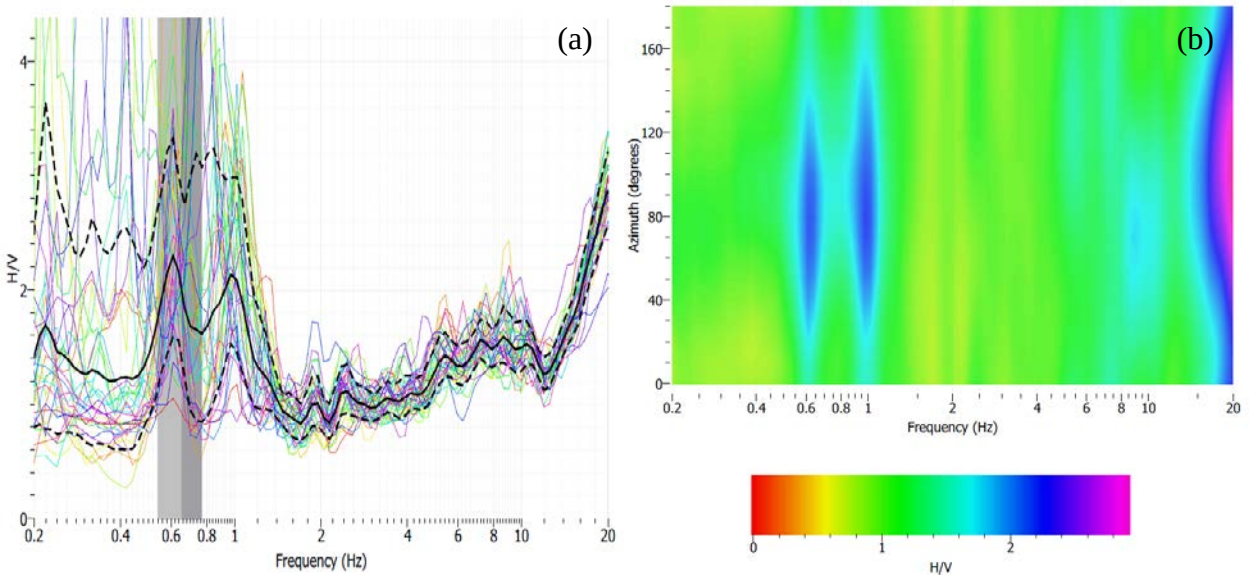


**Figure 5.7** Processing results of Station 3. (a) H/V processing results, and (b) H/V rotate analysis, indicating an around 0.6Hz seismic source which seems to come in directions from 30 degree to130 degree. The source around 1Hz and 20Hz are noise, we don't use them.

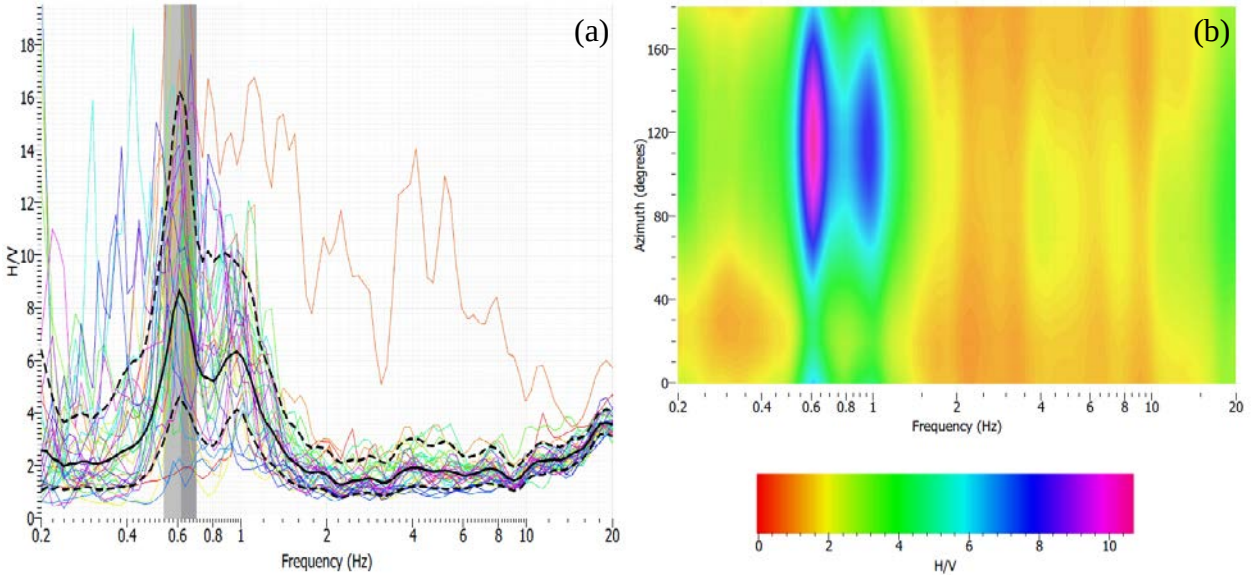


**Figure 5.8** Processing results of Station 4. (a) H/V processing results, and (b) H/V rotate analysis, indicating an around 0.6Hz seismic source which seems to come in directions from 50 degree to180 degree. The source around 1Hz is noise, we don't use it.

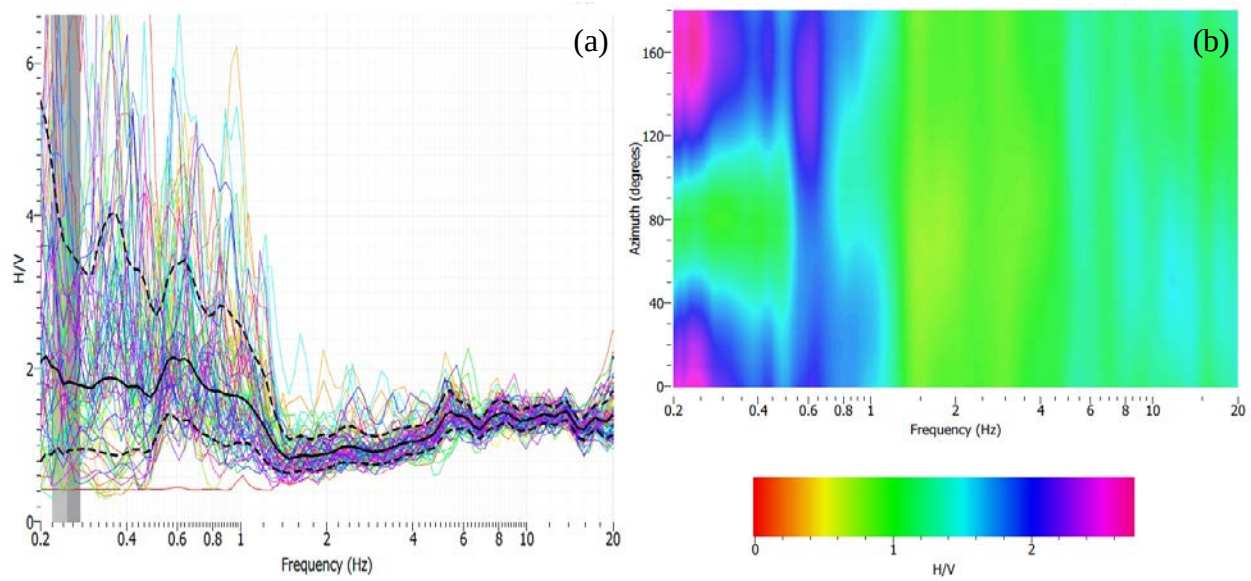


**Figure 5.9** Processing results of Station 5. (a) H/V processing results, and (b) H/V rotate analysis, indicating an around 0.6Hz seismic source which seems to come in directions from 110 degree to180 degree. The source around 0.2Hz is noise, we don't use it.

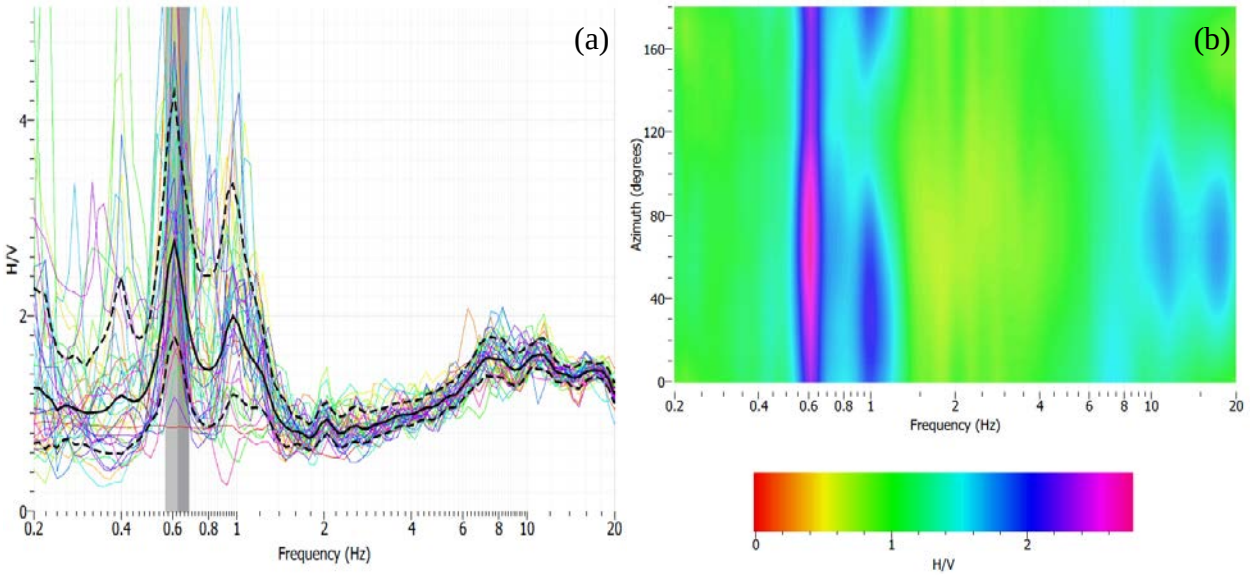


**Figure 5.10** Processing results of Station 6. (a) H/V processing results, and (b) H/V rotate analysis, indicating an around 0.6Hz seismic source which seems to come in all directions. The sources around 1Hz and 15Hz are noise, we don't use them.

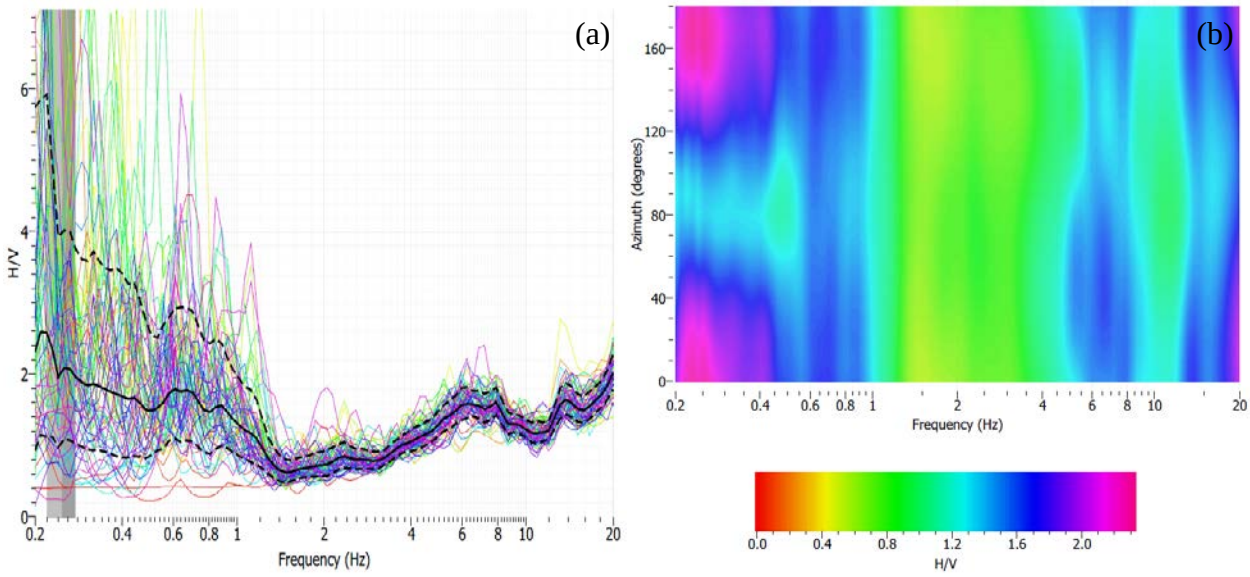


**Figure 5.11** Processing results of Station 7. (a) H/V processing results, and (b) H/V rotate analysis, indicating an around 0.6Hz seismic source which seems to come in all directions. The sources around 0.2Hz and 20Hz are noise, we don't use them.

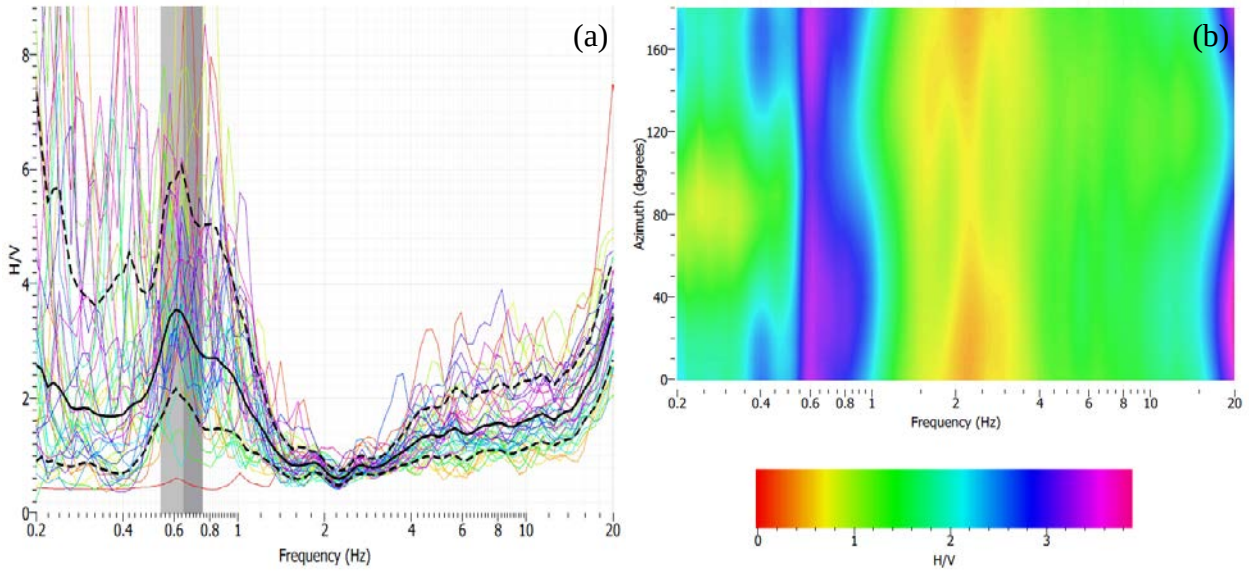


**Figure 5.12** Processing results of Station 8. (a) H/V processing results, and (b) H/V rotate analysis, indicating an around 0.6Hz seismic source which seems to come in all directions. The sources around 2Hz and 20 Hz are noise, we don't use them.

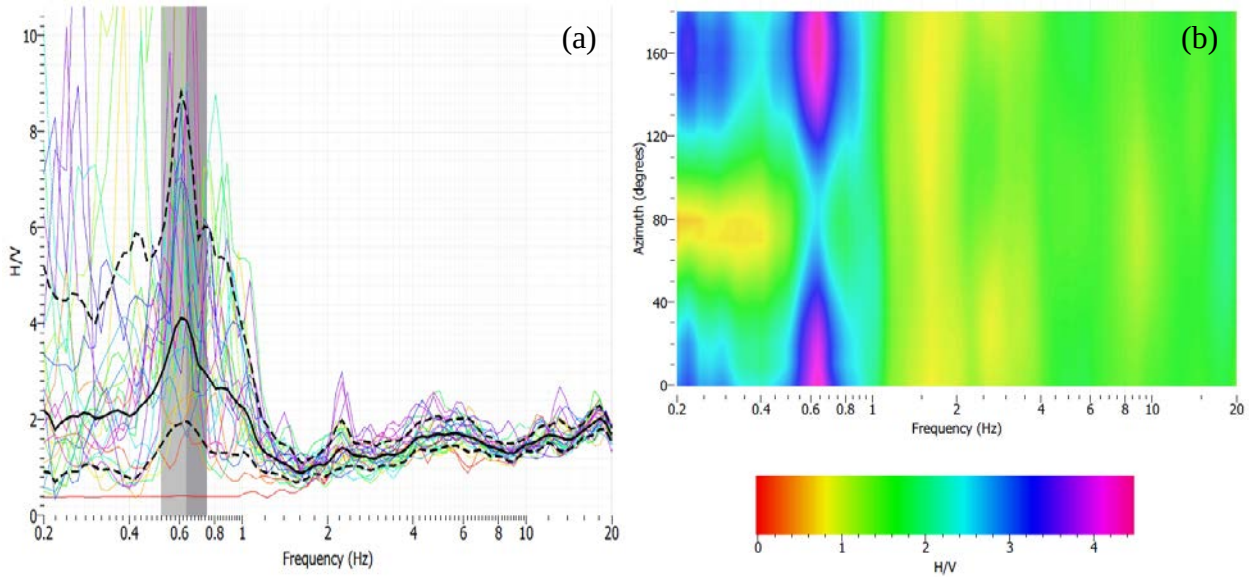


**Figure 5.13** Processing results of Station 9. (a) H/V processing results, and (b) H/V rotate analysis, indicating an around 0.6Hz seismic source which seems to come in directions from 0 degree to 40 degree and from 120 degree to 180 degree. The source around 0.2Hz is noise, we don't use it.

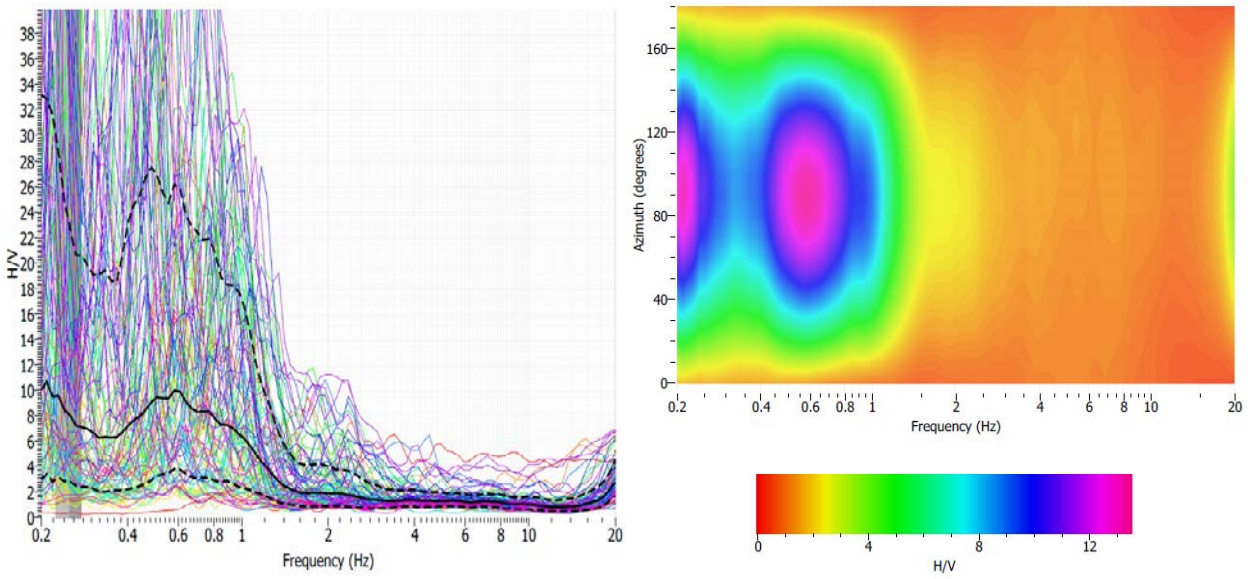


**Figure 5.14** Processing results of well site. (a) H/V processing results, and (b) H/V rotate analysis, indicating a 0.6 Hz seismic source which seems to come in directions from 40 degree to 140 degree. The source around 0.2Hz is noise, we don't use it.

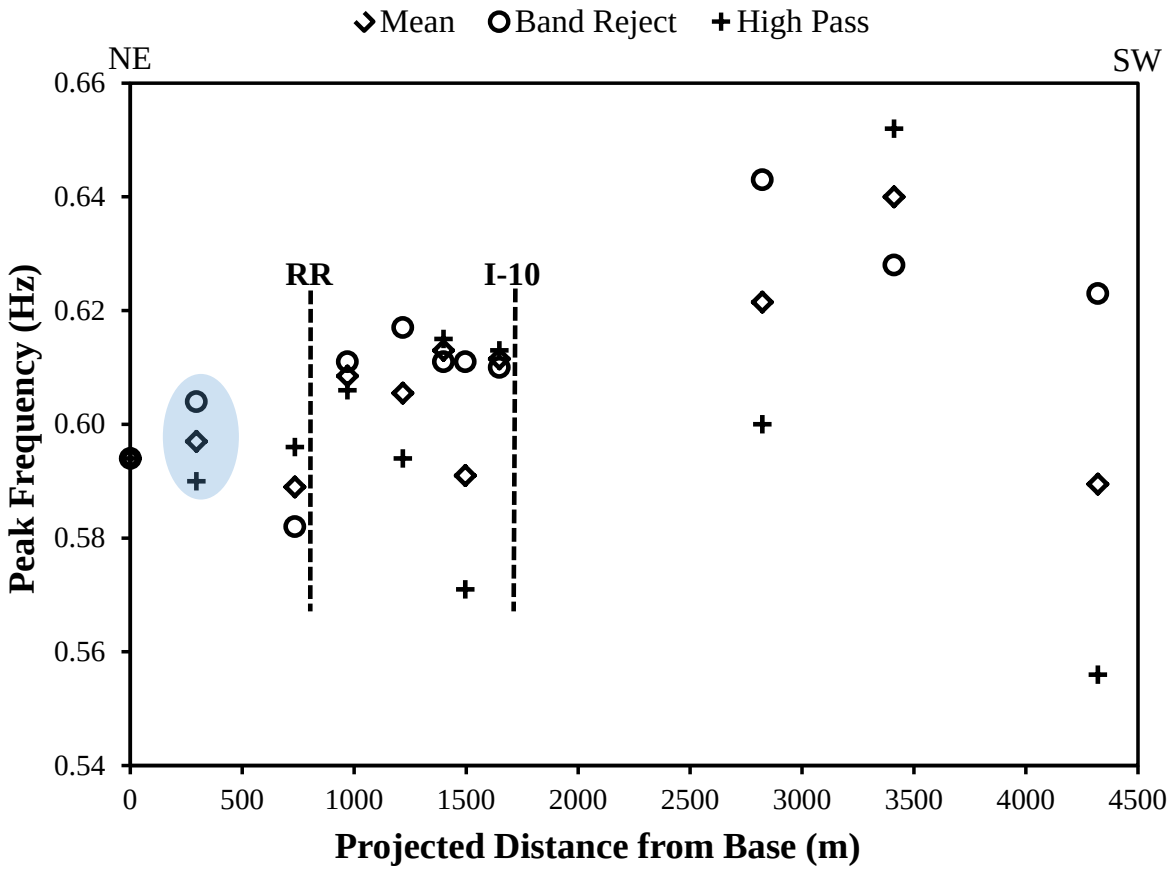


**Figure 5.15** The mean peak frequencies from processed data, and results from band-reject and high-pass filter methods. The well site data is in the blue ellipse.

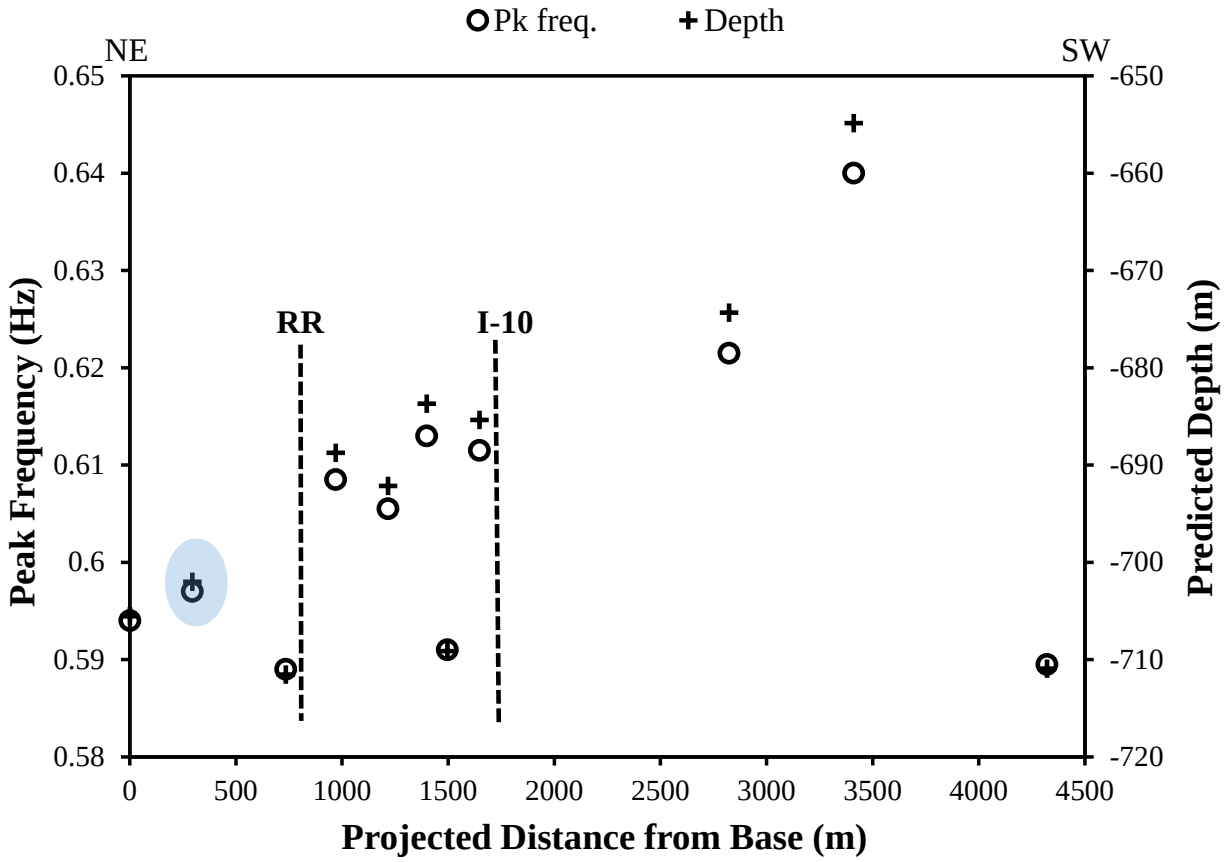


**Figure 5.16** The processing results (averaged from both filtering processes) of the passive seismic profile. The data in blue are from the well site, DW-9.

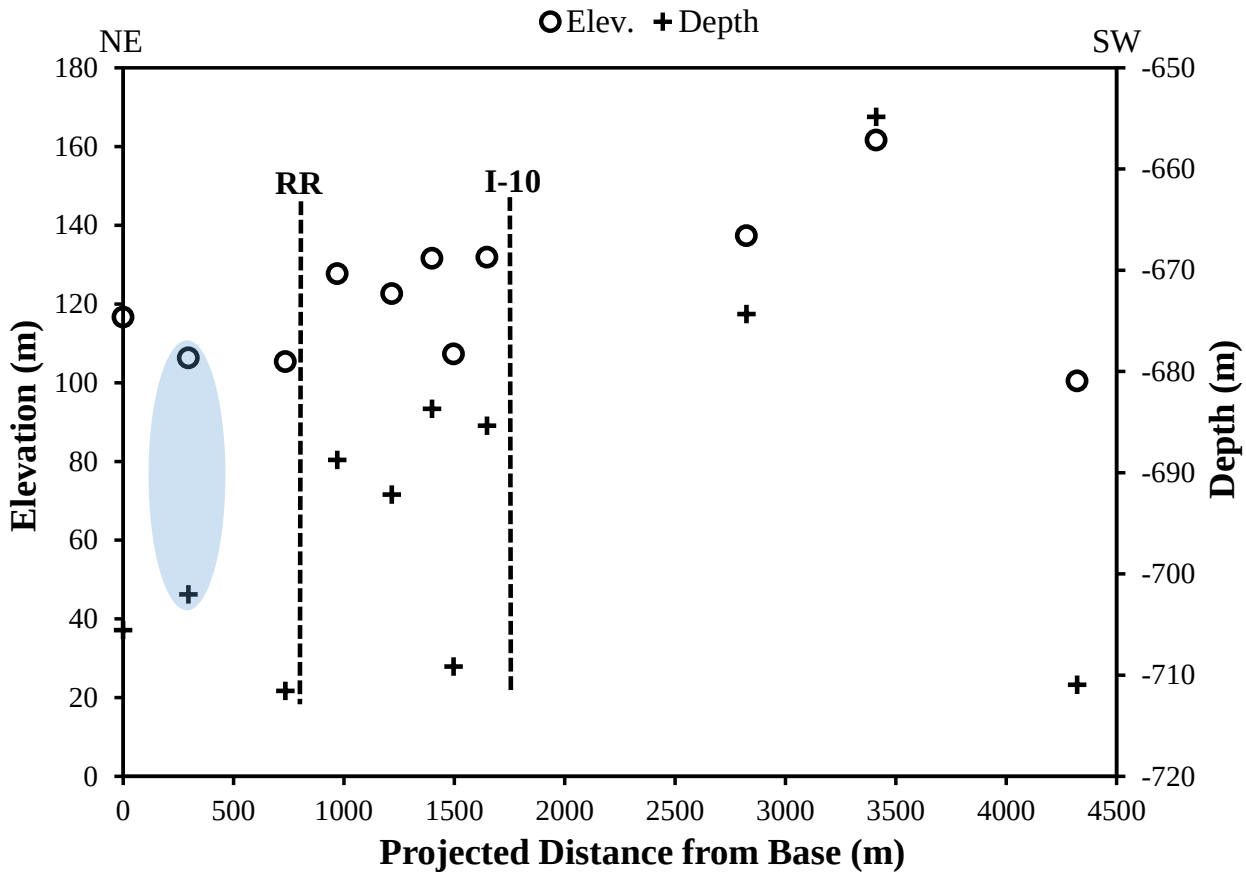


**Figure 5.17** Predicted elevations and depths using the averaged data from both filter types. The mean elevation in the survey area is 810 m AMSL. The data in blue are from the well site, DW-9.

# 6. Transient Electromagnetic Survey

## 6.1 Introduction

Transient Electromagnetic (TEM) is a geophysics method that is widely used for mapping subsurface layers. In this project, the TEM method was used to investigate depth to layers and depth to water table in the survey area. Generally, the maximum exploration depth of the TEM central-loop induction method is about 2 to 3 times the loop size. For more information about the TEM method, see the paper "Introduction to TEM" (Zonge, 2009). A total of eight sites were recorded within two days for this project. A postulated fault is located northeast of Interstate 10 (I-10) and we are trying to find which side of the fault is higher, so data were collected by setting four loops on each side of Interstate 10 (I-10). The transmitter loop sites were 200m X 200m.

## 6.2 Locations

The TEM data were recorded at eight sites in the Tucson Basin. On 3-1-2014, only two loops were measured, loop 1 and loop 2. On the second day 3-2-2014, another 6 loops were measured. For loop 6, a homeless camp was at the initial planned location, so it had to be shifted about 300m southwest of that location. Loop 1, 2, 7 and 8 are at on the northeast side of I-10. Loop 3, 4, 5 and 6 are at on the southwest side of I-10. Because of the existence of the solar array (northeast corner of the survey area) and the subdivision (southwest corner of the survey area), we cannot put a 200m x 200m loop there, and small loops cannot give us the depth needed, so there are no measurements in those two areas. The locations of eight loops are shown in Figure 6.1.

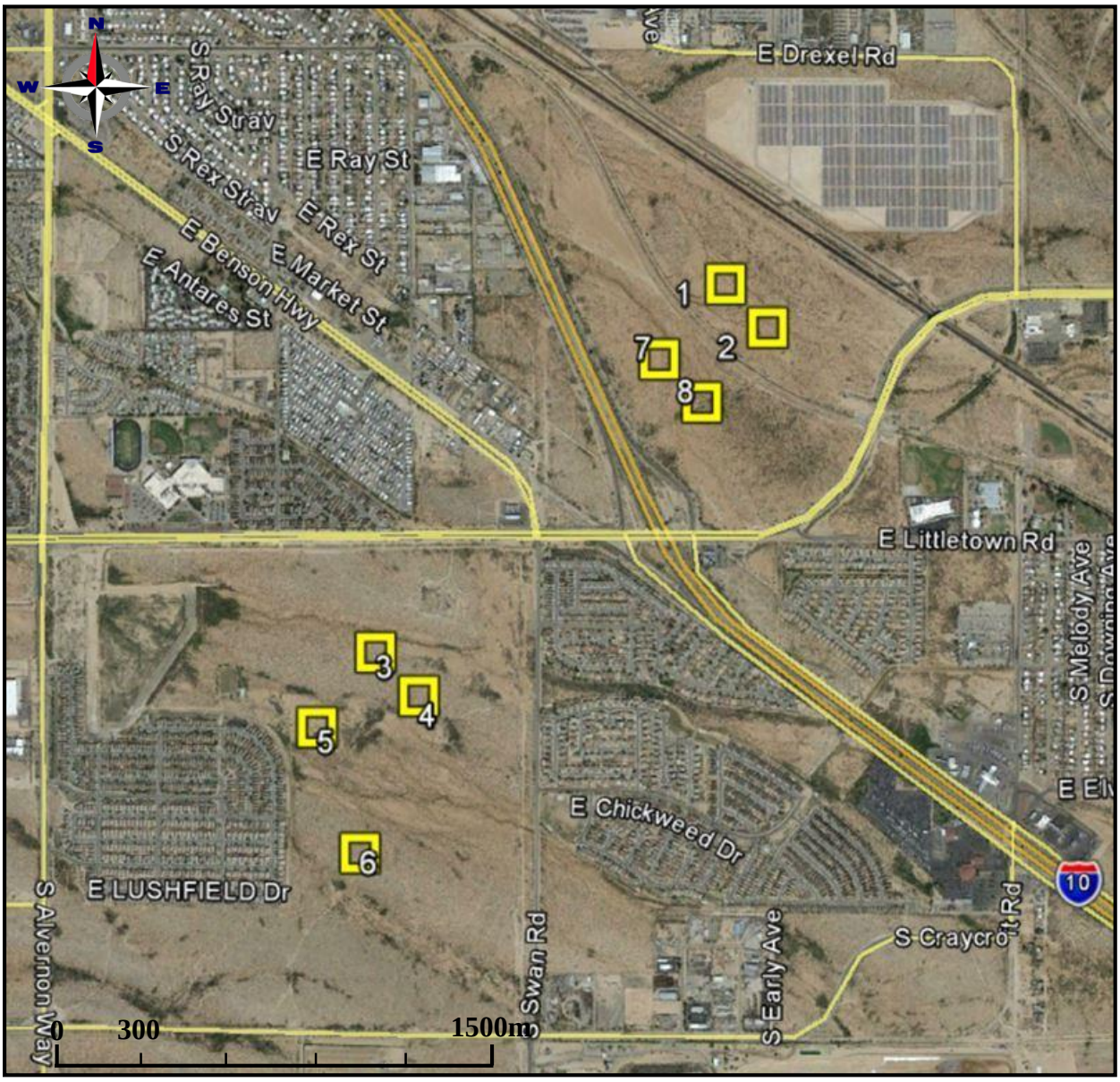


**Figure 6.1** TEM survey stations. The loop size for TEM survey is 200m × 200m. There are 8 loops in the survey area.

## 6.3 Instrumentation and Field procedures.

The TEM equipment for these measurements includes the GDP $32^{II}$ multi-function receiver (Zonge 2012), the ZT-30 TEM transmitter (Zonge, 2013a) and the XMT-32S transmitter controller (Zonge, 2013b). The XMT-32S transmitter controller controls ZT-20 TEM transmitter to generate 8Hz and 16Hz square waves into a 200m x 200m loop. The GDP $32^{II}$ multi-function

receiver is connected to a vertical magnetic-field sensor at the center of the loop. The receiver measures the off-time signal, which can be used to obtain the resistivity information of the earth. The GDP $32^{II}$ multi-function receiver must first be synchronized with the XMT-32S transmitter controller before measurements. A current of 2.2Amps was used in these measurements. Two 12-VDC batteries were connected in series to provide the power to the transmitter.

We tried to keep the transmitter loop as square as possible and away from fences, the rail-tracks, the solar array, and the subdivision. We used GPS to measure the distance between loop corners. After loop set up, we calculated the center position and then acquired our measurements at that location.

## 6.4 Data Processing

After TEM data were obtained in the field, we downloaded the data from the GDP $32^{II}$ to a computer. The raw data were sorted and organized and then processed using Zonge International's proprietary suite of software called DATPRO. Then, the data were trimmed or edited for data that were inconsistent with the overall decay curve. The data were then inverted by the Zonge STEMINV inversion program, using the smooth-inversion method (MacInnes and Raymond, 2009). We finally obtained a smooth layered-earth model for each station. The one-dimensional inversion results are shown in Appendix B. The measured decay curve is compared with the best-fit calculated decay curve. The solid line is the best-fit decay curve and the plus symbol line is the measured decay curve. The red plus symbols are time windows not used in the calculation. The one-dimensional earth models are shown on the right side of each plot.

## 6.5 TEM processing results.

With the inversion results from STEMINV, we plotted 2D cross sections. We used Golden Software's Surfer 11 to display the inversion data. The gridding method we used was the Kriging method. Because we only have 8 stations in total, and the separation is quite large between the stations on the NE and the stations on the SW, the results in the middle of the cross section are not reliable. Thus, in the contour plots, we blanked that area. For these 8 stations, we divided the data into two lines, the north line and the south line. Each line has 4 loops. With 8Hz

and 16Hz, we have 4 contour plots, as shown in Figure 6.2 to Figure 6.5. We projected the loop locations to the main profile lines.

## 6.6 Interpretation

Based on the four TEM-model contour plots, both sides of the profiles have a very low resistivity region below the more resistive surface layers. On the northeast side of I-10, the low-resistivity region starts around 750m in elevation and continues very deep. On the southwest side, this region starts around 720m in elevation and continues very deep. This low-resistivity region is likely caused by high TDS in the water and high shale content. Referring to the hydrogeologic cross section (Figure 1.5), the top of these low-resistivity areas is in the area of the water-table depth. Another important feature from these contour plots relates to the offset in the top boundary of these low-resistivity regions. Using the same resistivity contour line, the northeast side of I-10 is always shallower than the southwest side of I-10. All four plots contain this feature (Figures 6.2, 6.3, 6.4, 6.5). This feature indicates the water table on the northeast side of I-10 is shallower thn that on the southwest side of I-10.

The 8Hz pulse repetition frequency has a somewhat deeper depth of investigation than the 16 Hz. From the 8Hz contour plots (Figures 6.2, and 6.3), the deep resistivities also show an offset.

Resistivity well-log information from DW-9 (Figure 6.6), shows a resistivity increase using the 16 and 64 inch normal resistivity tools, starting at 1400 ft (427m) depth, and increasing more at 1800 ft (549m) depth, till the end of the well log at 2200 ft (671m) depth. The resistivity increase around 400m in elevation on the left side of Figures 6.2 and 6.3 is similar to the resistivity increase around 1400 ft (427m) depth in Figure 6.6. From the 8Hz contour plots (Figures 6.2 and 6.3), the deep boundary of the low-resistivity regions also show a change in elevation along the profile. For example, the 12 ohm-m contour line is around 400m on the left side of Figures 6.2 and 6.3, but on the right side it is much deeper. It is possible that the variations in this deep boundary are due to facies changes across the section, rather than an offset due to faulting.

## 6.7 References

Maclnnes S., Raymond M., 2009, Zonge Data processing smooth-model TEM inversion. Zonge International.
Zonge, 2009. Introduction to TEM. (http://www.zonge.com.au/docs/tem/intro_tem.pdf)

Zonge, 2012. GDP-32$^{II}$. Geophysical receiver. Multi-function receiver.

(http://www.zonge.com/legacy/PDF_Equipment/Gdp-32ii.pdf)

Zonge, 2013a, ZT-30 Geophysical transmitter.

(http://www.zonge.com/legacy/PDF_Equipment/Zt-30.pdf)

Zonge, 2013b, XMT-32S Transmitter Controller.

(http://www.zonge.com/legacy/PDF_Equipment/Xmt-32s.pdf)

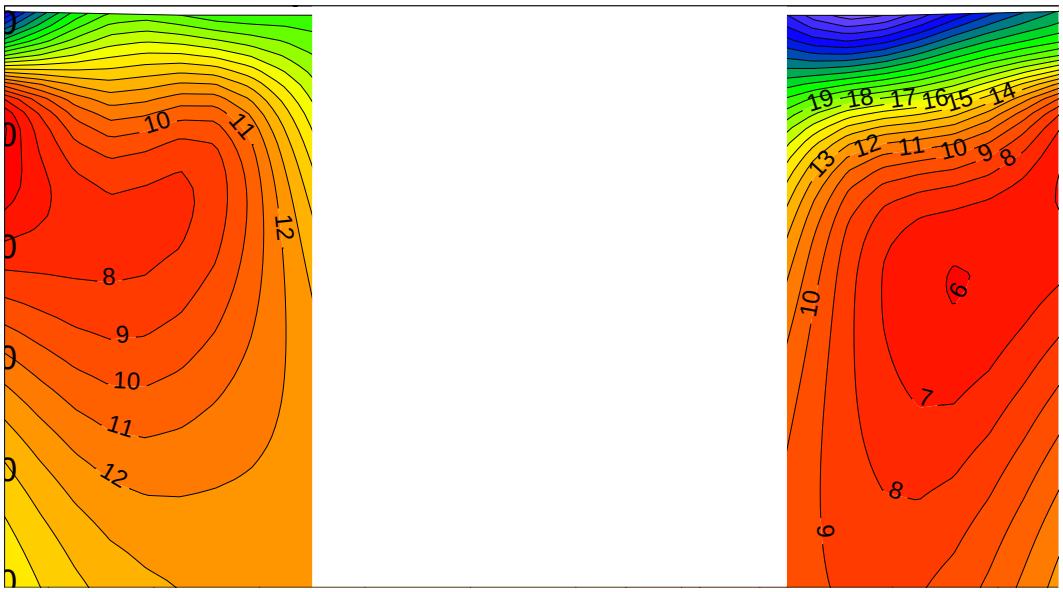


**Figure 6.2** Cross section of 8Hz TEM data inversion results at the north line. Between loop 7 and loop 3, the no-data region is interpolated by Surfer, which is not reliable, so we blanked this area. The locations are projected to the main profile for better comparison.

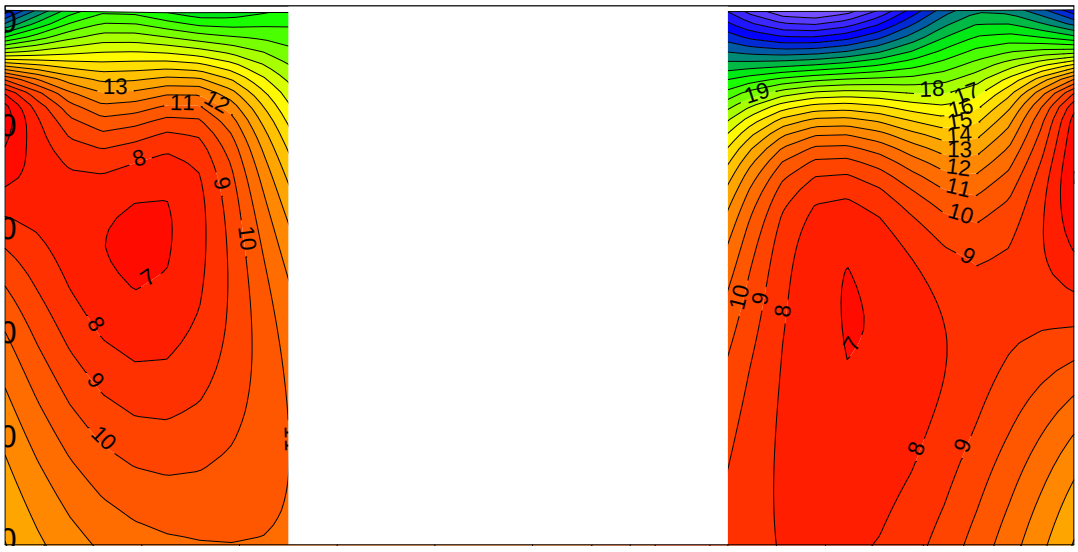


**Figure 6.3** Cross section of 8Hz TEM data inversion results at the south line. With the same reason in Figure 6.2, we blanked them. The locations are projected to the main profile for better comparison.

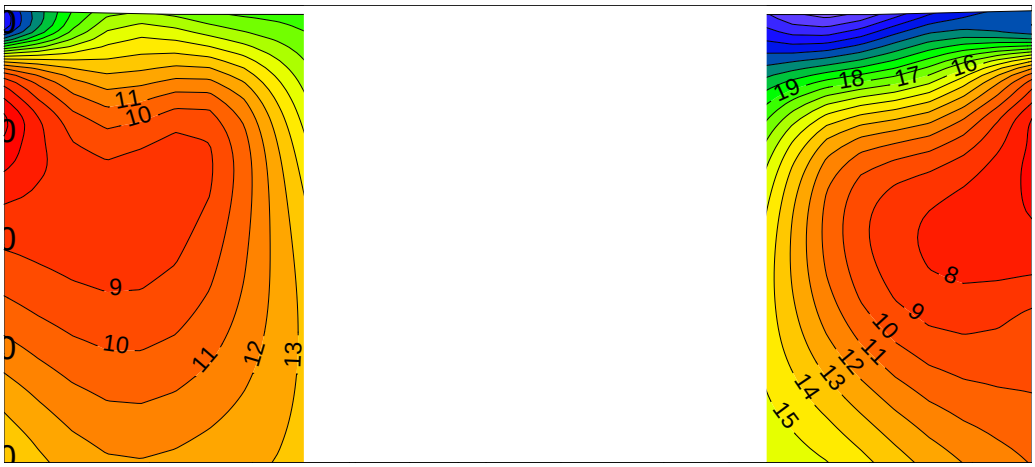


**Figure 6.4** Cross section of 16Hz TEM data inversion results at the north line. With the same reason in Figure 6.2, we blanked them. The locations are projected to the main profile for better comparison.

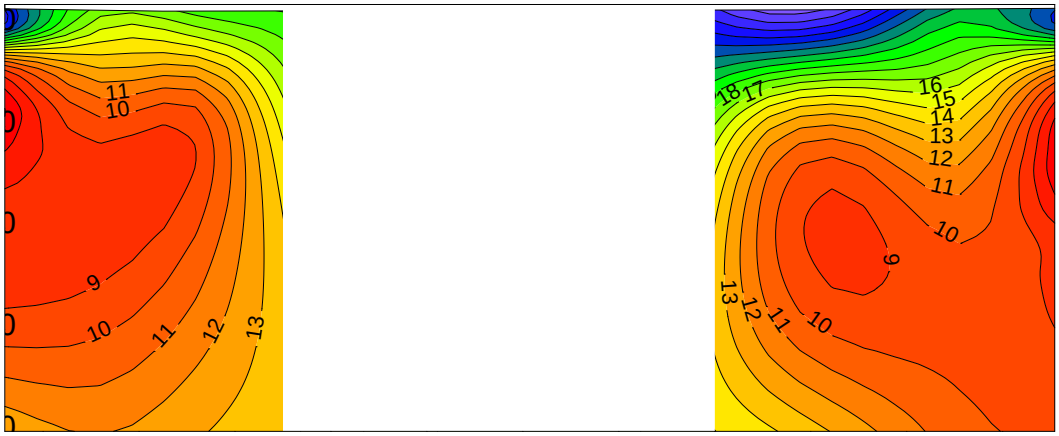


**Figure 6.5** Cross section of 16Hz TEM data inversion results at the south line. With the same reason in Figure 6.2, we blanked them. The locations are projected to the main profile for better comparison.

(a)

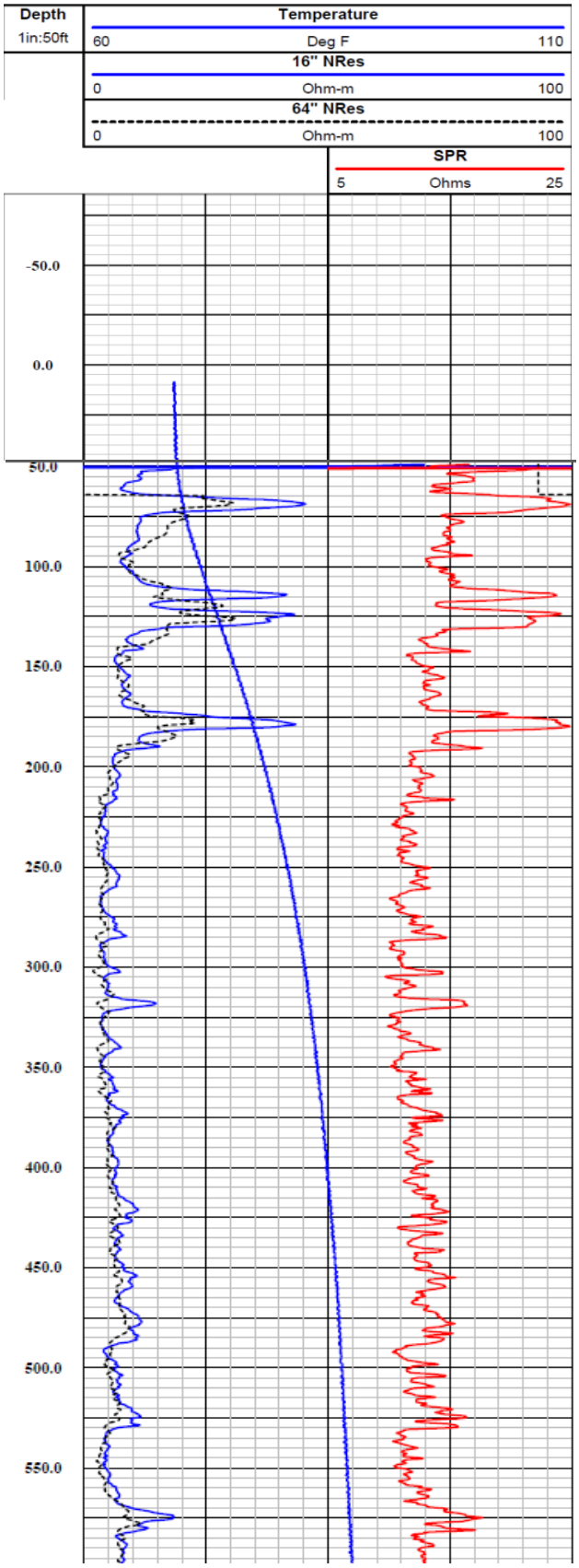
Depth
1in:50ft
Temperature
60
Deg F
110
16" NRes
0
Ohm-m
100
64" NRes
0
Ohm-m
100
SPR
5
Ohms
25
-50.0
0.0
50.0
100.0
150.0
200.0
250.0
300.0
350.0
400.0
450.0
500.0
550.0

(b)

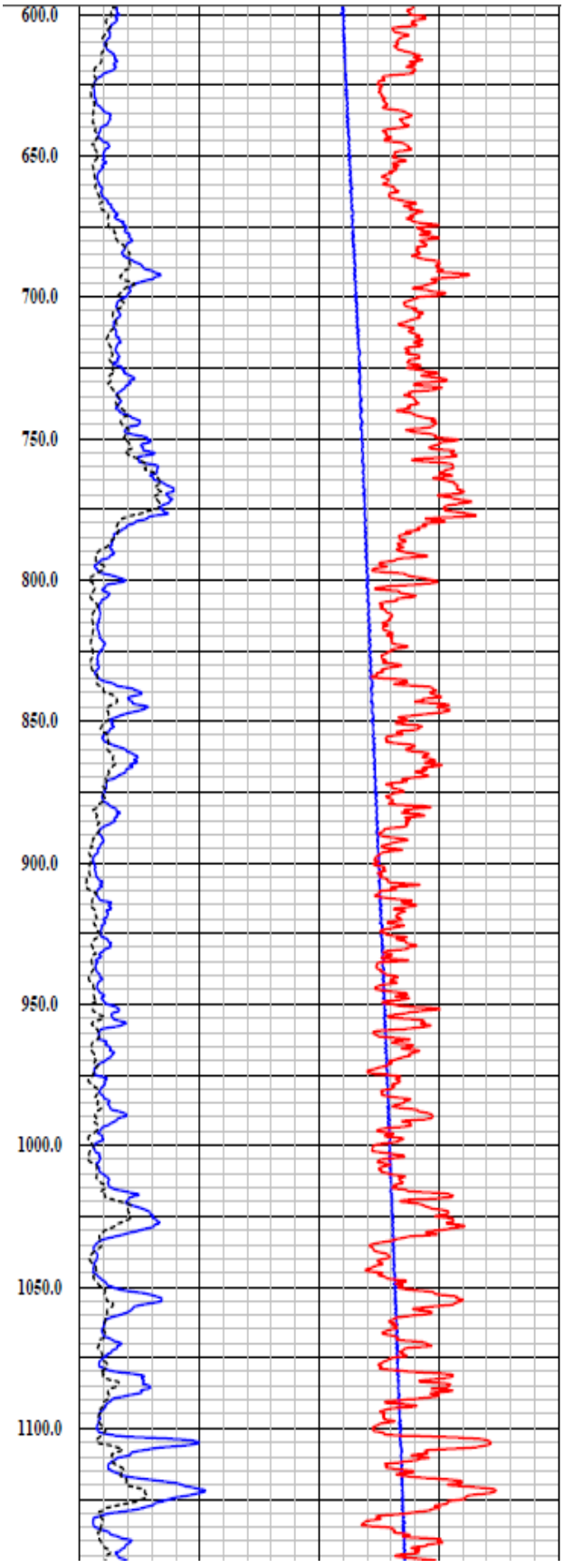

(c)

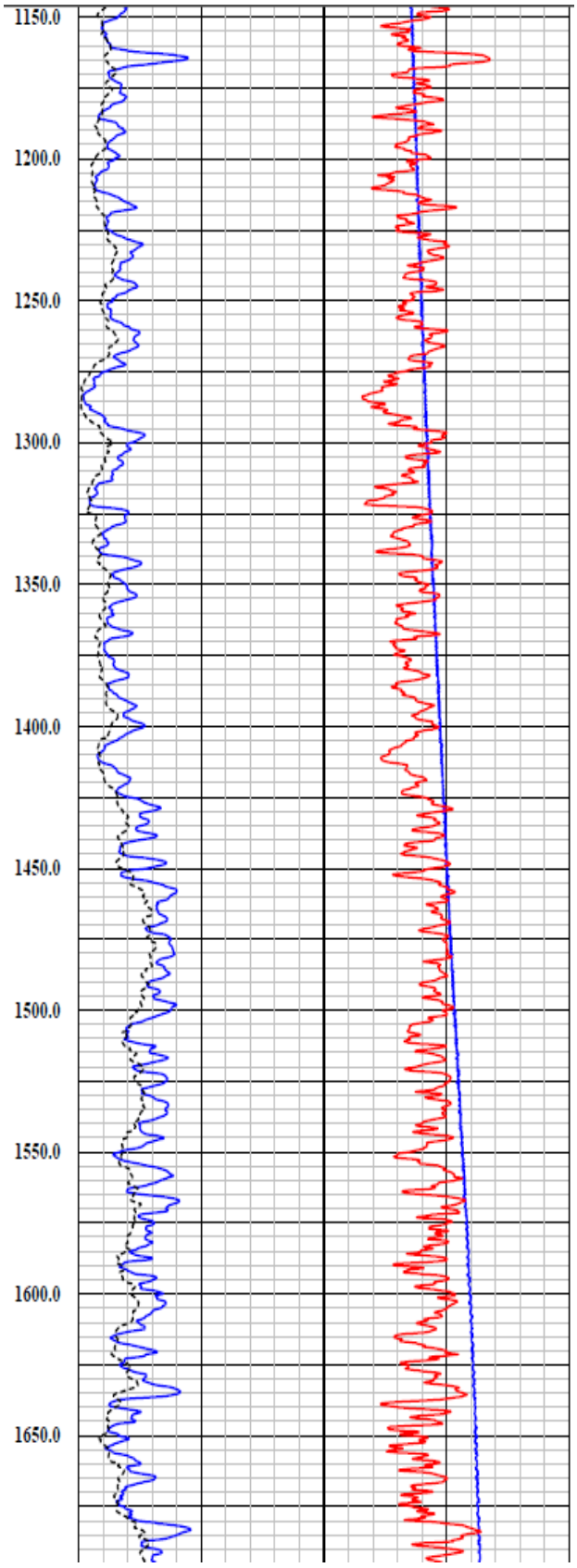
1150.0
1200.0
1250.0
1300.0
1350.0
1400.0
1450.0
1500.0
1550.0
1600.0
1650.0

(d)

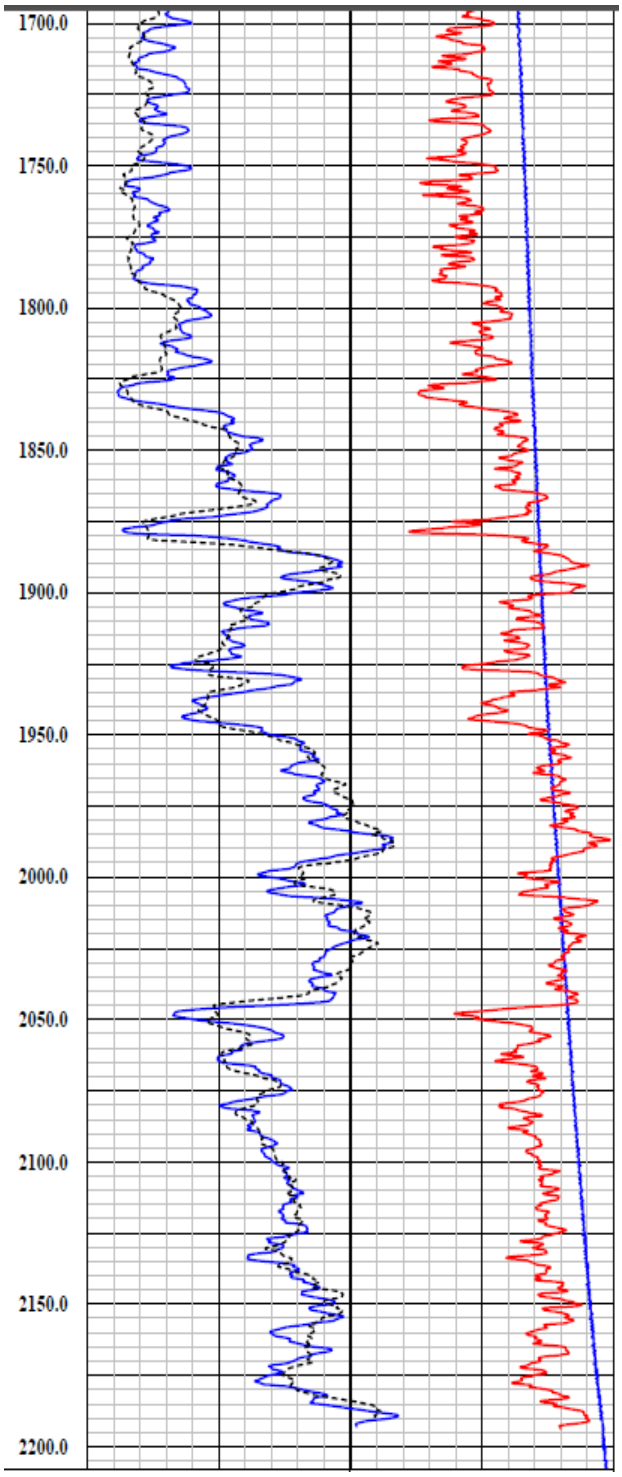


**Figure 6.6** Partial information of Well-log DW-9. 16" normal resistivity and 64" normal resistivity oscillate from 50 (15m) to 200 ft (61m) at shallow depth and increase after 1400 ft. Single point resistance has the same pattern.

# Appendix A: Magnetic Field Data

April 6 2014 Data:

| | | | | | | | | | |
|---|---|---|---|---|---|---|---|---|---|
| | Projected distance from Base | Uncorrected Reading (nT) | base reading | longitude 12S | latitude | projected x | projected y | correction | corrected reading |
| MC-1 | 2085.965005 | 47318.79 | 47408.8 | 510209 | 3555403 | 510234 | 3555378 | -35.3 | 47354.09 |
| MC-2 | 2037.881743 | 47337.91 | 47407.2 | 510243 | 3555437 | 510268 | 3555412 | -36.9 | 47374.81 |
| MC-3 | 1986.970055 | 47330.98 | 47408.2 | 510280 | 3555472 | 510304 | 3555448 | -35.9 | 47366.88 |
| MC-4 | 1936.058367 | 47335.05 | 47409.2 | 510316 | 3555508 | 510340 | 3555484 | -34.9 | 47369.95 |
| MC-5 | 1886.560892 | 47335.29 | 47408.6 | 510351 | 3555543 | 510375 | 3555519 | -35.5 | 47370.79 |
| MC-6 | 1837.063418 | 47334.45 | 47408 | 510387 | 3555577 | 510410 | 3555554 | -36.1 | 47370.55 |
| MC-7 | 1316.632827 | 47369.78 | 47408.7 | 510757 | 3555943 | 510778 | 3555922 | -35.4 | 47405.18 |
| MC-8 | 1382.393757 | 47352.2 | 47406.1 | 510707 | 3555900 | 510731.5 | 3555876 | -38 | 47390.2 |
| MC-9 | 1435.426766 | 47359.41 | 47405.4 | 510671 | 3555861 | 510694 | 3555838 | -38.7 | 47398.11 |
| MC-10 | 1486.338454 | 47345.49 | 47404.4 | 510637 | 3555823 | 510658 | 3555802 | -39.7 | 47385.19 |
| MC-11 | 1536.543036 | 47347.51 | 47404.8 | 510599 | 3555790 | 510622.5 | 3555767 | -39.3 | 47386.81 |
| MC-12 | 1587.454724 | 47347.37 | 47405 | 510565 | 3555752 | 510586.5 | 3555731 | -39.1 | 47386.47 |
| MC-13 | 1636.245092 | 47333.85 | 47405.2 | 510529 | 3555719 | 510552 | 3555696 | -38.9 | 47372.75 |
| MC-14 | 1611.496354 | 47350.32 | 47406.2 | 510545 | 3555738 | 510569.5 | 3555714 | -37.9 | 47388.22 |
| MC-15 | 1624.224276 | 47344.38 | 47406.2 | 510538 | 3555727 | 510560.5 | 3555705 | -37.9 | 47382.28 |

February 22 2014 Data:

| | Projected distance from Base | Uncorrected Reading (nT) | base reading | longitude 12S | latitude | projected x | projected y | correction | corrected reading |
|---|---|---|---|---|---|---|---|---|---|
| G-10 | 4336.686 | 47258.5 | 47436.3 | 508649 | 3553780 | 508642.5 | 3553787 | -7.8 | 47266.3 |
| M-3 | 4265.268 | 47276.9 | 47438.3 | 508704 | 3553826 | 508693 | 3553837 | -5.8 | 47282.7 |
| M-4 | 4166.98 | 47279.7 | 47439.7 | 508772 | 3553897 | 508762.5 | 3553907 | -4.4 | 47284.1 |
| M-5 | 4066.571 | 47287.4 | 47439.8 | 508843 | 3553968 | 508833.5 | 3553978 | -4.3 | 47291.7 |
| M-6 | 3966.162 | 47311.5 | 47439.7 | 508914 | 3554039 | 508904.5 | 3554049 | -4.4 | 47315.9 |
| MS-01 | 3869.995 | 47297.4 | 47440.1 | 509024 | 3554065 | 508972.5 | 3554117 | -4 | 47301.4 |
| MS-02 | 3793.628 | 47303.7 | 47441.3 | 509143 | 3554054 | 509026.5 | 3554171 | -2.8 | 47306.5 |
| MS-03 | 3725.746 | 47295.6 | 47441.6 | 509246 | 3554047 | 509074.5 | 3554219 | -2.5 | 47298.1 |
| MS-04 | 3645.135 | 47307.9 | 47441.3 | 509347 | 3554060 | 509131.5 | 3554276 | -2.8 | 47310.7 |
| MS-05 | 3563.818 | 47269.1 | 47441.4 | 509419 | 3554103 | 509189 | 3554333 | -2.7 | 47271.8 |
| MS-07 | 3527.049 | 47297.7 | 47441.9 | 509430 | 3554144 | 509215 | 3554359 | -2.2 | 47299.9 |
| MS-06 | 3498.057 | 47302.1 | 47440.6 | 509419 | 3554196 | 509235.5 | 3554380 | -3.5 | 47305.6 |
| MS-08 | 3417.447 | 47325.6 | 47442.1 | 509433 | 3554296 | 509292.5 | 3554437 | -2 | 47327.6 |
| MS-09 | 3353.807 | 47308.66 | 47442.1 | 509428 | 3554391 | 509337.5 | 3554482 | -2 | 47310.66 |
| MS-10 | 3278.854 | 47309.9 | 47441.5 | 509424 | 3554501 | 509390.5 | 3554535 | -2.6 | 47312.5 |
| M-16 | 3244.913 | 47311.6 | 47442.3 | 509435 | 3554538 | 509414.5 | 3554559 | -1.8 | 47313.4 |
| M-17 | 3140.261 | 47319.7 | 47442.9 | 509503 | 3554618 | 509488.5 | 3554633 | -1.2 | 47320.9 |
| M-18 | 3042.68 | 47326 | 47442.8 | 509573 | 3554686 | 509557.5 | 3554702 | -1.3 | 47327.3 |
| M-19 | 2954.292 | 47327.1 | 47442.6 | 509636 | 3554748 | 509620 | 3554764 | -1.5 | 47328.6 |
| G-7 | 2843.983 | 47338.4 | 47441.2 | 509712 | 3554828 | 509698 | 3554842 | -2.9 | 47341.3 |
| M-21 | 2736.503 | 47338.2 | 47441.9 | 509772 | 3554920 | 509774 | 3554918 | -2.2 | 47340.4 |
| M-22 | 2638.215 | 47339.3 | 47441.9 | 509843 | 3554988 | 509843.5 | 3554988 | -2.2 | 47341.5 |
| M-23 | 2540.635 | 47346.5 | 47442.9 | 509916 | 3555053 | 509912.5 | 3555057 | -1.2 | 47347.7 |
| M-24 | 2436.69 | 47343.2 | 47444.2 | 509989 | 3555127 | 509986 | 3555130 | 0.1 | 47343.1 |
| G-6 | 2337.695 | 47349 | 47441.3 | 510058 | 3555198 | 510056 | 3555200 | -2.8 | 47351.8 |

| | | | | | | | | | |
|---|---|---|---|---|---|---|---|---|---|
| M-26 | 2271.227 | 47357.9 | 47440.4 | 510118 | 3555232 | 510103 | 3555247 | -3.7 | 47361.6 |
| MN29 | 1224.002 | 47405 | 47432 | 510827 | 3556004 | 510843.5 | 3555988 | -12.1 | 47417.1 |
| MN28 | 1196.425 | 47389.6 | 47432.8 | 510866 | 3556004 | 510863 | 3556007 | -11.3 | 47400.9 |
| MN27 | 1147.634 | 47396.3 | 47432.6 | 510887 | 3556052 | 510897.5 | 3556042 | -11.5 | 47407.8 |
| MN26 | 1095.308 | 47385.4 | 47432.8 | 510937 | 3556076 | 510934.5 | 3556079 | -11.3 | 47396.7 |
| MN25 | 1029.547 | 47391.2 | 47430.7 | 510966 | 3556140 | 510981 | 3556125 | -13.4 | 47404.6 |
| MN24 | 999.1419 | 47394.3 | 47430.7 | 511005 | 3556144 | 511002.5 | 3556147 | -13.4 | 47407.7 |
| MN23 | 946.1089 | 47392.3 | 47431 | 511047 | 3556177 | 511040 | 3556184 | -13.1 | 47405.4 |
| MN22 | 893.783 | 47383.1 | 47431 | 511079 | 3556219 | 511077 | 3556221 | -13.1 | 47396.2 |
| MN21 | 816.7083 | 46839 | 47431.5 | 511140 | 3556267 | 511131.5 | 3556276 | -12.6 | 46851.6 |
| MN20 | 702.8641 | 47402.2 | 47431.7 | 511250 | 3556318 | 511212 | 3556356 | -12.4 | 47414.6 |
| MN19 | 661.8519 | 47394.2 | 47430.8 | 511302 | 3556324 | 511241 | 3556385 | -13.3 | 47407.5 |
| MN18 | 627.2037 | 47391.7 | 47432.1 | 511352 | 3556323 | 511265.5 | 3556410 | -12 | 47403.7 |
| MN17 | 591.1413 | 47401.9 | 47430.5 | 511402 | 3556324 | 511291 | 3556435 | -13.6 | 47415.5 |
| MN16 | 555.7859 | 47398.3 | 47430.7 | 511455 | 3556321 | 511316 | 3556460 | -13.4 | 47411.7 |
| MN15 | 518.3093 | 47411.7 | 47430.1 | 511508 | 3556321 | 511342.5 | 3556487 | -14 | 47425.7 |
| MN14 | 485.0753 | 47408.4 | 47429.1 | 511558 | 3556318 | 511366 | 3556510 | -15 | 47423.4 |
| MN13 | 439.8204 | 47414.7 | 47429.9 | 511606 | 3556334 | 511398 | 3556542 | -14.2 | 47428.9 |
| MN12 | 385.3732 | 47411.8 | 47430 | 511651 | 3556366 | 511436.5 | 3556581 | -14.1 | 47425.9 |
| MN11 | 347.8965 | 47425.3 | 47430.1 | 511701 | 3556369 | 511463 | 3556607 | -14 | 47439.3 |
| MN10 | 306.1772 | 47415.9 | 47432.5 | 511750 | 3556379 | 511492.5 | 3556637 | -11.6 | 47427.5 |
| MN9 | 254.5584 | 47369.7 | 47432.9 | 511756 | 3556446 | 511529 | 3556673 | -11.2 | 47380.9 |
| MN8 | 219.9102 | 47385.9 | 47431.5 | 511756 | 3556495 | 511553.5 | 3556698 | -12.6 | 47398.5 |
| MN7 | 183.8478 | 47406.2 | 47433.4 | 511757 | 3556545 | 511579 | 3556723 | -10.7 | 47416.9 |
| MN6 | 146.3711 | 47408.4 | 47433.4 | 511759 | 3556596 | 511605.5 | 3556750 | -10.7 | 47419.1 |
| MN5 | 110.3087 | 47416 | 47435.4 | 511760 | 3556646 | 511631 | 3556775 | -8.7 | 47424.7 |
| MN2 | 96.16652 | 47422.5 | 47434.6 | 511649 | 3556777 | 511641 | 3556785 | -9.5 | 47432 |
| MN4 | 76.36753 | 47382.3 | 47434.4 | 511758 | 3556696 | 511655 | 3556799 | -9.7 | 47392 |
| MN1 | 70.71068 | 47437.4 | 47436.2 | 511667 | 3556795 | 511659 | 3556803 | -7.9 | 47445.3 |
| MN3 | 48.08326 | 47407.4 | 47433.8 | 511749 | 3556745 | 511675 | 3556819 | -10.3 | 47417.7 |

February 8 2014 Data:

| | | | | | | | | | |
|---|---|---|---|---|---|---|---|---|---|
| | Projected distance from Base | Uncorrected Reading (nT) | base reading | longitude 12S | latitude | projected x | projected y | correction | corrected reading |
| | 90.5 | 47395.68 | 47416.8 | 511667 | 3556795 | N/A | N/A | -27.30 | 47422.98 |
| M-35 | 877.44 | 47367.16 | 47430.4 | 511070 | 3556253 | | | -13.70 | 47380.86 |
| M-34 | 950.19 | 47393.16 | 47432.2 | 510960 | 3556154 | | | -11.90 | 47405.06 |
| M-33 | 1026.94 | 47383.92 | 47431.4 | 510960 | 3556154 | | | -12.70 | 47396.62 |
| M-32 | 1124.41 | 47387.81 | 47426.5 | 510886 | 3556087 | | | -17.60 | 47405.41 |
| M-31 | 1223.76 | 47382.67 | 47434.6 | 510811.71 | 3556021.14 | | | -9.50 | 47392.17 |
| M-30 | 1253.35 | 47388.34 | 47434.5 | 510764 | 3555973 | | | -9.60 | 47397.94 |
| M-29 | 1325.01 | 47380.38 | 47436.4 | 510671 | 3555878 | | | -7.70 | 47388.08 |
| M-28 | 1424.24 | 47369.60 | | 510505.52 | 3555709.84 | | | | 47369.60 |

# Appendix B: TEM Data Fits and Models

In this appendix, we show the smooth-model TEM inversion results for all the loops. The left sides of the figures display the measured decay curve with the best-fit calculated decay curve. The right sides of the figures show the inverse one-dimensional earth model for each station.

For 8Hz data

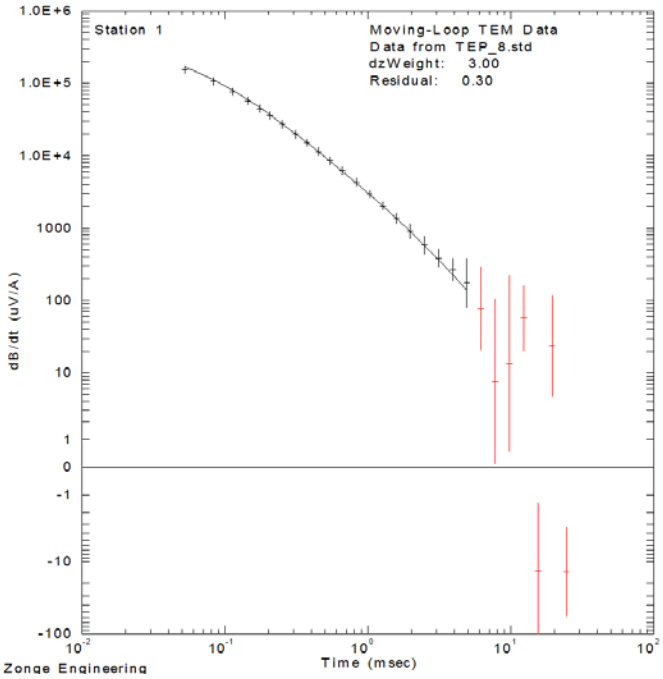


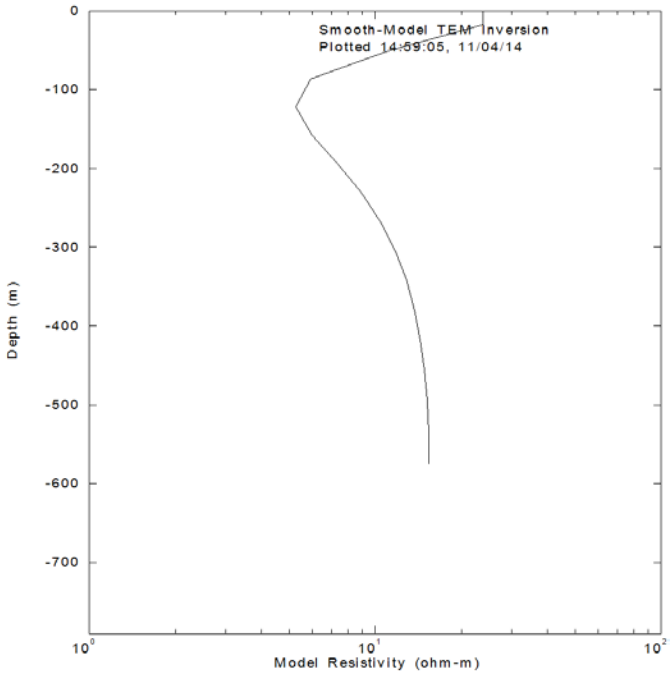


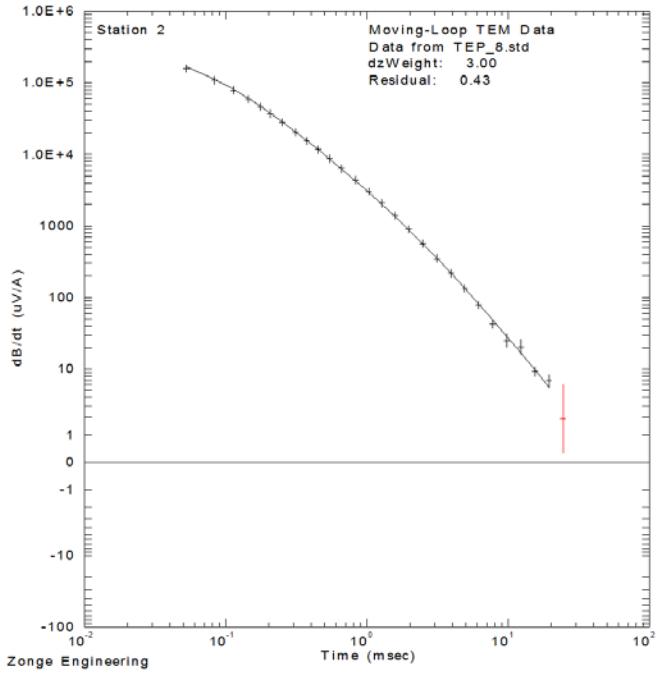


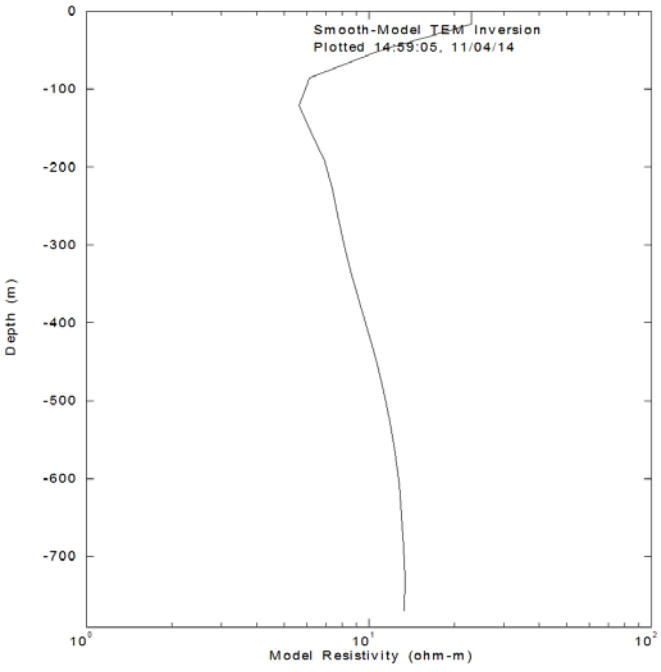

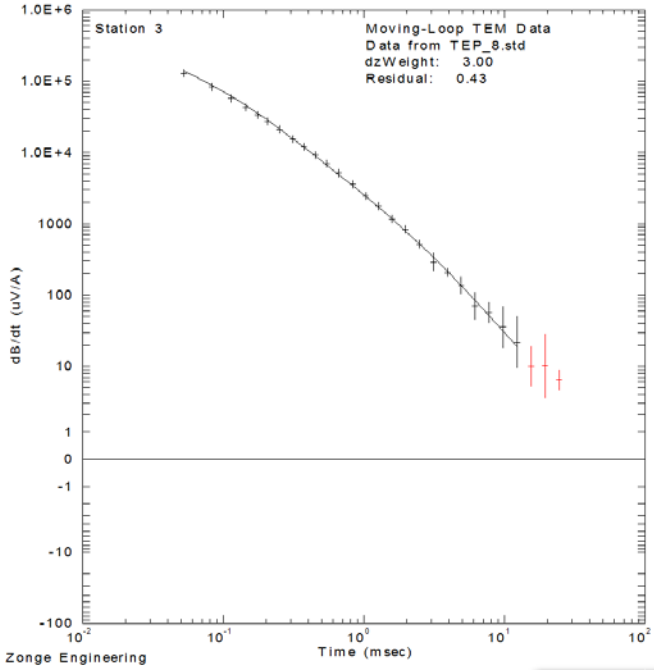
Station 3
Moving-Loop TEM Data
Data from TEP_8.std
dzWeight: 3.00
Residual: 0.43
dB/dt (uV/A)
Time (msec)
Zonge Engineering

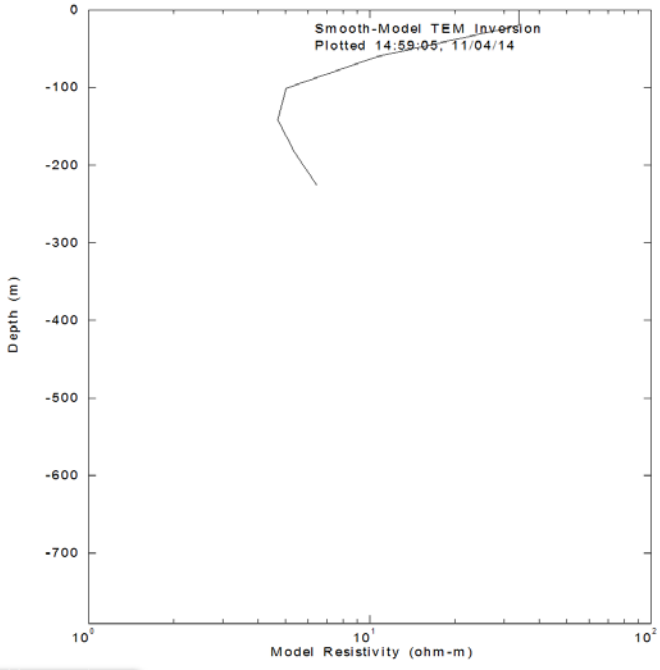
Smooth-Model TEM Inversion
Plotted 14:59:05, 11/04/14
Depth (m)
Model Resistivity (ohm-m)

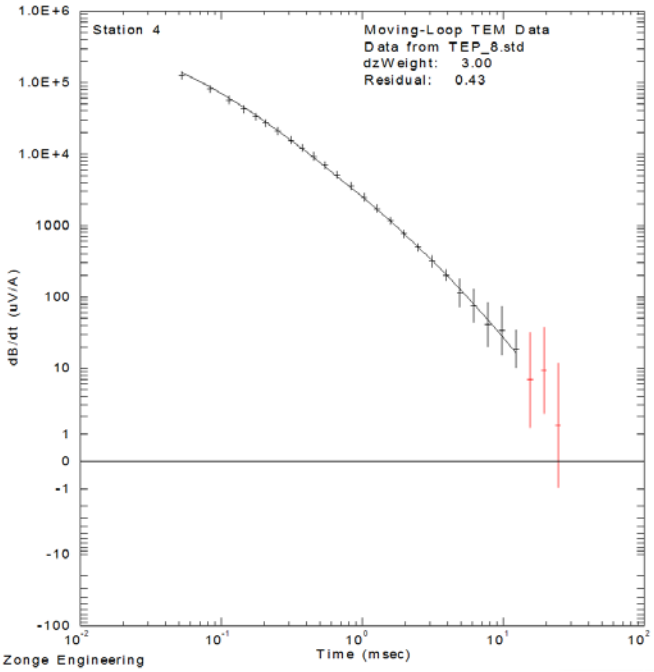
Station 4
Moving-Loop TEM Data
Data from TEP_8.std
dzWeight: 3.00
Residual: 0.43
dB/dt (uV/A)
Time (msec)
Zonge Engineering

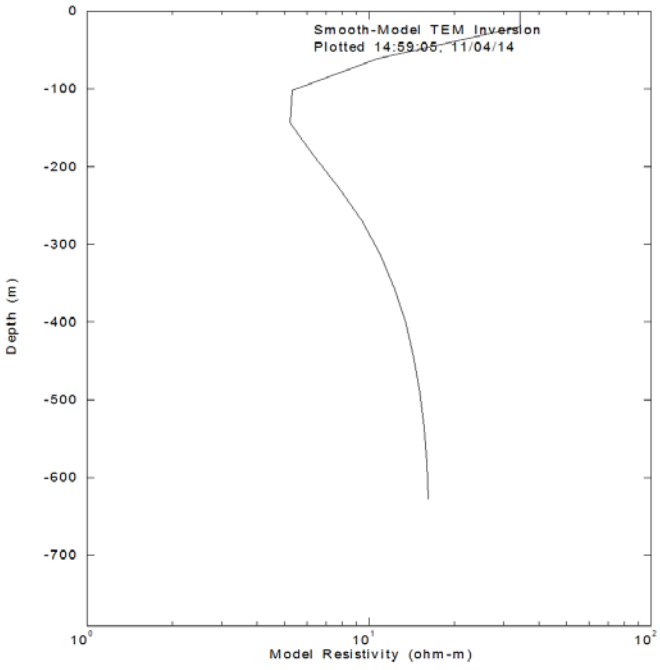
Smooth-Model TEM Inversion
Plotted 14:59:05, 11/04/14
Depth (m)
Model Resistivity (ohm-m)

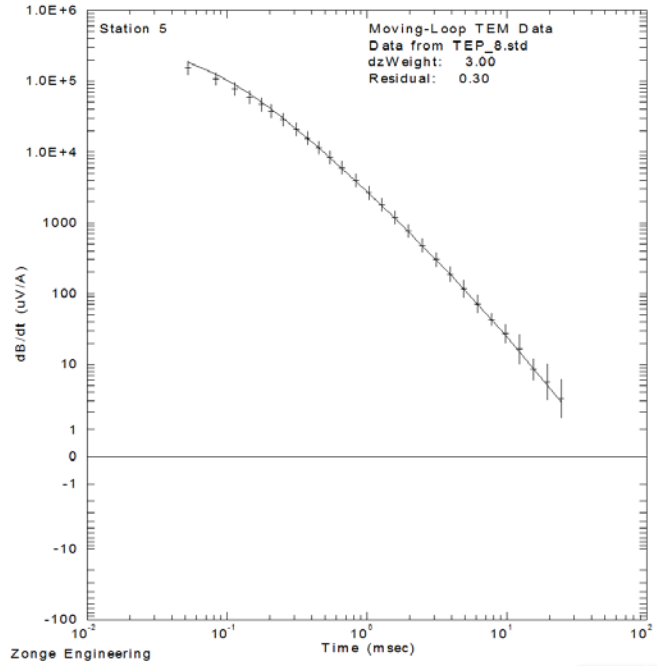
Station 5
Moving-Loop TEM Data
Data from TEP_8.std
dzWeight: 3.00
Residual: 0.30
dB/dt (uV/A)
Time (msec)
Zonge Engineering

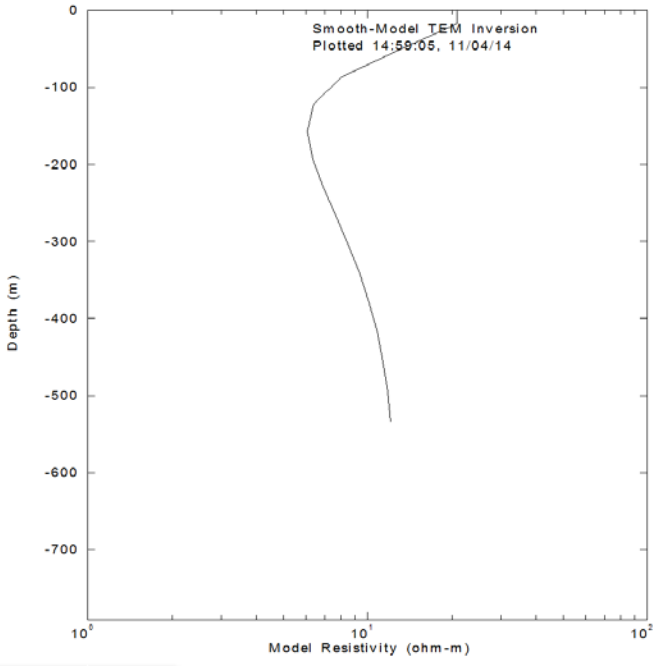
Smooth-Model TEM Inversion
Plotted 14:59:05, 11/04/14
Depth (m)
Model Resistivity (ohm-m)

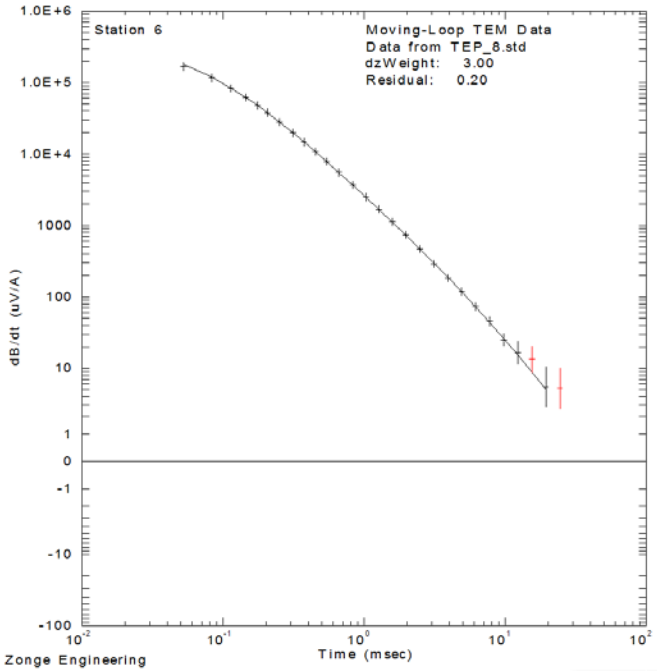
Station 6
Moving-Loop TEM Data
Data from TEP_8.std
dzWeight: 3.00
Residual: 0.20
dB/dt (uV/A)
Time (msec)
Zonge Engineering

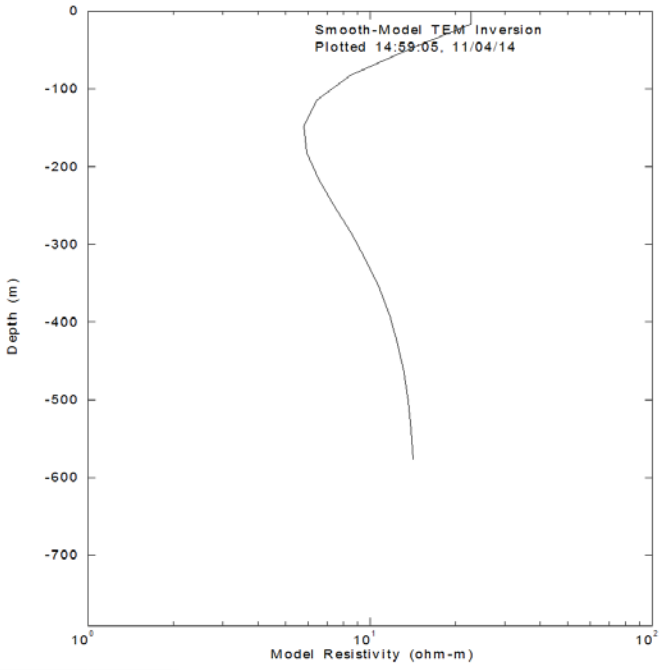
Smooth-Model TEM Inversion
Plotted 14:59:05, 11/04/14
Depth (m)
Model Resistivity (ohm-m)

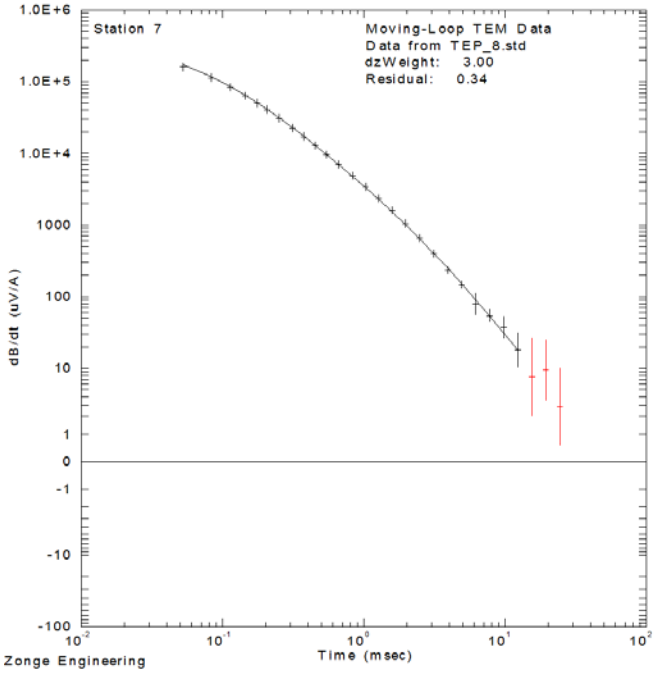
Station 7
Moving-Loop TEM Data
Data from TEP_8.std
dzWeight: 3.00
Residual: 0.34
dB/dt (uV/A)
Time (msec)
Zonge Engineering

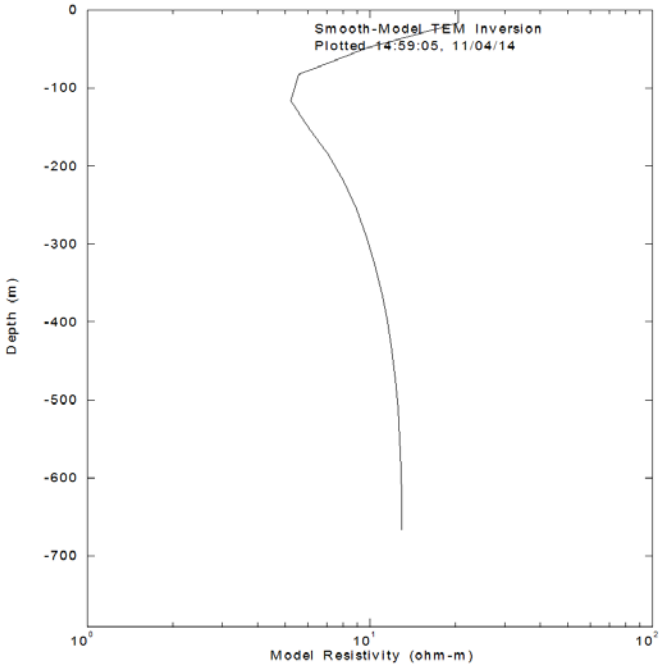
Smooth-Model TEM Inversion
Plotted 14:59:05, 11/04/14
Depth (m)
Model Resistivity (ohm-m)

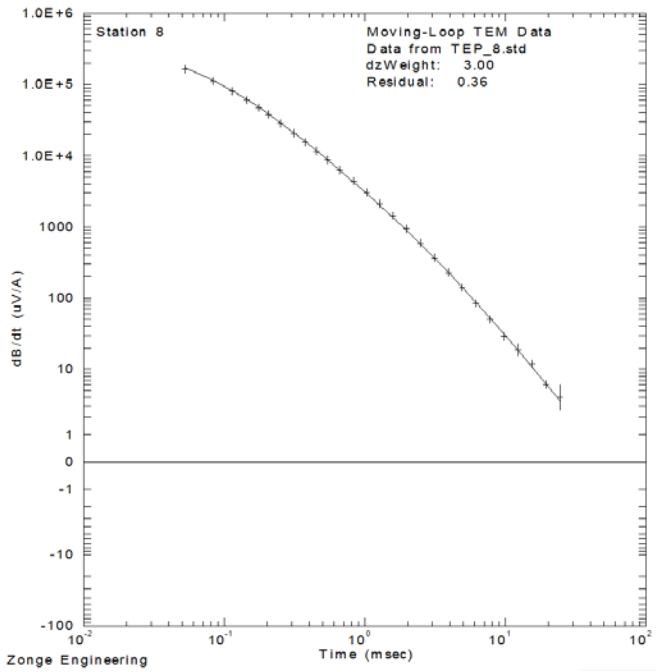
Station 8
Moving-Loop TEM Data
Data from TEP_8.std
dzWeight: 3.00
Residual: 0.36
dB/dt (uV/A)
Time (msec)
Zonge Engineering

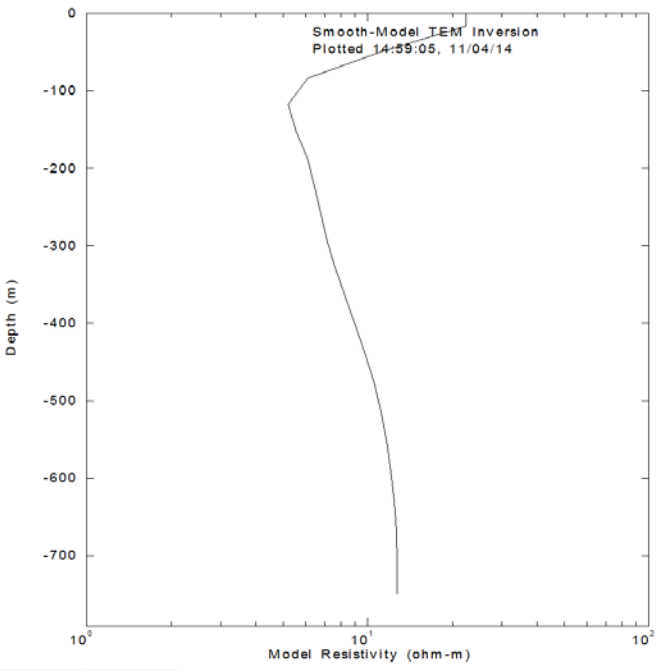
Smooth-Model TEM Inversion
Plotted 14:59:05, 11/04/14
Depth (m)
Model Resistivity (ohm-m)

For the 16Hz data

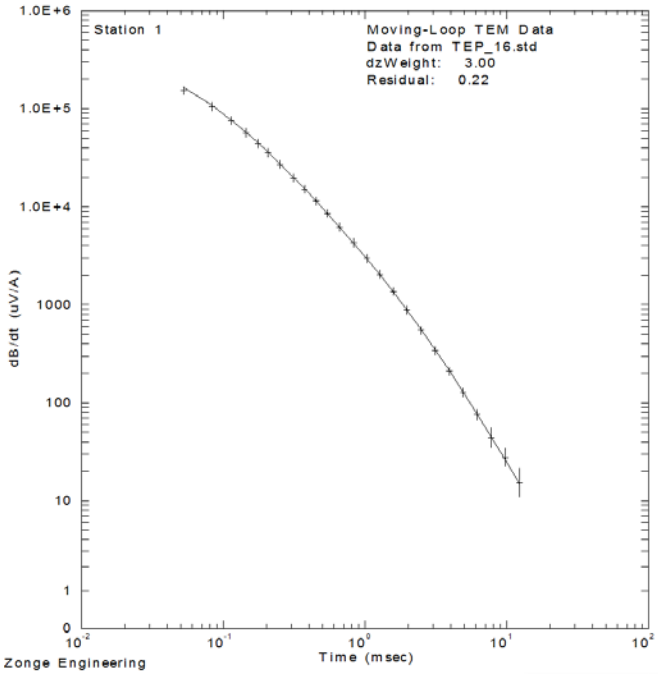


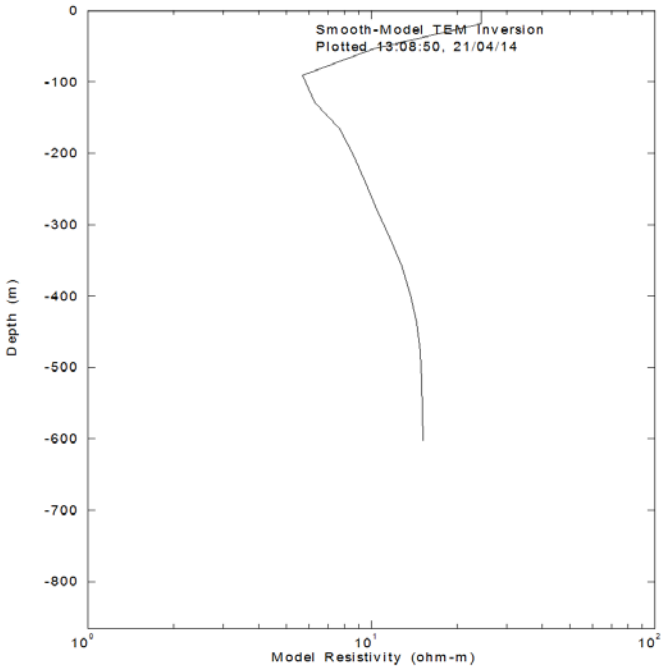


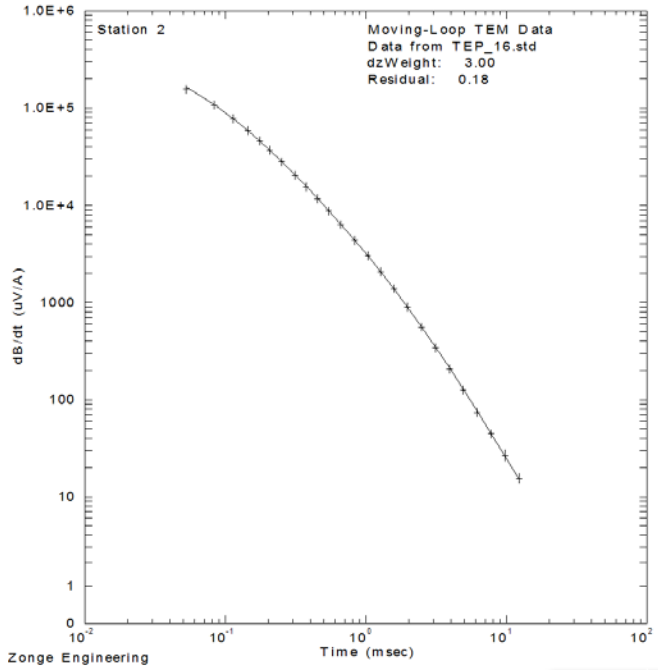


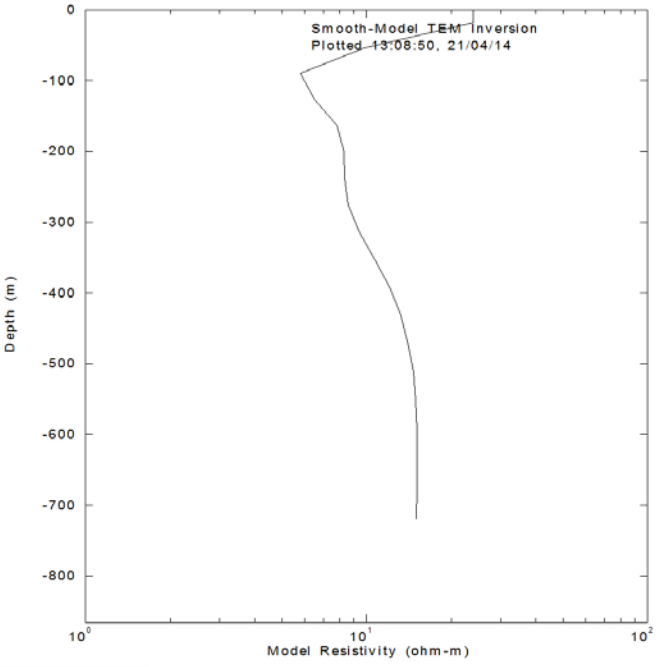

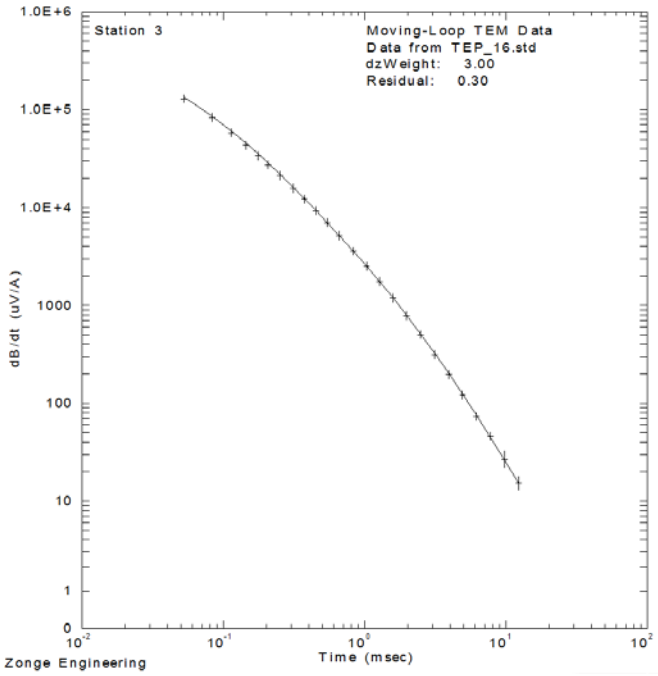
Station 3
Moving-Loop TEM Data
Data from TEP_16.std
dzWeight: 3.00
Residual: 0.30
dB/dt (uV/A)
Time (msec)
Zonge Engineering

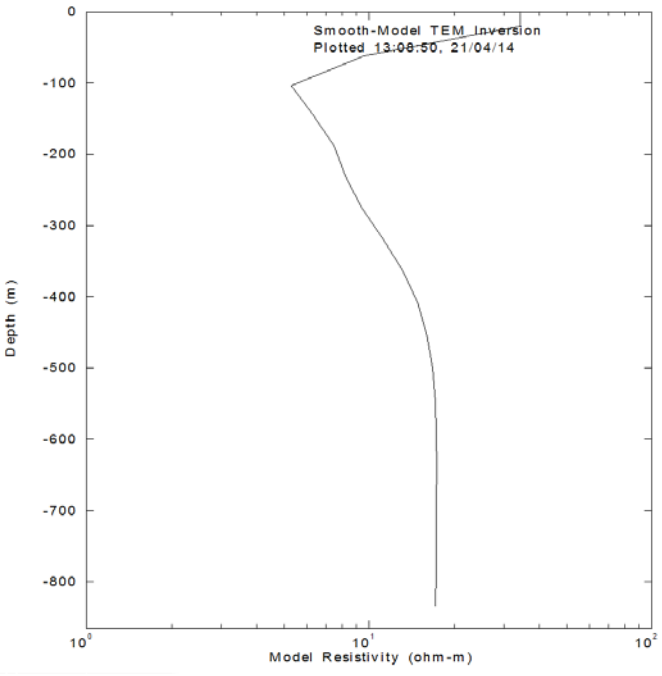
Smooth-Model TEM Inversion
Plotted 13:08:50, 21/04/14
Depth (m)
Model Resistivity (ohm-m)

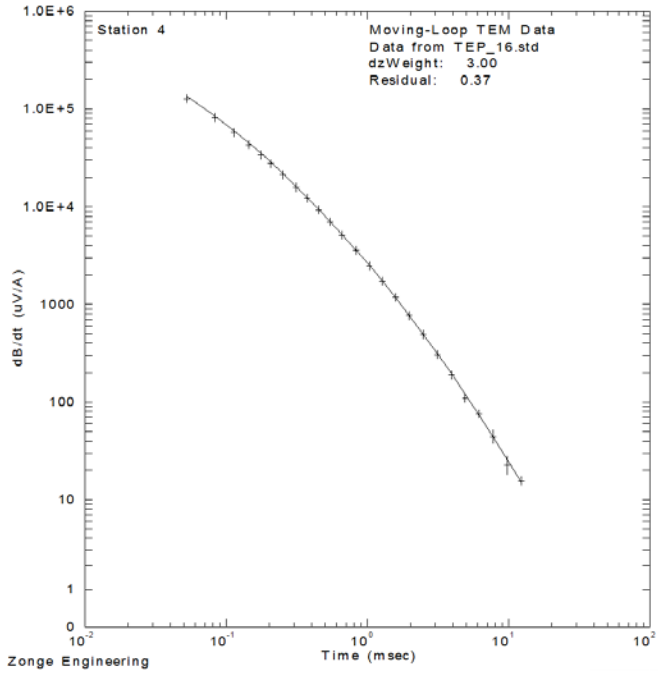
Station 4
Moving-Loop TEM Data
Data from TEP_16.std
dzWeight: 3.00
Residual: 0.37
dB/dt (uV/A)
Time (msec)
Zonge Engineering

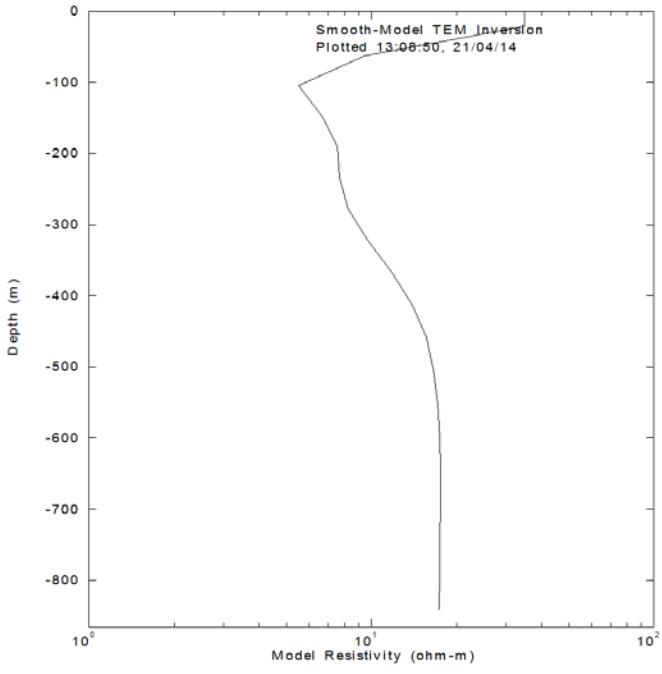
Smooth-Model TEM Inversion
Plotted 13:08:50, 21/04/14
Depth (m)
Model Resistivity (ohm-m)

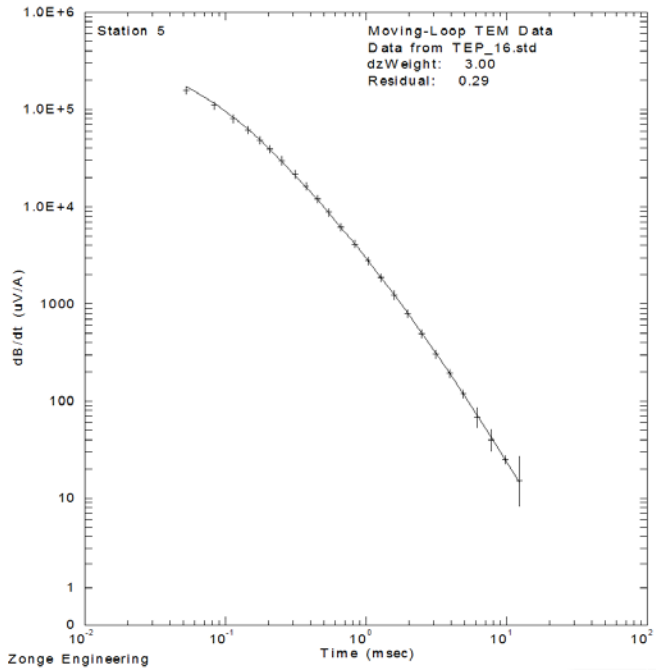
Station 5
Moving-Loop TEM Data
Data from TEP_16.std
dzWeight: 3.00
Residual: 0.29
dB/dt (uV/A)
Time (msec)
Zonge Engineering

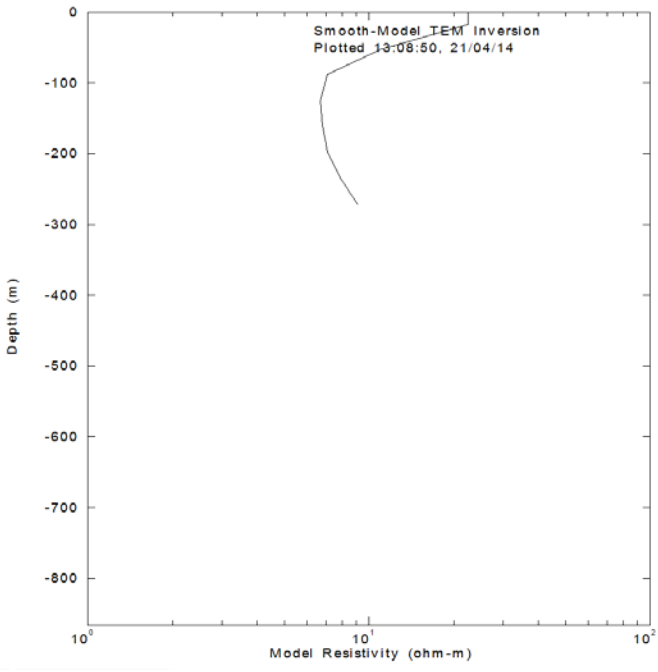
Smooth-Model TEM Inversion
Plotted 13:08:50, 21/04/14
Depth (m)
Model Resistivity (ohm-m)

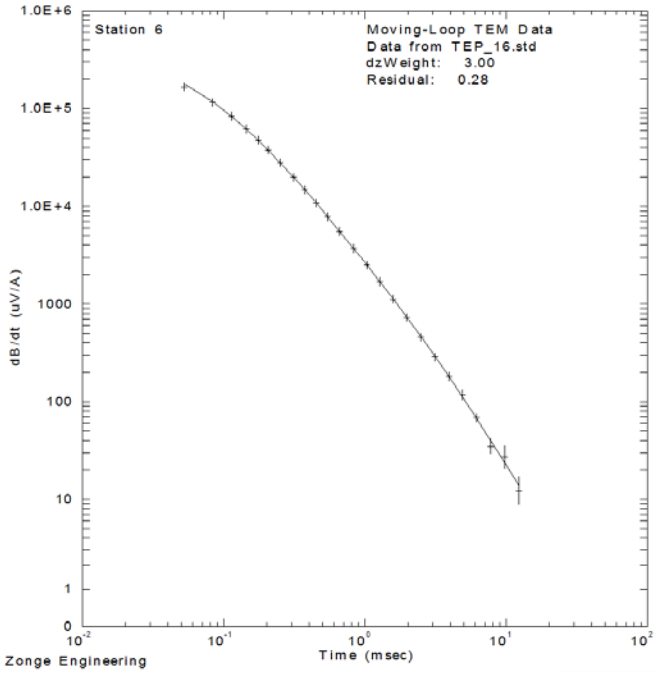
Station 6
Moving-Loop TEM Data
Data from TEP_16.std
dzWeight: 3.00
Residual: 0.28
dB/dt (uV/A)
Time (msec)
Zonge Engineering

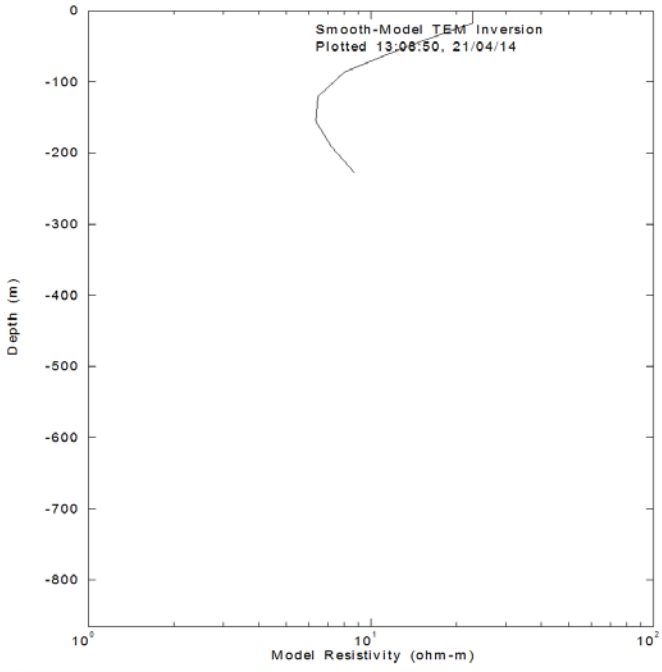
Smooth-Model TEM Inversion
Plotted 13:08:50, 21/04/14
Depth (m)
Model Resistivity (ohm-m)

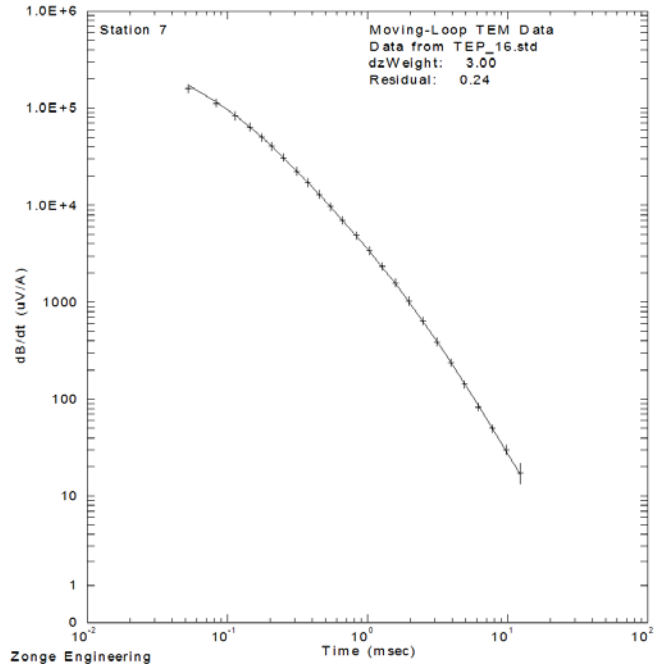
Station 7
Moving-Loop TEM Data
Data from TEP_16.std
dzWeight: 3.00
Residual: 0.24
dB/dt (uV/A)
Time (msec)
Zonge Engineering

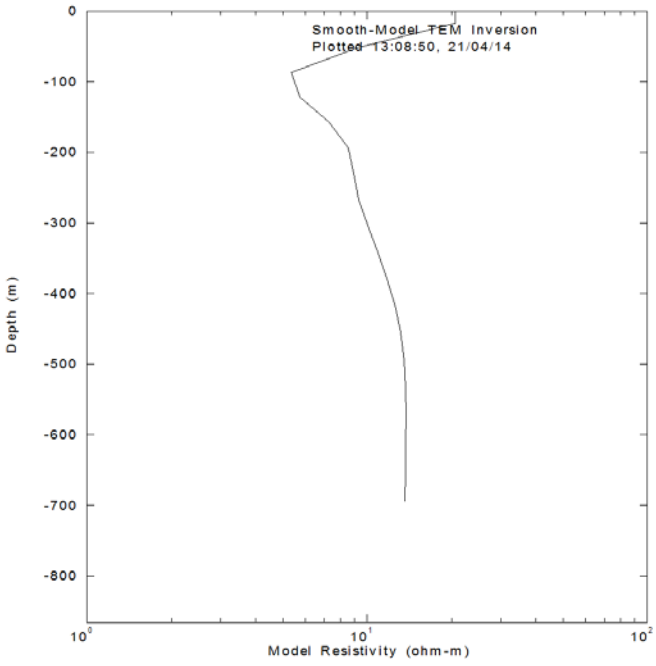
Smooth-Model TEM Inversion
Plotted 13:08:50, 21/04/14
Depth (m)
Model Resistivity (ohm-m)

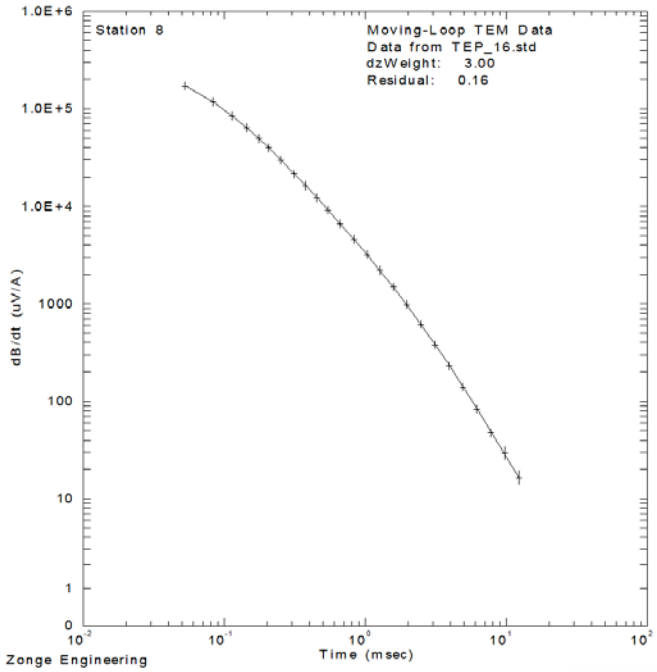
Station 8
Moving-Loop TEM Data
Data from TEP_16.std
dzWeight: 3.00
Residual: 0.16
dB/dt (uV/A)
Time (msec)
Zonge Engineering

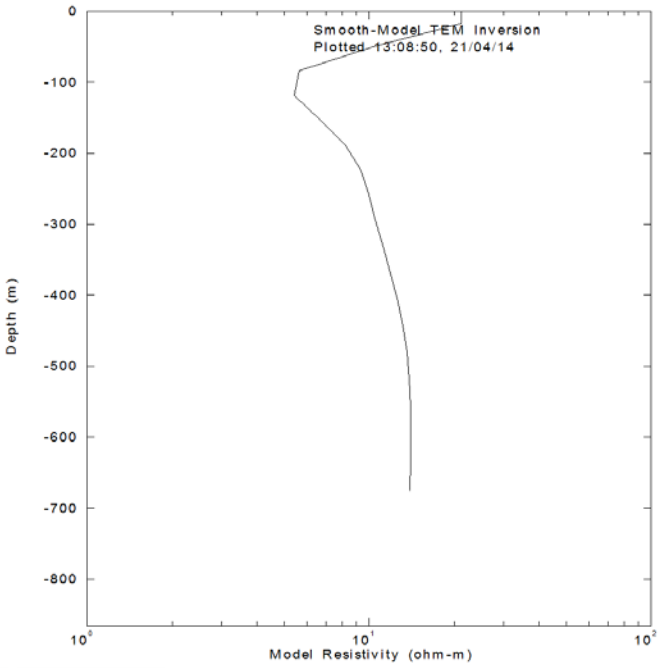
Smooth-Model TEM Inversion
Plotted 13:08:50, 21/04/14
Depth (m)
Model Resistivity (ohm-m)